Probing the Nature of Cellulosic Fibre Interfaces with Fluorescence Resonance Energy Transfer

A Dissertation
Presented to
The Academic Faculty

By

Cameron Ian Thomson

In Partial Fulfillment
Of the Requirements for the Degree
Doctor of Philosophy in the
School of Chemistry and Biochemistry

Georgia Institute of Technology

August 2007

Probing the Nature of Cellulosic Fibre Interfaces with Fluorescence Resonance Energy Transfer

Approved By:

Dr. Arthur J. Ragauskas
School of Chemistry and Biochemistry
Georgia Institute of Technology

Dr. Yulin Deng
School of Chemical and Biomolecular Engineering
Georgia Institute of Technology

Dr. Larry Bottomley
School of Chemistry and Biochemistry
Georgia Institute of Technology

Dr. Tim Patterson
School of Mechanical Engineering
Georgia Institute of Technology

Dr. L. Andrew Lyon
School of Chemistry and Biochemistry
Georgia Institute of Technology

Date Approved: June 18th, 2007

Acknowledgements

I have been fortunate to receive a great deal of advice and assistance from friends, family and colleagues throughout my graduate education. I would like to first thank my thesis advisor Dr. Art Ragauskas for encouraging me to work independently and pursue whatever topic interested me. I feel this freedom has allowed me to gain a great deal from my graduate school experience. I would like to thank my thesis defense committee members, Dr. Larry Bottomley, Dr. Yulin Deng, Dr. Andrew Lyon and Dr. Tim Patterson for their advice and support during my research.

Many of my colleagues have contributed to this work in various ways. I would like to thank Rob Lowe for collaborating with me on this project and helping me bring my ideas to fruition. I had many helpful and enjoyable discussions with Dr. Derek Page, Dr. Hiroki Nanko and Lauri Lehtonen about paper and fibre physics and the nature of the fibre bond that must be acknowledged. Delphine Nain gave invaluable advice about image analysis and image processing and contributed greatly to the writing of the MATLAB program code. I would like to thank Tom Dyer and Richard Chandra for collaborations and helping me adjust to life in graduate school and in the Ragauskas group when I first arrived in Atlanta. I appreciate and acknowledge the guidance and friendship of my fellow students: Andy DeMaio, Brett Brotherson, Doug Cameron, Mike Carlson, Courtney Sorrell, Kane Barker, Dongcheng Zhang, Zheng Dang, Kim Nelson, Aaron Jacobson,

John Litvay, Jeremy Meyers and Fran Jacobson. All of whom contributed in some manner to my experience at Georgia Tech.

Rallming Yang, Lenong Allison, Dr. Yunqiao Pu, Dr. Jianguo Zhang, Kristina Knutson, Shaobo Pan and Tuwanda Strowbridge provided technical assistance in the laboratory that allowed me to complete my research tasks. I would like to thank Major Hank White for keeping me company during many late nights at the PTB building. Above all I would like to thank Shanna Young for her love and support throughout my research program.

It is also important to acknowledge Dr. George Pan and Dr. Steven Pitts who were my first research mentors. They kindled my passion for research and were instrumental in making me the researcher that I am today. I am indebted to them.

Lastly, I would like to thank my parents and my family for always supporting and encouraging me in my education.

Table of Contents

List of Tables

List of Figures

List of Equations

Summary

Among the most fundamental and practically important properties of paper are the physical and chemical parameters involved in fibre-fibre bonding. Inter-fibre bonding is solely responsible for internal cohesion in paper, because all stresses transferred between fibres operate through fibre-fibre bonds. Although several differing technologies are currently being pursued to improve fibre-fibre bonding the fundamentals of this process are still poorly defined. The future development of cellulosic fibre materials will require an improved understanding on the fibre-fibre interface. Current techniques are unable to provide useful information on the structure of the fibre-fibre interface at relevant length scales or under ambient conditions. A new tool is required that is capable of providing structural information about the formation and behaviour of fibre-fibre interfaces at the nanoscale.

Fluorescence resonance energy transfer (FRET) is identified as a tool for the study of fibre interfaces with nanometre resolution. In order to develop this tool, it was necessary to successfully label cellulosic fibres with a fluorescent dye pair capable of FRET. A protocol for covalent linkage of fluorophores to natural and regenerated cellulosic fibres was developed and the absorptive and emissive properties of these dyes were characterized. The fluorescent response of these dyed fibres in paper sheets was studied using steady-state fluorescence spectroscopy.

Fluorescence micrographs of fibre crossings were analyzed using the FRETN correction algorithm. The results suggested that energy transfer from coumarin dyed fibers to fluorescein dyed fibres was occurring. The FRETN surface for spruce fibre interfaces was distinctly different from that observed in viscose fibre. The effects of refining, wet pressing and fibre fraction on the spruce fibre interface were investigated with FRET microscopy. It was determined that the method was able to detect statistically significant differences when fibre fraction and wet pressing were varied. Image analysis of fluorescence micrographs of white spruce fibres indicates a FRET signal is being produced at fibre crossings and that it can be manipulated with wet pressing load.

The coalescence of fibre interfaces during drying was observed with the technique and a logarithmic relationship between increasing average FRETN values and drying time was identified. The FRET signal from once-dried fibre crossings increases dramatically after rewetting and wet pressing for a second time. This indicates that the material within the fibre bonds is still compliant after a single drying cycle.

Lastly, a model system of polysaccharides films was employed to investigate the difference between natural and regenerated cellulose fibre interfaces. It was found that cellulose is less capable of reducing the average interfibre distance either through resistance to deformation or the inability to participate in interdiffusion. On the other hand, the xylan films demonstrated a wet pressing

response that was similar to that observed for natural wood fibres. The results of the FRETN analysis of the polysaccharide film model systems indicate that lower molecular weight carbohydrates are likely to be significant contributors to fibre interface development.

Chapter 1: Introduction

The primary resource of the paper industry is the lignocellulosic fibre derived from renewable plant resources. Although there may be heightened interest in renewable products, the paper industry must overcome numerous technical barriers associated with lignocellulosic fibres in order to generate competitive products. Whether lignocellulosic fibres are used in paper-like products or in other types of composite materials, the fibre-fibre and fibre-matrix interfaces are critical to material performance. Papermakers have manipulated these fibre interfaces for hundreds of years with a variety of mechanical and chemical processes which bear close resemblance to those used today. Recently, approaches involving the modification of fibre surface chemistry have been explored with the goal of controlled fibre interface development. Further understanding of the structure and behaviour of cellulosic fibre interfaces will allow for directed manipulation of fibre-fibre interfaces and a host of improved material properties.

Currently there are no techniques available that are capable of defining the structure of fibre-fibre interfaces at the length scales relevant to molecular interactions. This dissertation presents a new tool for the investigation of cellulosic fibre interfaces. A review of the techniques used by researchers in the past to investigate fibre-fibre interfaces is presented to provide some context for the current work.

Chapter 2: Literature Review

Any discussion of fibre-fibre interfaces must include a consideration of the chemical composition and structure of the fibres themselves. Although there are a wide variety of natural and synthetic cellulosic fibres used in the manufacture of paper, non-wovens and fibre-reinforced composites, this review will focus on the properties of lignocellulosic fibres derived from wood. Lignocellulosic fibres find their origin as plant cell walls in plants with persistent stems such as trees. Wood itself can be described as a fibre reinforced composite whereby relatively rigid plant cell walls composed primarily of carbohydrates are embedded in a polymer matrix. Furthermore, the fibre cell wall itself is also composite-like in structure with the various polymers organized. Lignocellulosic fibres are liberated from wood using a variety of chemical and mechanical treatments designed to soften or degrade the composite matrix. These procedures modify the final composition and performance of the resultant fibres and will be discussed briefly.

2.1 Chemical Composition of the Cell Wall

Lignocellulosic fibres are primarily composed of three main natural polymers: cellulose, non-cellulosic carbohydrates commonly known as hemicellulose and lignin. These components are distributed throughout the cell wall with varying degrees of organization and will be discussed in further detail below [1].

2.1.1 Cellulose

Cellulose is the most plentiful material in nature primarily because it is the major constituent of the plant cell wall typically making up 40-50% of native wood by weight. Cellulose is a linear polysaccharide composed of D-glucose monomers connected by 1,4-β glycosidic bonds as shown in Figure 1 [2]. Cellulose has an chain length of nearly 10,000 cellobiose monomer units in native wood but can decrease to less than 2000 after pulping [3]. Suckling *et al.* have observed that the average chain length of cellulose in *Pinus radiata* is approximately 9,000 but decreases to 4,000 – 5,000 after kraft pulping [4].

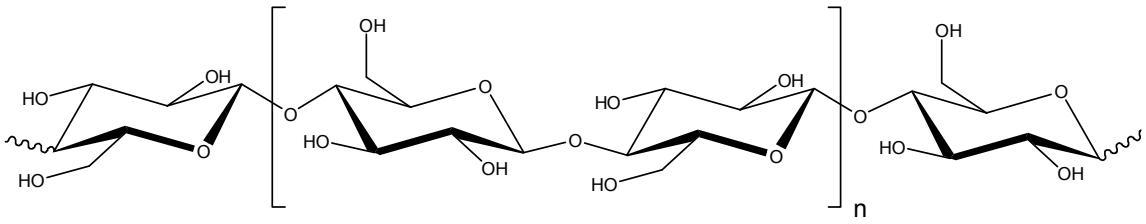

Figure 1. Chemical structure of cellulose

1,4-β-D-glucopyranose monomers and cellobiose repeating units [2].

Cellulose macromolecules can be organized into crystalline structures due to the presence of numerous hydroxyl groups on the chain backbone which lead to both intermolecular and intramolecular hydrogen bonds. In the cell wall, cellulose is organized into thin crystalline structures known as microfibrils that are helical about the fibre axis. In most wood species, elementary fibrils with a width of 3.5 nm are first constructed by the crystallization of 36 parallel cellulose chains [5]. Microfibrils are then formed by aggregation of these elementary fibrils into bundles that can reach 50 nm in width. Hult *et al.* calculated the width of

cellulose microfibril aggregates in kraft pulps to be on the order of 14-20 μm using CPMAS ^{13}C NMR data [6, 7].

Table 1. Cellulose degree of polymerization

Change in DP due to kraft pulping and ECF bleaching for softwoods [4, 8].

Cellulose Source	Cellulose Degree of Polymerization
Native wood	9000 - 10000
Unbleached kraft pulp	4000 - 6000
Fully bleached kraft pulp	1500 - 2000

Cellulose has six crystalline polymorphs of which cellulose I and II are the most commonly found [2]. Cellulose I is composed of parallel cellulose chains and is the native form produced in plants and other organisms [5]. Natural cellulose I exists as two sub-allomorphs, I_α and I_β, which can both be described as dense, highly hydrogen bonded sheets of parallel chains with less hydrogen bonding between the sheets which are arranged in stacks [9, 10]. The main difference between the two allomorphs is the stacking of these sheets is displaced in the chain direction. The two allomorphs are often found together although bacterial cellulose tends to be rich in I_α while cotton tends to be higher in cellulose I_β [11]. The ratio of cellulose I_α and I_β in woody plants depends greatly on the species. In general, softwoods are higher in I_α, while hardwoods contain more I_β. Cellulose II is the most common alternative polymorph found in synthetic cellulosic materials and is obtained from cellulose I by mercerization or various cellulose regeneration processes. Cellulose II consists of antiparallel cellulose chains that are arranged into less dense sheets. There is significant hydrogen bonding both within sheets and between sheets in cellulose II [2, 10].

Table 2. Distribution of cellulose crystalline allomorphs

In several cellulose sources from

Cellulose source	Cellulose crystalline allomorphs		
	I_α (%)	I_β (%)	II (%)
Native spruce wood	74	26	-
Cotton	41	59	-
Bacterial cellulose	62	30	trace
Bleached spruce kraft pulp	30	61	9
Viscose	-	-	100

Despite the chemical resistance afforded to cellulose by its largely crystalline structure, alkaline pulping and modern bleaching practices do degrade the cellulose macromolecule. In addition to the drop in cellulose DP, the degree of crystallinity and distribution of polymorphs in cellulose fibres also changes during pulping [6]. Cellulose crystallinity can be measured using IR, X-ray powder diffraction [12] or CP/MAS ^{13}C NMR methods [11, 13]. Alkaline pulping results in conversion of cellulose I_α to cellulose I_β and a small amount of cellulose II [11]. The overall crystalline cellulose content typically increases after conventional kraft pulping and ECF bleaching due to removal of amorphous material.

2.1.2 Hemicellulose

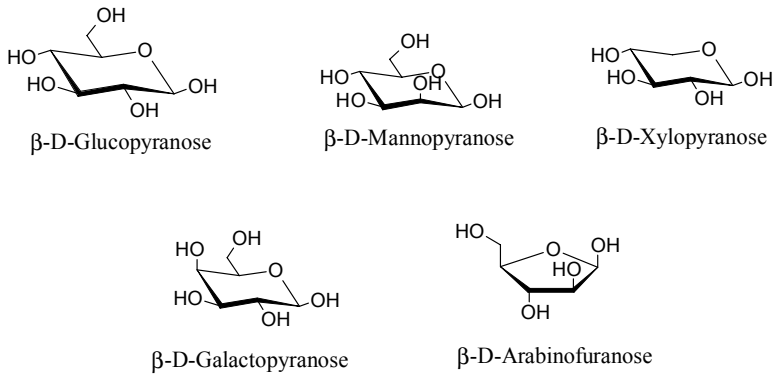

Figure 2: Common sugar monomers in hemicellulose

Hemicellulose is entrained within the cell wall matrix along with the lignin and cellulose [14]. Hemicelluloses are branched heteropolysaccharides that consist of a number of different sugar building units that are linked together in a variety of bonding arrangements. Prevalent hexose units include glucose, mannose and galactose, while the pentoses are primarily xylose and arabinose. Hemicellulose has an average degree of polymerization of only 100 to 200 units and has varying degrees of branching sugars off of the main chain [15]. Hemicellulose is an amorphous polymer and this is attributed to the low degree of polymerization and the branched structure.

Both the proportions and the composition of hemicellulose vary from species to species as can be seen in Table 3. Hemicellulose content is typically 20 to 30% of oven dry wood in softwoods and 25 to 35% in hardwoods [15]. The hemicellulose of hardwoods is primarily comprised of xylan with lesser amounts of unbranched glucomannan. Softwood hemicellulose is principally composed of

branched galactoglucomannan with lesser amounts of arabinoxylan and trace amounts of arabinogalactan [16].

Table 3. Chemical composition of representative hardwoods and softwoods

From Timell [17].

Softwoods	Cellulose (%)	Lignin (%)	Glucuronoxylan (%)	Glucomannan (%)	Other (%)
Pinus taeda	42	30	9	17	3
Picea glauca	41	27	13	18	1
Abies balsamea	42	29	9	18	2
Pinus strobus	41	29	9	18	3
Tsuga Canadensis	41	33	7	16	3
Thuja occidentalis	41	31	14	12	2
Hardwoods					
Acer rubrum	45	24	25	4	2
Populus tremuloides	48	21	24	3	4
Betula papyrifera	42	19	35	3	1
Eucalyptus goniocalyx	44	30	18	4	4
Fagus grandifolia	45	22	26	3	4
Ulmus americana	51	24	19	4	2

Xylans are a major class of hemicelluloses present in virtually all forms of lignocellulosic materials. Hardwoods, softwoods, cereal straws, grasses, sugarcane, bagasse, and corn stovers all contain xylan to some extent. There are two predominant types of xylan – acetylglucuronoxylan and arabinoglucuronoxylan [18]. Both polymers have homosaccharide backbones of 1,4-β-linked xylopyranose units, but the branching of the polymers is different. Figure 3 shows acetylglucuronoxylan with 30-70% of the 2 positions are substituted with acetyl groups and about 10% with 4-O-methylglucuronic acid groups [18]. This type of xylan is prevalent in the hardwoods.

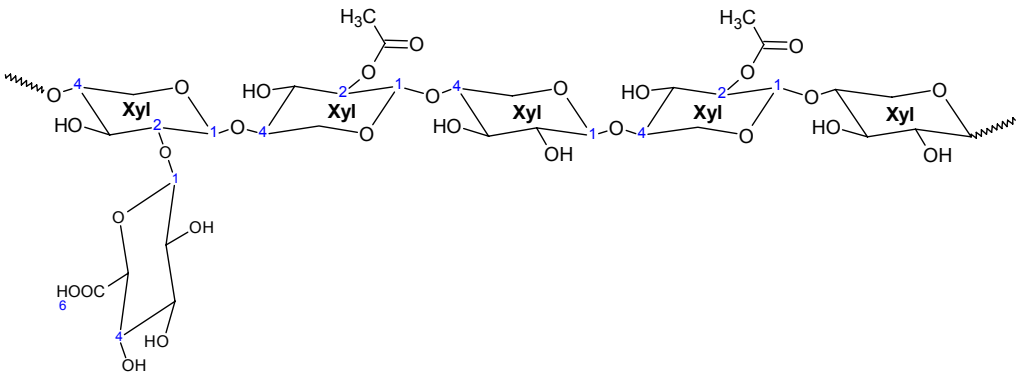

Figure 3: Xylan structure found in hardwoods

1,4-β-linked xylopyranose units and acetyl groups at C2 positions and 4-O-methyluronic acid branches at C2 position [18].

In softwoods, the xylan has the same basic structure, but usually with no attached acetate groups. Softwood xylan shown in Figure 4 has 4-methylglucuronic acid side chains at approximately 20% of the C2 positions but it also has arabinose sugars attached to either C2 or C3 [18]. In general, the softwood xylans are more branched with uronic acids but are less substituted overall because there are no acetate groups. The typical arabinose/uronic acid/xylose ratio is 1:2:8 [15, 17]. This tends to make softwood xylans less soluble than hardwood xylans in most aqueous solvents.

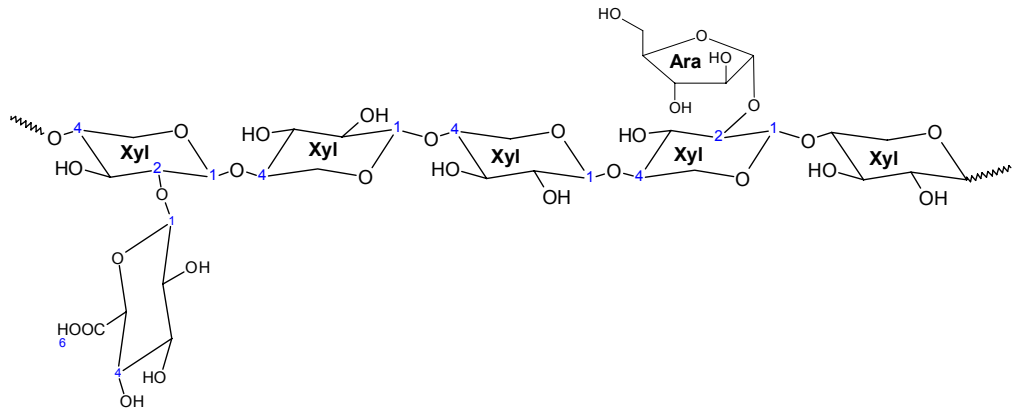

Figure 4. Xylan structure found in softwoods

1,3 linked arabinose units and 4-O-methylglucuronic acid at C2 [18].

Glucomannan is far more important than arabinoglucuronoxylan to the hemicellulose of softwood. Galactoglucomannan contributes to 15-20% of the dry wood mass of softwoods and thus is the principal component of the hemicellulose in the conifer species [17, 19, 20]. It is comprised of 1,4-β-linked glucose and mannose units that are partially acetylated at C2 and C3 and partly substituted by single galactose units attached to the 6 position [21]. It has an approximate DP of 100-150 and is found primarily in the lignified secondary wall. Softwoods generally have two different types of galactoglucomannan – one highly branched form with a 1:1:3 galactose/glucose/mannose ratio and another that is less branched with a 0.1:1:3 galactose/glucose/mannose ratio [15, 17]. In hardwoods, glucomannan has little or no branching and a lower glucose/mannose ratio of 1:1 or 1:2 [16, 17].

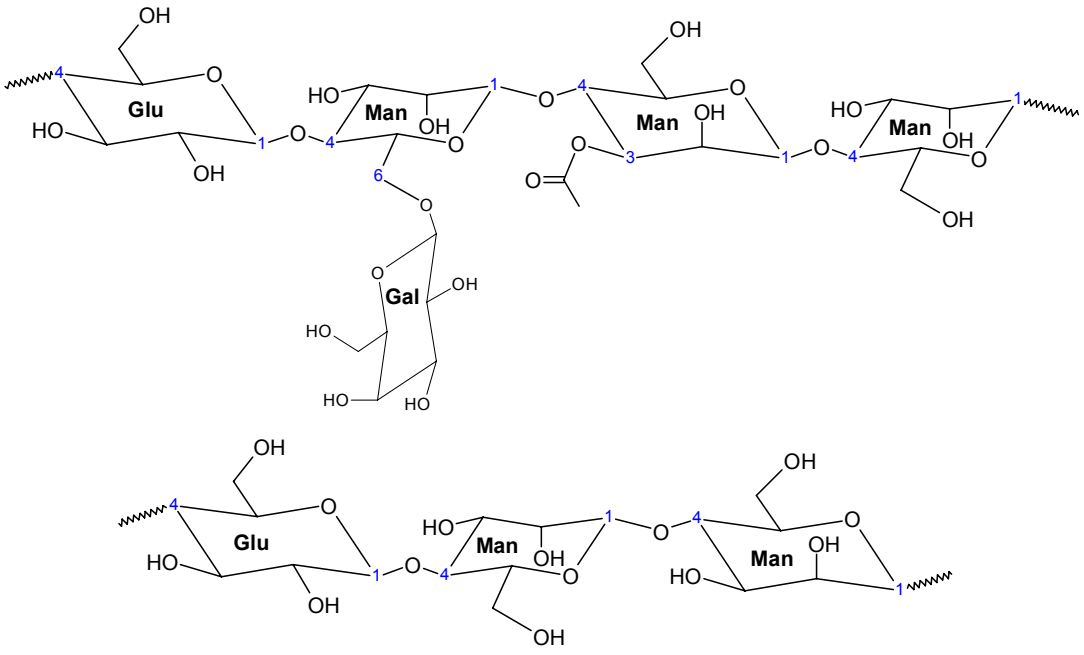

Figure 5: Structures of Glucomannan

Softwood galactoglucomannan (top) and hardwood glucomannan (bottom)[17].

The last major type of hemicellulose is arabinogalactan, a highly water soluble hemicellulose that is present in many woods to a minor extent (0.5-2%) but is the major component of larch hemicellulose (10-30%) [22]. The backbone of arabinogalactan is 1,3-β-linked galactopyranose units and it is highly branched with two unit sidechains of 1,6-β-linked galactose units or 1,3-β-linked arabinose units. The high degree of branching as shown in Figure 6 makes arabinogalactan highly soluble in aqueous solutions. Unlike the hemicelluloses in other species, larch arabinogalactan is actually deposited outside of the cell wall and can be fully extracted with hot water [17].

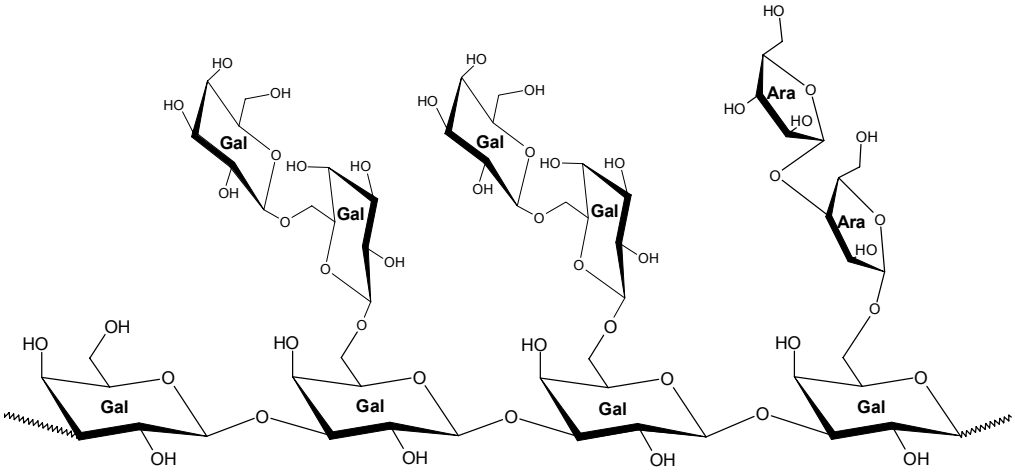

Figure 6: Structure of Arabinogalactan

Found in Larch species[17]

The hemicellulose fraction of the fibre wall is altered during modern alkaline pulping methods. The amorphous structure of hemicellulose allows for easy penetration of pulping liquors and its low degree of polymerization results in the rapid generation of soluble oligomers. In the initial phase of kraft pulping, 40% of hemicellulose is removed while only 10% of cellulose is removed, illustrating the

importance of the crystalline structure of cellulose to its chemical resistance [17, 23]. Hemicelluloses undergo peeling reactions that remove end units and ultimately convert them to isosaccharinic acids. Figure 7 illustrates the alkaline hydrolysis reactions that cleave the hemicellulose chain during alkaline pulping and reduce the degree of polymerization [23]. The liberated monomers can then undergo further degradation into mono- and di-carboxylic acids in the pulping liquor.

Table 4. Hemicellulose DP and average molar mass

Hemicellulose derived from softwood holocellulose and bleached kraft pulp [8, 24].

Hemicellulose source	Degree of Polymerization	
	Xylan	Glucomannan
Softwood holocellulose	90 - 145	90 - 130
Bleached softwood kraft	-	70 - 100

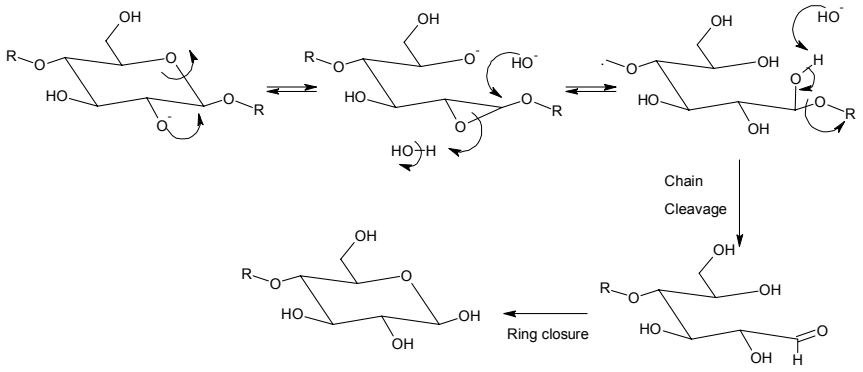

Figure 7: Alkaline cleavage of glycosidic bond

[23]

Hemicelluloses are also easily degraded under acidic conditions such as those experienced during sulfite pulping and some bleaching stages. Acid catalyzed hydrolysis (Figure 8) is an effective method for cleaving the glycosidic bond in polysaccharides. The results are similar to the alkaline hydrolysis except that the

monomers undergo a very different degradation pathway. Hexoses and pentoses are dehydrated in the presence of acid to form 5-hydroxymethylfurfural (HMF) and furfural, respectively.

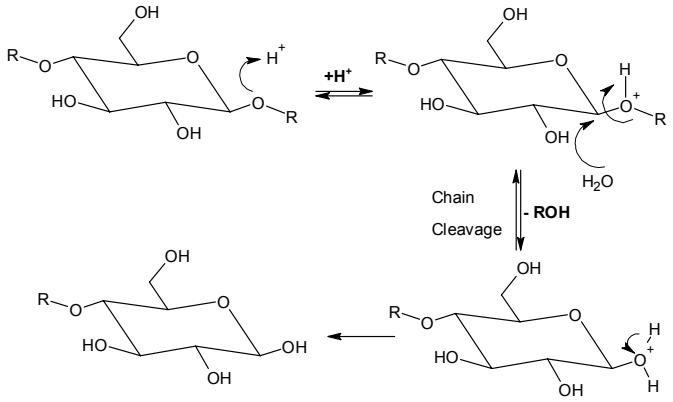

Figure 8. Acid hydrolysis of glycosidic bond

2.1.3 Lignin

Lignin is a complex three-dimensional network polymer made up of phenylpropane units [25]. The profusion of lignin in nature is due to its importance to the cell walls of both woody and non-woody plants. Trees are the most significant contributor to the production of lignin in the biosphere due to their relatively high lignin content and their ubiquitous presence on the planet. Although lignin is critical to the structural properties of wood, its removal is essential to the production of high quality and high strength paper. The pulp and paper industry devotes a vast amount of effort to capital intensive pulping and bleaching primarily designed to remove lignin from wood fibres. In spite of the efforts of many researchers over the past fifty years, the structure of native lignin is unknown, largely due to the difficulty in isolating lignin without modification.

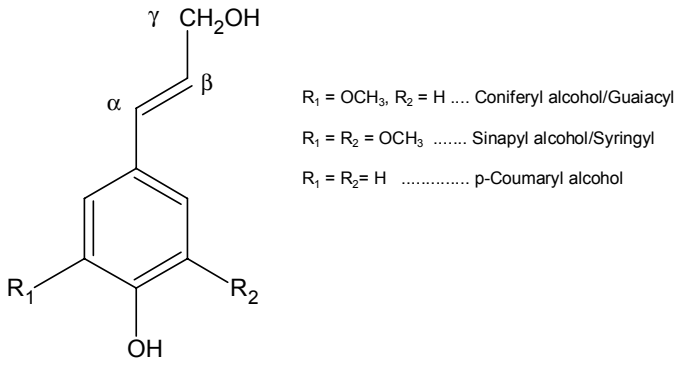

Figure 9: The building blocks of lignin

From [26]

Although the structure of native lignin is not yet known, a great deal of information has been inferred from lignin degradation products and model compound studies. Lignin formation originates from the polymerization of three different phenylpropane units known as monolignols: sinapyl, coniferyl and p-coumaryl alcohol (Figure 9) [27].

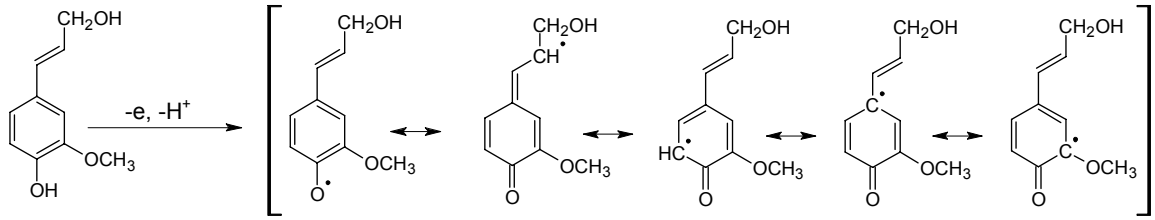

Figure 10: Resonance structures of lignin building blocks

Phenoxy radical precursors for lignin formation from [25, 28]

The polymerization of lignin is believed to occur via the formation and subsequent coupling of phenoxy radicals [25, 28, 29]. There are five main resonance structures (Figure 10) of the phenoxy radical and thus a wide variety of linkages are formed during the coupling. The multi-functionality of the phenoxy radical monomer ultimately results in the formation of a complex network

polymer. The phenylpropane units are connected by carbon – carbon or ether bonds. There are eight common interunit linkages in lignin as shown in Figure 11 [27]. The most abundant linkage in lignin is by far the β-O-4 ether linkage, which typically makes up approximately 50% of the total linkages in softwood lignin.

Table 5. Frequency of different lignin linkages

For hardwood and softwood lignin from [27, 29].

Type	Name	Softwood (%)	Hardwood (%)
β-O-4	β-aryl ether	45 - 50	60
α-O-4	α-aryl ether	6 - 8	7
β - 5	Phenylcoumaran	9 - 12	6
5 - 5'	Biphenyl and Dibenzodioxocins	18 - 25	7
4-O-5	Diphenyl ether	4 – 8	5
β - 1	1,2 - diphenylpropane	7 – 10	7
β - β	β - β linked structures	3	3

The distribution of covalent linkages in lignin is believed to play a significant role in its reactivity. Table 5 shows the frequency of linkages found in softwood lignin. Certain linkages are easily broken during pulping and bleaching, while other structures are less susceptible to certain modes of chemical attack. The frequencies of key functional groups that also contribute to lignin reactivity are summarized in Table 6. The difference in reactivity amongst the various lignin units and linkages is particularly evident when comparing post-pulping or post-bleaching residual lignin to native lignin.

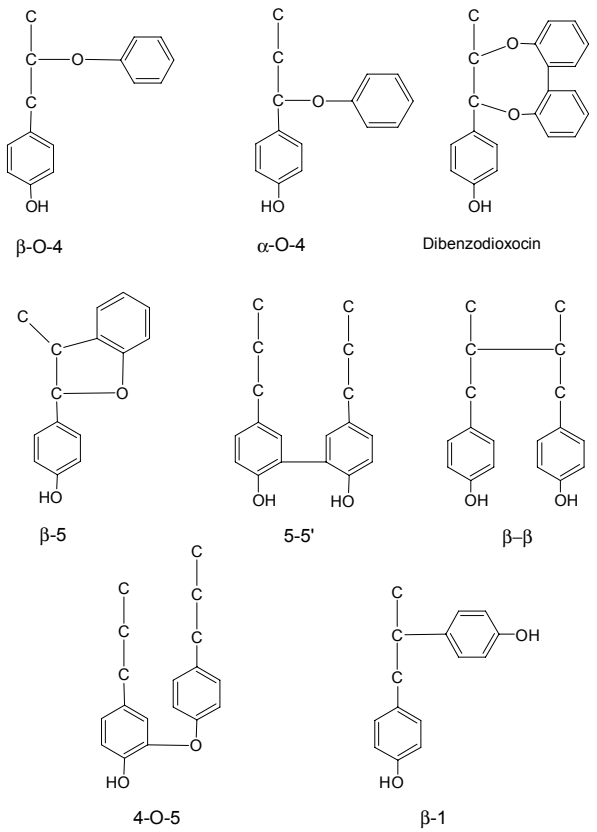

Figure 11: Structures of common lignin linkages

From [26, 30, 31]

Table 6. Functional groups in softwood lignin per 100 phenylpropane units

From [26]

Functional Group	Softwood Lignin (per 100 C-9)
Carbonyl	10 - 15
α-hydroxyl	15 - 20
Phenolic hydroxyl	15 - 30
Methoxyl	92 - 96

2.1.4 Cell Wall Architecture

Wood is cellular in structure with the cell walls composed of a group of natural polymers known as lignocellulose.[32] Lignocellulose is made up of three main components - cellulose, hemicellulose and lignin. These polymers are arranged within the cell wall in a number of configurations and at varying concentrations as

shown in Figure 12. The thickness of the cell wall layers and their chemical composition are widely varying between species and within the tree.

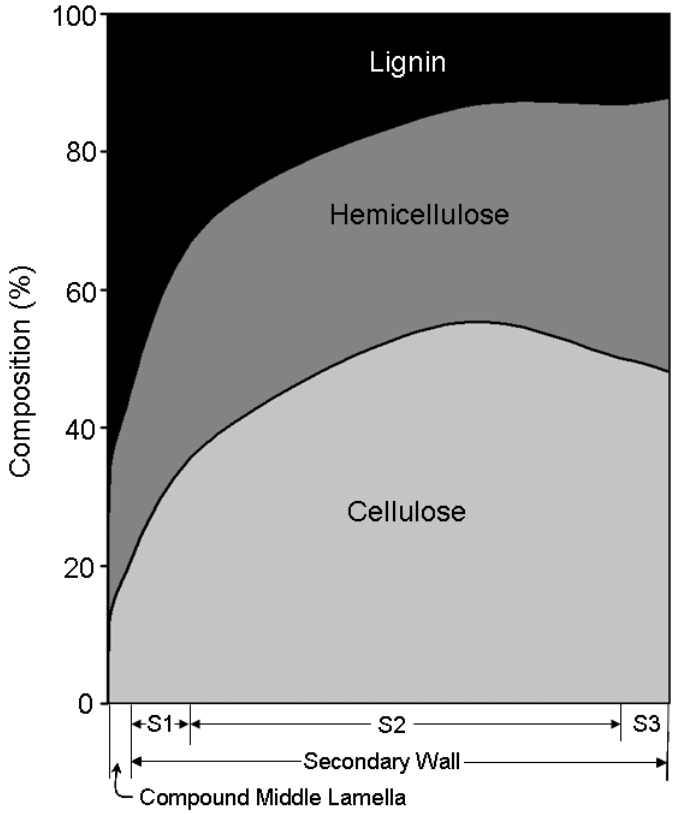

Figure 12. Distribution of cell wall components across cell wall layers

Content and relative cell wall layer thickness for softwood tracheids. Adapted from [32].

The majority of woody cells in softwoods are longitudinal tracheids that run in the direction of the tree axis. Tracheids are long thin walled tubes that average 1 – 4 mm in length, 35 – 45 μm in diameter with cell walls of 1 – 5 μm.[20] Other cell types include ray parenchyma, longitudinal parenchyma, epithelial parenchyma and ray tracheids, all of which make up a much smaller volume of the wood.[32] The parenchyma cells store and conduct food materials in the tree. Epithelial cells are thin-walled, excretory cells that are particularly important to resinous

trees such as the pine species, as they surround the longitudinal and transverse (with ray tracheids) resin canals.[32]

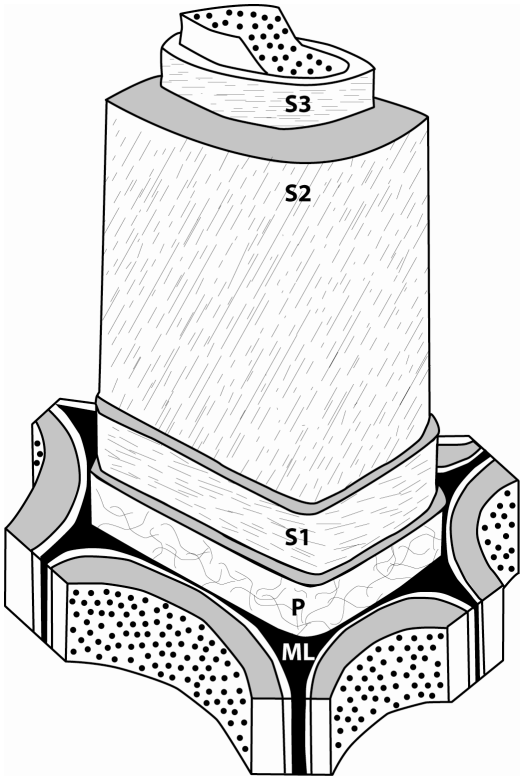

Figure 13. Illustration of a softwood tracheid (fibre) cell wall structure.
Adapted from Côté.[33]

The woody plant cell wall is made up of several layers as illustrated in Figure 13. The compound middle lamella is made up of the two primary walls from adjacent cells and the true middle lamella. The middle lamella is primarily composed of lignin and acts to hold fibres together in the wood ultrastructure. The primary wall is also highly lignified but it also contains cellulose microfibrils organized in a loose network almost perpendicular to the cell axis. As shown in Figures 12 and 13, this layer is quite thin but has a very high lignin content and low cellulose content.

The secondary wall is dense, consists predominantly of cellulose and is the primary contributor to the fibre's mechanical properties. It is made up of three different sub-layers – S1, S2 and S3.[32] The S2 layer makes up about 75% of the cell wall volume and has a low microfibril angle of about 10 to 30°. It is composed primarily of densely organized cellulose microfibrils that are highly aligned with the cell axis. The S1 and S3 layers are much thinner (10% and 8% by volume on average, respectively) and have higher microfibril angles of 50 to 70° and 60 to 90°, respectively.[32] Figure 13 shows the average relative thickness of each of the cell wall layers as well as their composition in terms of cellulose, lignin and hemicellulose.

Table 7. Comparison of wood and kraft pulp chemical composition

Native spruce wood [20] and bleached spruce kraft pulp [23].

	Spruce Native Wood (%)	**Spruce Bleached Kraft Pulp (%)**
Cellulose	41	81
Glucomannan	18	8
Glucuronoxylan	13	10
Lignin	27	0.05

The overall chemical composition of lignocellulosic fibres described in Table 7 and the distribution of those components in the cell wall as illustrated in Figure 13 changes quite dramatically upon pulping and bleaching. Kraft pulping and subsequent bleaching stages remove over 99% of the main target lignin as well as approximately 10-15% of cellulose and 50-60% of hemicellulose as shown in Table 7. The resultant overall chemical composition of a typical bleached

softwood kraft pulp is 80-82% cellulose, 17-19% hemicellulose and routinely less than 0.5% lignin.

2.1.5 Fibre Surface Chemistry

Lehtonen *et al.* have described the main goal of pulping and papermaking processes as being the efficient creation and management of specific surface area [34]. The principal role of pulping is to liberate fibres from wood and thus create new specific surface area. Meanwhile, the papermaker achieves desired sheet properties through the distribution of specific surface area into bonded areas which contribute to strength and to unbonded areas which scatter light. Along the process from wood to bleached fibre, the chemistry of fibre surfaces is changing. This section will discuss the impact of the aforementioned primary goals on fibre surfaces, as well as some of the opportunities for the modification of fibre surface chemistry.

2.1.5.1 Impact of kraft pulping on fibre surface chemistry

In general, kraft pulping aims to remove as much lignin as possible without harming the carbohydrate portion of the fibre. However, the process also results in significant redistribution of cell wall components as well as chemical modification due to the high process temperatures and highly alkaline conditions. The majority of the work on the chemistry of pulp fibre surfaces has focused on determining surface lignin content with various analytical approaches involving X-ray photoelectron spectroscopy (XPS) also known as electron spectroscopy for

chemical analysis (ESCA). As shown in Table 8, several researchers have documented that the surface lignin content of both unbleached and bleached kraft fibres can be as much as an order of magnitude greater than the bulk concentration [35-39]. However Risen *et al.* have indicated that the various calculations and approaches for XPS determination of surface lignin content have a fairly wide variation [38].

Table 8. Literature values of bulk and surface lignin content

For unbleached kraft pulps as measured by XPS using the O/C ratio method [35-38].

Unbleached Kraft Pulps	Total Lignin Content (%)	Surface Lignin Content (%)
Li and Reeve		
aspen	1.8	28
aspen	4.0	34
aspen	6.4	33
Duchesne *et al.*		
spruce	0.8	12
spruce	3.1	18
spruce	4.7	14
Risen *et al.*		
mixed softwood	4.6	36
mixed hardwood	2.6	30
Laine *et al.*		
pine	4.0	16

Although the middle lamella and primary cell wall are higher in lignin than the other cell wall layers in native wood, the difference observed in kraft pulp fibres is more pronounced. This suggests that either surface lignin is less susceptible to pulping or that dissolved lignin is re-deposited on fibre surfaces. Li and Reeve have confirmed that retained middle lamella is not responsible for the high

surface lignin content [36]. They removed middle lamella material from aspen CTMP fibres with PFI refining and then subjected the fibres to kraft pulping conditions. The results of this work are summarized in Table 9 and clearly show that the surface lignin content is unaffected by middle lamella removal prior to pulping.

Table 9. Surface lignin in kraft pulped aspen CTMP

Li and Reeve's results for untreated and PFI refined CTMP subjected to kraft pulping [36].

Aspen CTMP Fibres	Surface lignin content before pulping (%)	Surface lignin content after pulping (%)
Untreated	43	22
PFI refined	16	23

More recently, researchers have begun to study the carbohydrate components on kraft pulp fibre surfaces. These studies typically involve peeling of fibre surfaces by mechanical [19], chemical [40], or enzymatic [41] means followed by capillary electrophoresis or size exclusion chromatography of the peeled material. In general, the surface layers of chemical pulps are higher in hemicellulose than the rest of the fibre although the differences are typically less dramatic than those seen for lignin. Dahlman *et al.* observed approximately 30% more hemicellulose in the surface material of unbleached kraft pulps relative to the inner material as summarized by Table 10 below [19]. Surface material was removed mechanically and defined as the outer 1% by mass. They also observed that the surface hemicellulose in unbleached kraft pulp had higher average molar mass.

Table 10. Surface hemicellulose content and average molar mass of kraft pulp

Hemicellulose (mass %) and average hemicellulose fraction molar mass in unbleached hardwood and softwood kraft pulps from Dahlman *et al.* [19]

Unbleached kraft pulp	Glucomannan (%)	Xylan (%)	Hemicellulose (%)	M_w (g/mol)	M_n (g/mol)
Hardwood					
Inner layer	1.6	27.0	28.6	15000	12100
Surface layer	1.9	46.3	48.2	19600	15900
Softwood					
Inner layer	8.7	10.8	19.5	15800	11600
Surface layer	9.3	16.4	25.7	20700	14700

Dahlman *et al.* also observed that the surface material of unbleached kraft pulps contained higher levels of 4-O-methylglucuronic acid and hexenuronic acid than the inner material. However, since the difference in uronic acid content was considerably lower than the difference in hemicellulose content, it must mean that the surface hemicellulose contains a lower degree of substitution of uronic acids [19].

2.1.5.2 Impact of bleaching on fibre surface chemistry

Most higher value papers are comprised of bleached pulps. Pulp bleaching typically involves several steps employing a variety of active chemicals to remove lignin and chromophores from pulp. Chlorine dioxide, sodium hydroxide, oxygen, hydrogen peroxide and ozone are the most common chemicals used in bleaching stages. Sodium hypochlorite and chlorine are not used in North America due to the creation of environmentally unfriendly organochlorine compounds. This review will focus on the impact of typical bleaching sequences on softwood kraft fibre surfaces. A more detailed review of pulp bleaching chemistry and technology has been published by Dence and Reeve [42].

Even after bleaching, the surface coverage of lignin is higher than the bulk concentration for kraft pulps. Risen *et al.* found higher levels of lignin on the surface of TCF bleached softwood kraft pulps using three different methods – ESCA, ESCA with mercurization and the mechanical peeling method [38]. All three methods showed higher levels of lignin on the surface and indicated that the initial oxygen delignification stage removed the most surface lignin, while subsequent stages had diminishing impact on both bulk lignin content and surface lignin coverage. Laine *et al.* examined the impact of both ECF and TCF bleaching sequences on surface lignin content. From the data shown in Table 11, he noted a significant drop in surface lignin after the first chlorine dioxide stage in ECF sequences and after the first ozone stage in TCF sequences [43]. Overall the ECF sequences involving oxygen delignification and several chlorine dioxide stages were the most efficient at removing surface lignin with final coverages of 1-3%.

Table 11. Surface and bulk lignin content of bleached softwood pulps.
From Laine *et al.* measured by ESCA using O/C ratio [43].

Bleaching sequence	Total Lignin Content (%)	Surface Lignin Content (%)
Unbleached	4	16
OZEP	0.5	5
OPZEP	0.1	4
ODEDED	0.1	1
DEDED	0.2	3

Dahlman *et al.* also examined the changes in hemicellulose on kraft pulp fibre surfaces after bleaching [19]. They determined that the surface layers retained

higher levels of xylan after ECF bleaching, but that the difference between inner and surface layers had decreased considerably as shown in Table 12. In particular the ECF bleaching sequence drastically diminished the uronic acid content both on the surface and in the bulk.

Table 12. Surface and inner cell wall layer hemicellulose content.

From Dahlman *et al* measured by mechanical peeling and capillary electrophoresis [19].

Kraft pulp	Cellulose (%)	Glucomannan (%)	Xylan (%)	Hexenuronic acid (mmol/kg)
Unbleached				
Inner layer	80.5	8.7	10.8	30
Surface layer	74.3	9.3	16.4	40
Oxygen delignified				
Inner layer	81.7	7.3	10.9	32
Surface layer	76.8	7.8	15.4	38
ECF bleached				
Inner layer	83.6	6.7	10.6	5
Surface layer	81.1	6.2	12.7	<3

Sjoberg *et al* also examined the distribution of hemicellulose in fully bleached dissolving pulps via enzymatic peeling methods [41]. Hardwood and softwood pulps prepared either by sulfite or prehydrolysis kraft pulping all had higher xylan concentrations on the surface particularly the outer 1-5% by mass. They also observed five times higher mannose values in the surface layer compared to the bulk content for the softwood prehydrolysis kraft pulps. Freese *et al.* also examined dissolving pulps using a chemical peeling method involving surface acetylation with acetic anhydride followed by extraction of the acetylated material with dichloromethane [40]. They observed approximately twice as much xylose

and mannose content in the surface layer (5% by mass) of prehydrolysis kraft pulps.

2.2 Fibre-Fibre Bonding and Lignocellulosic Fibre Interfaces

The strength of paper is inherently linked to the ability of pulp fibres to form inter-fibre bonds. Given its importance, it is no surprise that the structure and mechanism of formation of the fibre bond has been a key subject for the paper physics community. An inter-fibre bond can be defined as the area between two fibres sufficiently close such that molecular interactions can occur between the surfaces of the fibres [44]. Several molecular interactions participating in bond formation [45] have been proposed including: hydrogen bonding [46], van der Waals forces [47, 48], and electrostatic interactions [49]. While these interactions may operate under different constraints, they each must be accompanied by two fibre surfaces that are in close proximity, on the order of 2-10 angstroms, to each other.

2.2.1 Importance of Inter-fibre Bonding

The role of bonding in the ultimate strength of paper has been investigated by many researchers but is perhaps best introduced using Page's theory for the tensile strength of paper [50]. Page's theory involves two important premises [50]. The first is that the stress at failure is distributed between fibres that break along the rupture zone and fibres that are pulled out at the rupture zone. If the rupture zone is much smaller than the length of a fibre, then it is assumed that

the force required to cause breakage is equal to the ultimate strength of the fibres themselves. Fibre strength is usually expressed as a function of the zero span tensile strength (Z) while assuming a random sheet (isotropic distribution of fibres). The second major assumption is that the distribution of fibres along the rupture zone that either break or are pulled out is determined by the relative force required to pull out a fibre versus that required to break a fibre. The pull out force can be further broken down into the area of fibre-fibre contact and the shear strength per unit area of contact. These considerations are combined with fibre dimensions to give the Page equation for tensile strength of paper:

$$\frac{1}{T} = \frac{8}{9Z} + \frac{12A}{bPL \cdot (RBA)}$$

Equation 1. Page's equation for the tensile strength of paper

Where *T* is the tensile strength, *Z* is the zero span strength, *A* is the fibre cross-sectional area, *b* is the specific bond shear strength per unit area, *P* is the perimeter of the fibre cross section, *L* is the fibre length and RBA is the relative bonded area of the sheet.

Of the variables in Equation 1, only the fibre dimensions and the fibre strength are relatively easy to obtain and are well defined. The two important remaining variables are the specific bond strength and the relative bonded area, neither of which are well defined or easily measured. Facile determination of the shear strength of single fibre bonds is readily achievable; however it is not a simple problem to quantify the load bearing area over which that shear stress operates.

Researchers have closely examined the structure of fibre bonds in order to determine the relative bonded area to varying degrees of success.

As the sheet consolidates due to the surface tension forces of receding water, fibre surfaces approach one another and various molecular interactions begin to occur as the solids content continues to rise ultimately resulting in the formation of a fibre-fibre joint. The number of bonding interactions and the nature of those interactions determine the efficacy of the bonded area to transfer load between fibres.

2.2.2 Physical Structure of Fibre Bonds

Numerous researchers have collected information and developed theories about the fibre bond based on either the direct observation of individual fibre crossings or inference from various ensemble averaged measurements of paper sheet properties. In tandem, these two strategies have given the paper industry a great deal of practical information regarding the development of fibre bonds in paper.

2.2.2.1 Direct observation of fibre-fibre bond structure

Although direct methods of examining fibre-fibre bonding can be limited by difficult sample preparation and data collection methodology, they provide the most detailed information regarding the actual structure of the fibre bond. Page [51] and co-workers [52-54] employed light microscopy with polarized vertical illumination to examine fibre-fibre bonds in paper sheets and on glass. They

observed areas of optical contact at the fibre-glass interface and for fibre-fibre intersections. Optical contact occurs at an interface where light is no longer scattered between two objects with the same index of refraction and implies a separation of a few or several hundred angstroms. Page and Tydeman [53] observed few or closely spaced interference fringes around optical contact areas suggesting that the entire area was in contact. Page and Sargent [52] calculated the distance between two bonded fibres to be on the order of 150 Å by comparing the intensity of light from the contact zone with that of the first bright interference fringe. Ratliff [55] originally proposed that the distances necessary for optical contact are close enough to generate surface tension forces that should lead to complete physical contact. This idea is shared by several workers [51, 56] including Emerton [57] who presented attractive forces using a cylindrical capillary model from Barkas [58]. Their calculations predicted that the attractive forces due to the surface tension of water could approach 70 atmospheres at a separation of 200 Å.

Electron microscopy has also been used to study the fibre-fibre bond; results of these studies support the observations from conventional optical microscopy. However, the tremendous resolving power of electron microscopy has also allowed researchers to further characterize fibre-fibre bond structure. Asunmaa and Steenberg [59] examined thin sections of fibre-fibre crossings with transmission electron microscopy and observed areas of apparent interfibre contact as large as 100 μm^2 between Norway spruce kraft pulp fibres. They

assumed that fibre material was in contact when no gap was observed in the images obtained using a microscope with a resolution limit of 20 Å. They also observed the presence of fibrillar material within the fibre-fibre bond and noted local interruptions in the contact areas caused by surface morphology. Asunmaa and Schwab [60] later noticed fibrillar bonding and local interruptions in contact areas between aspen holocellulose fibres. Some of these interruptions were approximately 1 μm^2 in area and were often characterized by inter-fibre gaps on the order of 150 nm wide densely filled with bridging microfibrils.

Jayme and Hunger [61] made similar observations based on their electron micrographs of replicas of spruce sulphite pulps. They obtained electron micrographs of replica fibre contact zones that had been torn apart and the former contact zones showed that the resultant raised or broken microfibrils likely to participate in molecular bonding constituted only 10-20% of the total area in optical contact. Page and Sargent [52] observed similar behaviour in micrographs of paper glazed to glass. They also observed raised microfibrils at the apparent contact zones. However, they identified two possible scenarios to interpret this data. In the case of raised microfibrils, these were generated when the product of adhesion to the glass that was stronger than internal cohesion of those microfibrils. They further suggested that some microfibrils could participate in adhesion to the glass substrate but would not be raised if they were more strongly associated to the fibre substrate.

2.2.2.2 Indirect investigations of fibre-fibre bond structure in paper

The more commonly used indirect methods for investigating fibre-fibre bonding are based on two important premises that are also part of Page's original theory described earlier. The first premise is that the overall ultimate strength of the paper sheet can be expressed as a function of two main factors: fibre strength and bonding. The second premise is that the contribution from bonding can be further separated into two important factors: the efficiency of the interfacial fibre-fibre area to transfer load and the relative bonded area. Almost all of the information about bonding derived in this manner is based on the work done by Page [50], Haselton [62], and Ingmanson and Thode [56].

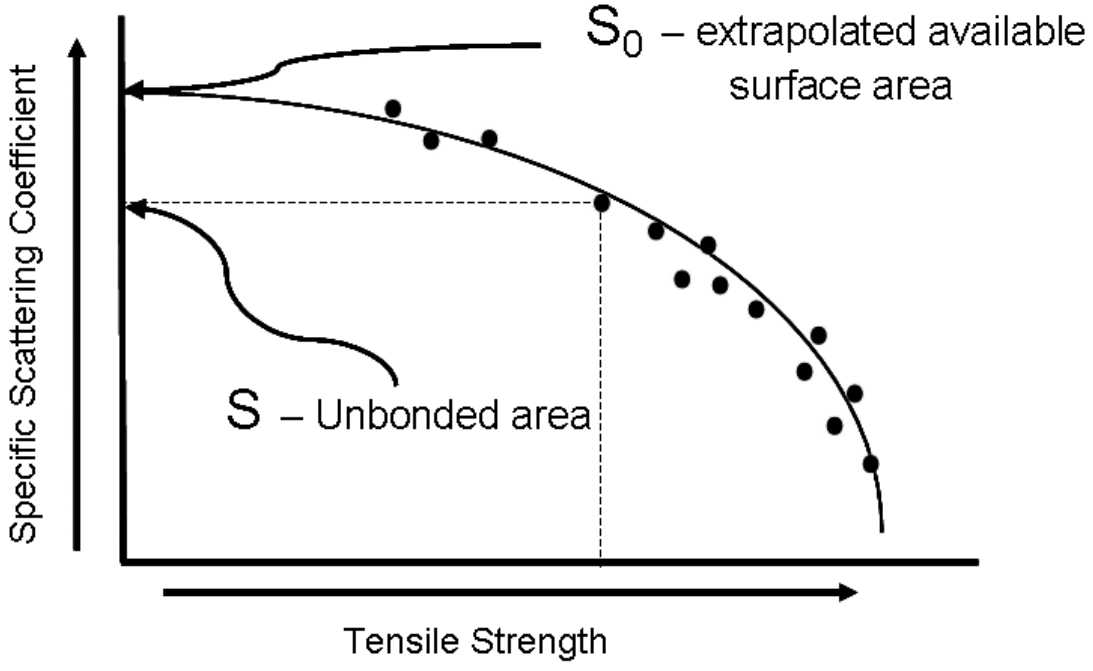

Figure 14. Ingmanson and Thode method of determining RBA in paper

Stylized graph of scattering coefficient versus tensile strength based on [56].

This approach is based on determining the relationship between free specific surface area and tensile strength for a given fibre source followed by extrapolation to zero tensile strength to obtain the relative bonded area as shown in Figure 14.

$$RBA = \frac{(A_0 - A)}{A_0}$$

Equation 2. Equation for relative bonded area estimation

The specific surface area itself can be determined by a variety of methods. Equation 2 is used to calculate the relative bonded area from a curve similar to that in Figure 14, where A_0 is the total available specific surface area and A is the free specific surface area of a partially bonded sheet. One particular problem with this approach as it applies to bonding is that it assumes that whatever method is used to manipulate the relative bonded area does not impact the specific bond strength. It is questionable whether refining, wet pressing or other means of improving relative bonded area do not simultaneously impact the specific bond strength as well.

Much of the prior work has examined the light scattering of paper by applying the Kubelka-Munk theory which allows for the separation of diffuse reflectance into two dependent parameters defined by the absorption and scattering coefficients [63, 64]. The scattering coefficient is related to the free specific surface area from which an approximation of the bonded area of a paper sheet can be derived as shown previously in Figure 14. The Kubelka-Munk treatment for paper optical

properties has been further refined by Scallan and Borch [65-67] using a Stokes layer model which better approximates the morphology of a paper sheet. Scallan developed Equations 3a and 3b for determining the absorption coefficient, *k*; and the scattering coefficient, *s,* in paper:

$$\frac{k}{s} = \frac{(1 - R_\infty)^2}{2R_\infty} \quad \text{(a)}$$

$$s = \frac{1}{W(1/R_\infty - R_\infty)} \ln \frac{(1 - R_0 R_\infty)}{(1 - R_0/R_\infty)} \quad \text{(b)}$$

Equation 3. Scallan-Borch equations (3a and 3b) for determining absorption and scattering coefficients from paper

Where R_∞ is the reflectivity of an optically thick stack of sheets, R_0 is the reflectivity of a single sheet, and W is the basis weight of the sheet in g/m^2.

Many researchers have questioned bonded area results derived from light scattering since scattering efficiency decreases dramatically when small particle surfaces are separated by less than λ/2 (~250 nm) [45, 68]. However, it is unclear at what level the light scattering of a heterogeneous system such as paper is better modeled by particles behaving independently or as a surface. Nordman [69], Haselton [70], and Ebeling [71] have all acknowledged this issue with respect to accurate measurement of free specific surface area of paper using light scattering. These are the same limitations of optical contact as described in the previous section. It has been noted that the correlation between pore size distributions determined by mercury intrusion porosimetry and light

scattering coefficient was greatly aided by the omission of pore sizes less than 200 nm [72, 73]. However, Lehtonen and Dyer also noted that this proved true for the correlation with specific surface areas determined by nitrogen gas adsorption as well and suggested that mercury intrusion porosimetry may lead to degradation of sheet structure due to very high pressures required to force mercury into such small pores [73].

In 1953, Haselton [62] investigated the use of nitrogen gas adsorption and the Brunauer-Emmett-Teller (BET) method to calculate specific surface area in paper and pulp [74]. This approach calculates the free specific surface area of paper based on the adsorption isotherm of a gas. In this case, the method is limited only by the size of the nitrogen molecule which is assumed to have a diameter of 4.5 Å. Since this method does not depend on the use of light scattering, it has been extensively used for the determination of the specific surface area of paper and pulp fibres.

There are a number of concerns about the suitability of the BET method for the analysis of paper surface area and of the accuracy of the results. First of all, there is some question whether the conditions under which BET analysis is performed provides relevant results. These concerns are based on the extensive moisture removal that occurs during sample preparation. Numerous researchers have commented on the importance of water in fibre-fibre bonding [57, 71, 75]. Haselton [70, 76] and Swanson and Steber [77] compared the BET surface areas

with those determined by light scattering for papers in which the relative bonded area was manipulated via beating and wet pressing. Although the experimental BET results do have a linear relationship with specific scattering coefficient they clearly have a non-zero intercept as shown in Figure 15. Haselton addresses this issue on page 110 of his dissertation: "*When the straight line plot is extrapolated to lower scattering and area values, it is seen that it does not pass through the origin*." The lack of agreement between light scattering and BET gas adsorption suggests that there may be a systematic error in one or both measurements.

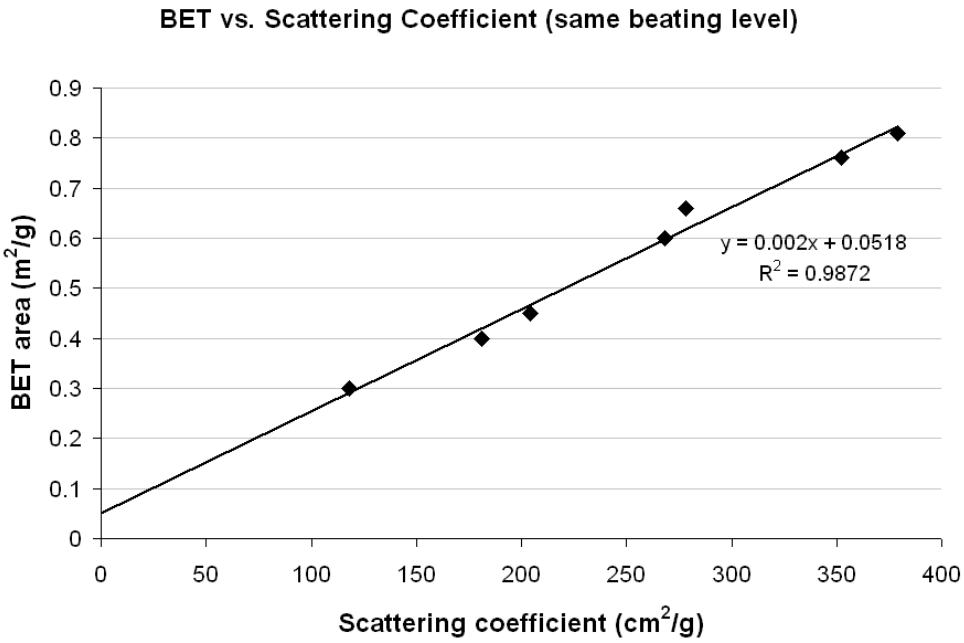

Figure 15. Graph of BET surface area vs. scattering coefficient for paper.
Data from Haselton's thesis [70].

Barber found a number of fundamental problems with the application of gas adsorption isotherms to the measurement of specific surface area or pore size distributions in cellulosics [78]. He observed that cellulose had a low adsorptive

potential and a heterogeneous distribution of surface energy sites. This leads to the formation of multilayers adsorbed gas molecules on the more energetic areas, which results in gross errors in surface area measured by BET. Barber discovered that two thirds of the cellulose surface had a lower adsorptive potential than liquid argon. Thus, after a surface coverage of only 0.3, argon had a higher affinity for liquid argon than it did for the bare cellulose surface. Barber determined that BET surface area measurements were between 2.25 and 3.97 times smaller than the more accurate Ross and Olivier method and that the ratio between the two methods was dependent on the mean adsorptive potential. Dietrich came to the same conclusions using similar methods but found that nitrogen had a slightly higher affinity reaching 0.56 surface coverage before actively forming multilayers [79]. Unfortunately the accuracy of Barber and Dietrich's work is difficult to ascertain as it has not been published in peer-reviewed journals and has not been cited in the literature.

Perhaps more importantly, Ebeling [71] has noted that electron micrographs by Asunmaa and Steenberg [59], Asunmaa and Schwab [60], Davies [80] and Bates [81] suggest that there may be regions in fibre-fibre bonds that are inaccessible to the nitrogen molecule, which Ebeling termed "occluded unbonded surfaces." Such unbonded surfaces would not be detected by BET and depending on the inter-fibre distances may not be probed via light scattering either. An illustrated interpretation of Ebeling's theory is shown in Figure 16.

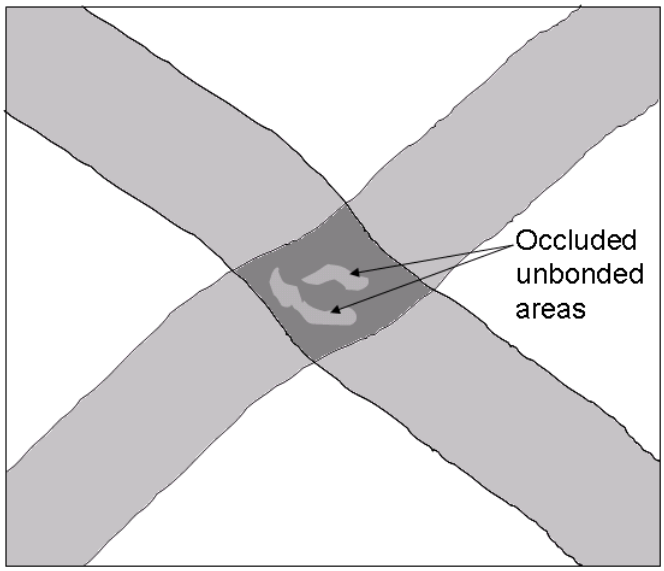

Figure 16. Schematic of a fibre crossing with Ebeling's occluded unbonded areas.

2.2.3 Adhesion and the Cellulosic Fibre Interface

Agreement on an all encompassing working definition of adhesion is difficult to realize given the wide range of materials and particles to which it is commonly applied. However, the cellulosic fibre interface would be described as adhesive in nature under almost any definition. Allen groups the mechanisms of adhesion into five categories: mechanical, adsorptive, chemical, electrostatic and diffusion [82]. In this case, it is logical to consider adhesion as the product of contributions from molecular interactions and mechanical considerations, both of which are likely to contribute to the ultimate strength of the fibre-fibre joint.

2.2.3.1 Contribution of molecular interactions to cellulosic fibre adhesion

Van der Waals forces, hydrogen bonding, and ionic interactions have all been implicated as primary contributors to the development of the fibre-fibre bond.

Given the high concentration of hydroxyl groups in the predominantly carbohydrate fibre wall, it is no surprise that the hydrogen bond was initially the most studied of the molecular interactions with respect to fibre bonding. Recently, researchers have focused on the influence of fibre charge and van der Waals forces on the fibre bond.

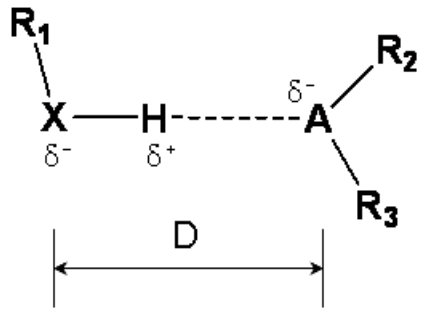

Figure 17. Hydrogen bonding

Hydrogen bonding is a unique molecular interaction that involves a bridging hydrogen atom between two atoms or molecules as shown in Figure 17. The most common hydrogen bonding occurs between atoms with high electronegativity such as nitrogen, oxygen or fluorine. However, weak hydrogen bonds have also been observed in π- systems and even sp^3 hybridized carbon [83]. Hydrogen bonds are approximately 2.2 – 3.2 Å in length measured as the separation between electronegative atoms and have dissociative energies ranging from 1 - 40 kcal/mol [83, 84]. In weak hydrogen bonding (1 – 5 kcal/mol), there is usually a clear distinction between the two bonds involved, where one is covalent in nature and the other is primarily electrostatic [85]. However, stronger hydrogen bonds (15 – 40 kcal/mol) appear to have a large degree of covalent

character whereby the second highly electronegative atom does have orbital overlap with the other two atoms [84, 86].

The importance of hydrogen bonding to interfibre bonding has been explored using a variety of methods. Several researchers have substituted hydroxyl groups on cellulose fibres by esterification with less polar groups [87-89]. Invariably this results in decreased sheet strength with little or no change in fibre strength. Nissan and Sternstein [90] attempted to calculate the contribution of hydrogen bonding to sheet strength from the acetylation data, but their approach has been criticized [71, 91]. Broughton and Wang noted that the polarity of the liquid used to form the sheet dictates the resultant strength of the sheet [92]. They proposed that non-polar liquids interrupted hydrogen bond formation. Although they acknowledged the contribution of surface tension forces, they further noted that soaking a regular handsheet in benzene led to decreased sheet strength and that sheets formed in butanol regained strength upon exposure to high humidity. The importance of water to fibre bonding beyond sheet consolidation is further indirect proof of the significance of hydrogen bonding to fibre bond strength.

Corte *et al* studied the gas-phase deuteration of loose fibre mats and paper via exchange with deuterium oxide and then tracked these changes with IR spectroscopy using the OH/OD stretch as a spectroscopic handle [93]. They calculated 3.8% exchangeable hydroxyl groups in loose fibre mats and only 2.1 -

2.4 % in paper. They then concluded that between 1.4 and 1.7% of hydroxyl groups were involved in hydrogen bonding. Ebeling has challenged the primary assumptions of Corte's work and suggests that the process may be diffusion controlled which would favour the loose fibre mats over the well bonded sheets [71].

Paper researchers have generally ignored the contributions of van der Waals forces to inter fibre bonding. This is likely because the prevailing assumption has been that their contribution must be small in relation to hydrogen bonding despite the fact that they undoubtedly exist in paper. Van der Waals forces are ubiquitous interactions that result from three different forces: Keesom forces which occur between two permanent dipoles; Debye forces which occur between a permanent dipole and an induced dipole; and finally London forces which are the interactions between two instantaneously induced dipoles. Van der Waals forces operate between atoms or molecules separated by less than 1 nm. However, macroscopic objects can be treated as a continuum and thus these forces are additive and can operate over separation distances much larger than 1 nm [94, 95]. Tabor examined mica surfaces and observed significant attractive van der Waals forces occurring at separations of 100 Å or less with retarded van der Waals forces occurring with separations of 100 – 300 Å. Hamaker calculated the distance dependence of these forces between parallel plates using Equation 4:

$$V_{vdW} = -\frac{A}{12\pi L^2}$$

Equation 4. Hamaker equation for van der Waals forces

Where V_{vdW} is the interaction free energy per unit area, A is the Hamaker constant and L is the separation distance [95].

Bergstrom used Lifshitz theory to estimate the Hamaker constant of Langmuir-Blodgett cellulose films using ellipsometry and found that the constants were relatively low in both air and water [96]. They did note the significant drop in water which correlates nicely with the low wet strength of paper. Notley *et al* used colloidal probe atomic force microscopy in a force-distance experiment to measure the interaction between a 13.5 μm radius regenerated cellulose microsphere and a regenerated cellulose film in water [97]. They calculated the Hamaker constant by fitting the Hamaker equation to their force distance data and observed a slightly lower value than Bergstrom's estimates (Table 13). They also observed significant attractive forces at separations less than 200 Å, which is similar behaviour to that observed by Tabor for mica.

Table 13. Estimated Hamaker constants of cellulose

	Hamaker constant (x10^{-21} J)	
	(in water)	(in air)
Bergstrom *et al.*	8.0	58.0
Notley *et al.*	3.5	-

Numerous researchers have observed that increased fibre carboxyl group content leads to improved sheet strength [35, 98]. It is not clear whether this

relationship is due to a change in bulk fibre properties or due to ionic interactions at the fibre surface. It is well known that increased fibre charge leads to increased fibre swelling. Cations associated with carboxyl groups create a concentration gradient between the fibre wall and the surrounding solution, which generates an osmotic pressure that forces water into the cell wall [99-101]. Scallan has posited that the overall swelling is a result of the hydration of macromolecules as well as the delamination of the cell wall [99]. Scallan and Grignon also found that the cationic species had an impact on final sheet properties in the order of $Al^{3+} < H^{+} < Mg^{2+} < Ca^{2+} < Li^{+} < Na^{+}$. Laine *et al* have shown that increasing the total fibre charge of bleached kraft pulps from 45 μeq/g to 125 μeq/g led to a tensile strength increase of approximately 260% [35]. They also found that the increasing fibre charge correlated with increased RBA as measured by light scattering which suggests that swelling is a factor.

Barzyk *et al.* modified bleached kraft pulps with chloroacetic acid and discovered that fibres with higher surface carboxyl group concentrations led to higher specific bond strengths as measured by light scattering [98]. However, Barzyk's surface and bulk treated pulps were prepared by once-drying and solvent exchange drying respectively in order to promote the distribution of acid groups via limiting diffusion. Laine *et al.* took a different approach and treated pulps with high molecular weight carboxymethylcellulose which is believed to be too large to permeate the cell wall thus insuring that the carboxyl groups are on the fibre surface [102]. The bulk treated fibres were prepared much the same way as

Barzyk prepared his bulk treated fibres [103]. They found that the light scattering coefficient dropped just 3% while the tensile index increased by 150% suggesting that the specific bond strength was the primary factor in the increased strength for the surface treated pulps [104]. Meanwhile the bulk treated pulps realized similar strength increases but with a decrease in light scattering of 33% which suggests that the sheet strength increased due to a different mechanism. However, as shown in Table 14 below, the surface charge of the bulk carboxymethylated pulps was similar to that of the surface treated pulps.

Table 14. Effect of bulk and surface carboxymethylation on sheet properties

Data from Laine *et al* for pulps in the Na^+ form [103].

	Total Charge (µeq/g)	Surface Charge (µeq/g)	Light Scattering Coefficient (m^2/kg)	Tensile Index (Nm/g)
Reference	39	3.5	33	22
Bulk treated	220	15	27.5	40
	480	29	21.5	82
Surface treated	51	13	30	56
	60	21	29	69
	74	29	28	76

Although it is not clear how increased fibre charge improves sheet strength, it does appear that there is a difference between enhanced bulk and surface charge. The increased strength of surface modified fibres does appear to increase strength without changing bonded area and thus may involve ionic molecular interactions.

2.2.3.2 Implications of surface material properties on cellulosic fibre adhesion

Too often, fibre-fibre bonds are discussed strictly in terms of molecular interactions. The contributions of surface roughness, mechanical interlocking and diffusion are routinely ignored in the literature; however natural fibre surfaces are highly amenable to these mechanisms due to their structure and surface properties. As mentioned in Section 2.2.2.1, several investigators have directly observed with SEM that the fibre surface is quite irregular. Natural fibres have rough surfaces which are highly fibrillated at several different length scales. Recent observations of the surfaces of natural wood fibres in the wet state with atomic force microscopy indicate that these surfaces are highly fibrillar in nature [105-107]. Several researchers have also observed that these fibrils are extended in solution [107, 108]. Furthermore, microindentation methods have indicated that natural wood fibre surfaces are highly compliant to depths of 200-800 nm into the cell wall [108].

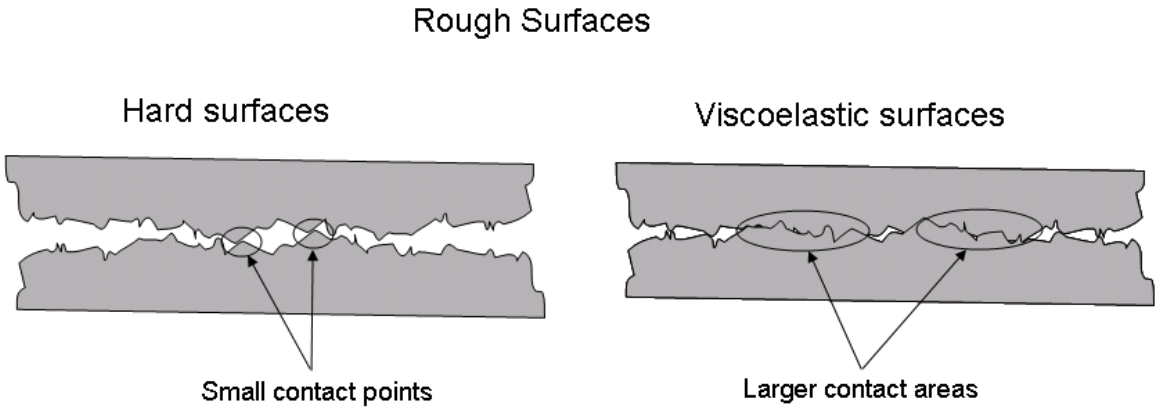

Figure 18. Contact area between hard and viscoelastic rough surfaces

Roughness is not necessarily a positive contributor to adhesion [109, 110]. In fact it often reduces contact area and actually decreases adhesion as shown in Figure 18. However, it is important to note that lignocellulosic fibres are viscoelastic materials, so roughness is not necessarily a problem for adhesion because the surfaces will deform under sufficient load. Furthermore, entanglement of polymer chains, microfibrils and macrofibrils is quite likely and should be expected to be a significant contributor to fibre-fibre bond strength.

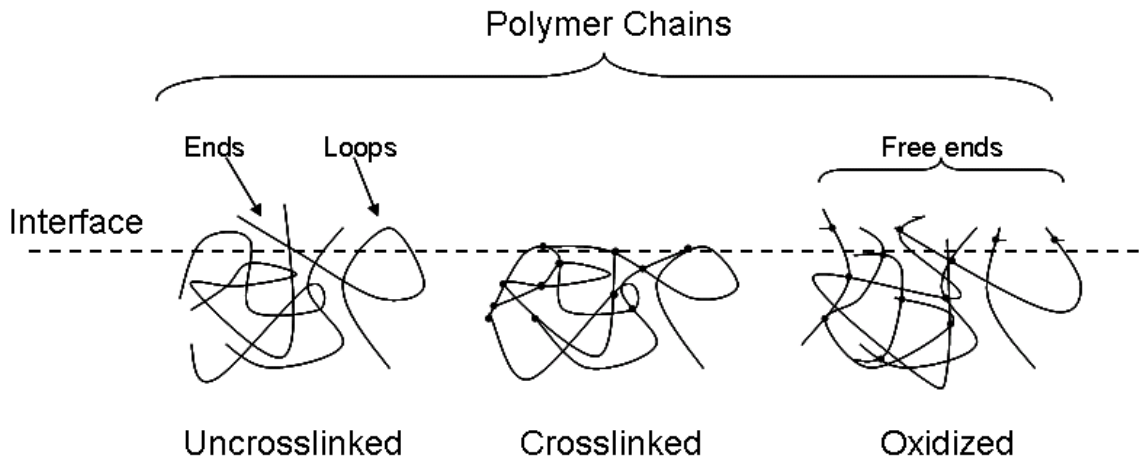

Figure 19. Schematic describing polymer interfaces

For uncrosslinked, crosslinked and oxidized chain scission of polystyrene and polyvinyl benzene chloride interfaces. Adapted from Maeda *et al* [111].

The impact of extended polymer chains and outermost polymer groups on the adhesion of polystyrene (PS) and polyvinyl benzyl chloride (PVBC) has been investigated by Maeda *et al* [111]. They postulated that the interdigitation of short chain segments would increase the number of van der Waals bonds by an order of magnitude and create significant steric barriers to shear forces. Using the surface force apparatus, they observed different adhesion hysteresis

responses based on whether the surfaces were uncrosslinked, crosslinked or degraded via UV chain scission in an oxygen atmosphere. The friction force dropped by two orders of magnitude when the polymer surface was crosslinked and that friction forces also increased as the polymer surfaces were exposed to UV irradiation with oxygen present. Long irradiation times led to adhesion and friction forces several orders of magnitude larger than even the uncrosslinked surface. Load and contact time were also found to be important factors. These results confirmed their interdigitation hypothesis as explained by Figure 19.

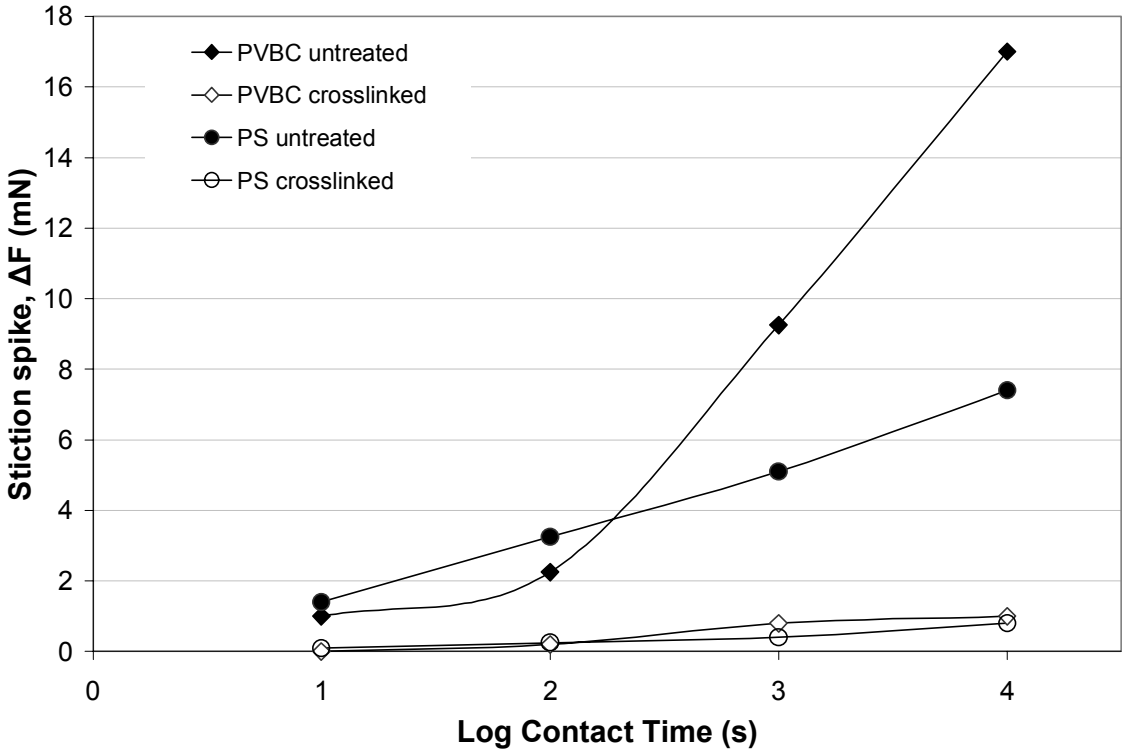

Figure 20. Relationship of friction force and contact time

For PS and PVBC surfaces from Chen *et al* [112].

Later work by Chen *et al.* from the same group had even more pertinent results for cellulosic fibre interfaces [112]. They used the same surface force apparatus set up as described above but this time used different molecular weight polymers

to increase the number of chain ends at the surface as well as the same crosslinking and chain scission protocols. They found increases in adhesion hysteresis as molecular weight went down, and particularly dramatic increase when the molecular weight of PS dropped below 10000 as shown in Figure 21 below. They also observed increased contact area with shorter contact times for the lower molecular weight PS surfaces and found that increased polarity did increase adhesion and friction forces although this was a secondary to the number of chain ends.

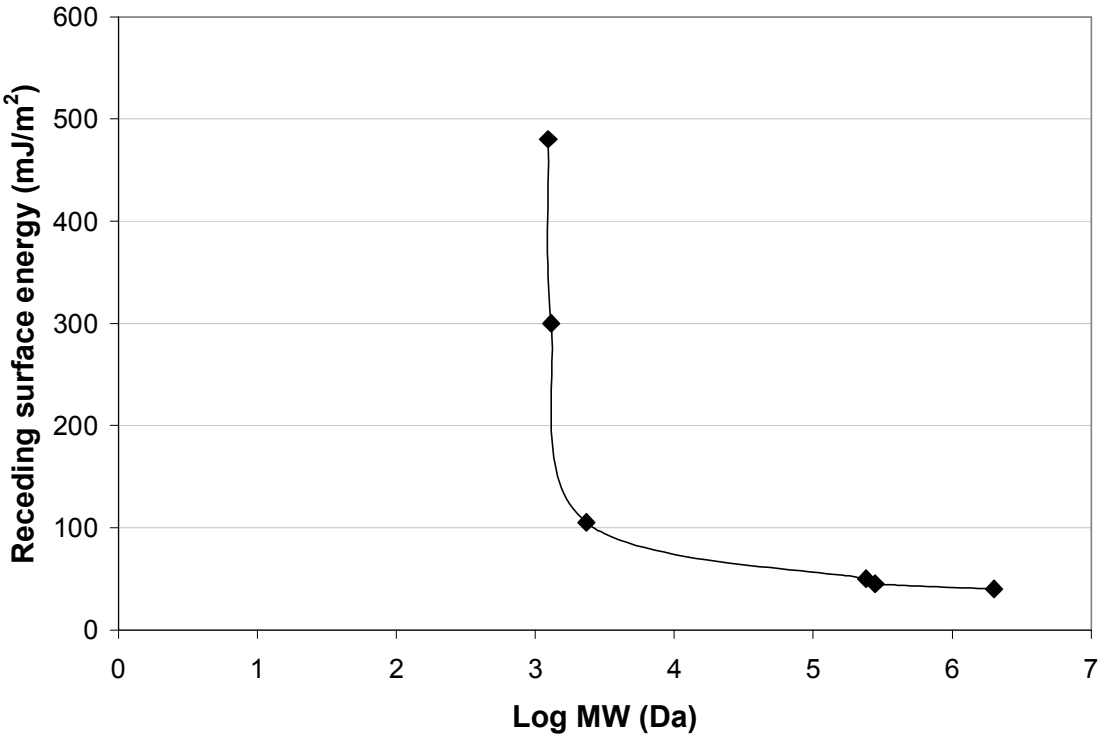

Figure 21. Plot of receding surface energy versus log polymer MW

The total surface energy required to shear PS surfaces from Chen *et al*.[112]

Israelachvili's concept of "interdigitation" with respect to polymer-polymer adhesion is very similar to Voyutskii's diffusion theory of adhesion [113], which has been suggested to contribute to fibre-fibre bonds by McKenzie [75].

Voyutskii identified important factors for the self-diffusion of high polymers, including contact time, pressure, temperature, layer thickness, molecular weight, viscosity and polarity. Voyutskii noted relationships between peeling forces and contact time, temperature, molecular weight and polarity for a variety of polymers that were very similar to the recent work of Israelachvili's group for polystyrene and polyvinyl benzene chloride described earlier.

These studies by Voyutskii and Israelachvili indicate that fibre surface characteristics, particularly at the molecular level, will greatly aid adhesion between cellulosic fibres. Since diffusion and interdigitation appear to be contribution factors, fibre-fibre bonding should respond favourably to lower molecular weight at the surface, higher temperatures, higher pressing loads, increased surface fibrillation, and longer contact times. Furthermore, it also indicates that natural fibres would likely display stronger adhesion than regenerated cellulose fibres because they have more polar surfaces and surfaces composed of lower molecular weight polymers. These considerations likely outweigh the contributions of the various molecular interactions, because these processes dictate the number of molecules capable of participating in such interactions.

2.3 Fluorescence Resonance Energy Transfer (FRET)

2.3.1 General Background on Electronic Spectroscopy

Light energy can be transferred to organic molecules under a process known as absorption. The valence electrons in every molecule have a series of discrete energy levels and are capable of moving from lower energy levels to higher ones if the energy of the quantum of light is equal to the energy spacing between the two levels. Simultaneously, the absorbed light that caused the electronic transition is capable of causing vibrational and rotational transitions. As a result, a great deal of chemical information can be derived from a system based on the electronic, vibrational and rotational transitions caused by its absorption of light.

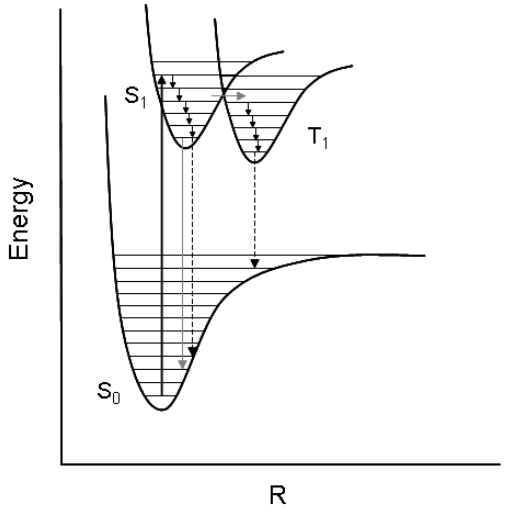

Figure 22: Potential energy surfaces for ground state and first excited state

Adapted from [114].

Figure 22 illustrates potential energy surfaces used to describe the energetic transitions of molecules. In the context of this illustration, electronic transitions can be described as transitions between potential energy surfaces, while

vibrational and rotational transitions occur within a given potential energy surface [115].

Once a molecule is excited to a higher energy level it is not able to remain there indefinitely and must eventually relax back down to its ground electronic state. There are a number of processes by which a molecule is able to relax back down to the ground state after excitation and these are commonly described in the form of a Jablonski diagram shown in Figure 23. It is useful to first make the distinction between radiative and non-radiative transitions; where radiative transitions involve the absorption or emission of light. Non-radiative transitions include vibrational relaxation from higher vibrational states down to the ground vibrational state, and internal conversion which is a collisional process by which energy is dissipated through collisions with other molecules.

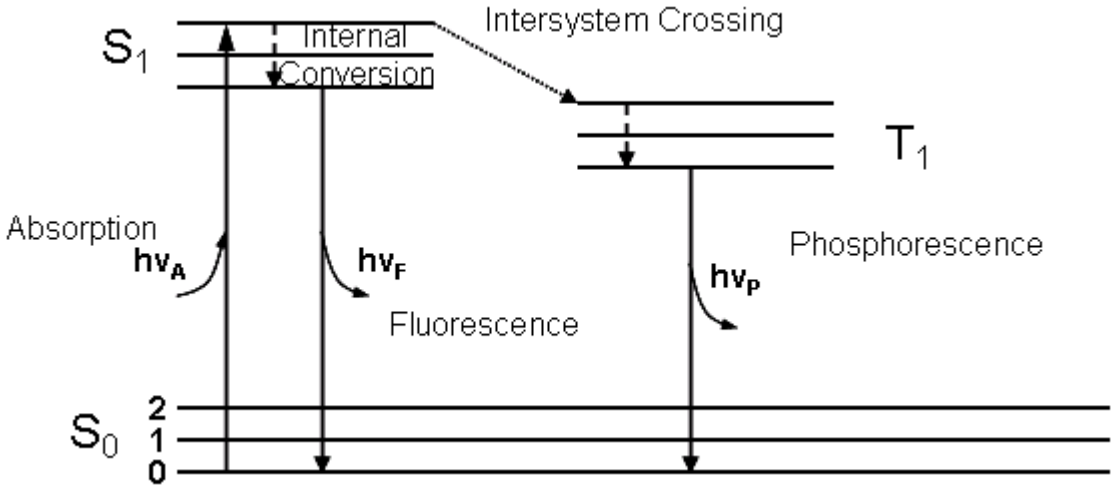

Figure 23: Jablonski diagram for electronic spectroscopy

Illustrating absorption and various relaxation pathways: fluorescence, internal conversion, intersystem crossing and phosphorescence [116].

Another non-radiative transition, known as intersystem crossing, involves the overlap of the excited singlet state and an excited triplet state, in which the electron in question is forced to change its spin. Once in the triplet state, the molecule can then continue to relax back down to the ground state either radiatively in a process known as phosphorescence or non-radiatively in a process similar to internal conversion. It should be noted that intersystem crossing to a triplet state and subsequent relaxation back to the ground state are all spin forbidden processes and thus are considerably slower than spin allowed processes occurring between singlet states. The time scales of these relaxation processes are shown in Table 15.

Table 15. Time scales for processes of relaxation.

From [117].

Process	Transition	Change in spin multiplicity	Time scale (s)
Fluorescence	Radiative $S_1 \rightarrow S_0$	0	10^{-9}
Internal conversion	Collisional $S_1 \rightarrow S_0$	0	$10^{-7} – 10^{-12}$
Vibrational relaxation	Collisional		10^{-14}
Intersystem crossing	$S_1 \rightarrow T_1$	1	$10^{-12} – 10^{-6}$
Phosphorescence	$T_1 \rightarrow S_0$	1	$10^{-7} – 10^{-5}$
Intersystem crossing	$T_1 \rightarrow S_0$	1	$10^{-8} – 10^{-3}$

Fluorescence is a radiative transition in which an electronically excited molecule can relax back down to the ground state with the emission of a photon of light without a change in spin multiplicity. The other processes all compete with fluorescence and the probability of a certain process prevailing is dictated by the

inherent chemical characteristics of the system in question as well as its chemical environment. There are three types of fluorescence possible: Stokes, anti-Stokes and resonance. Stokes fluorescence is the most commonly observed in solution and results in the emission of light with a longer wavelength and thus less energy than the absorbed light. Anti-Stokes fluorescence yields emitted photons with a shorter wavelength than the absorbed light and occurs in rare circumstances in which the ground state molecule has a great deal of vibrational energy or if thermal energy is added to the excited state. Resonance fluorescence is the result of virtually instantaneous re-emission of light of the same wavelength as that absorbed and is highly unlikely in solution.

Fluorescent molecules have two different spectra: excitation and emission spectra. The excitation spectrum is obtained with a fluorometer, by monitoring the emission intensity at a given wavelength while scanning through the spectrum of incident light. The excitation spectrum should be virtually equivalent to the absorption spectrum [118]. The emission spectrum is obtained at a given excitation wavelength while scanning through the spectrum of emitted light and monitoring the emission intensity.

Lastly, there are several useful characteristics of fluorescence spectra that are commonly used for a variety of analytical applications [118]. The first is the Stokes shift, which is the difference between the excitation and emission maxima and indicates the amount of energy dissipated while the molecule is in the

excited state. The equation is below where λ_{ex} is the excitation wavelength maximum and λ_{em} is the emission wavelength maximum.

$$Stokes\ shift = 10^7 \bullet \left(\frac{1}{\lambda_{\mathrm{ex}}}\right) - \left(\frac{1}{\lambda_{em}}\right)$$

Equation 5. Stokes' shift equation

Next is the fluorescence quantum yield, Φ_F, which is defined as the ratio of emitted photons over the total number of absorbed photons. The quantum yield is a measure of the efficiency of a fluorescent system.

$$\Phi_F = \frac{\#\ \text{of photons emitted}}{\text{total}\ \#\ \text{of photons absorbed}}$$

Equation 6. Definition of fluorescence quantum yield

The fluorescence lifetime, τ, is another useful characteristic and it is a measure of the mean time spent by the molecule in the excited state. Equation 7 is shown below where Γ is the radiative rate constant and k is an overall rate constant for all non-radiative processes. As in shown in Table 15, fluorescence lifetimes are on the order of nanoseconds. Delayed fluorescence is a separate possible process that results in a modification of the fluorescence decay into a two component system. If the first excited singlet and first excited triplet are relatively close in energy, it is possible for molecules to undergo intersystem crossing into the triplet state and then return to the singlet state to emit in the same fashion as

normal fluorescence. These singlet states are repopulated thermally and thus the delayed emission should correlate with increased temperature. Delayed fluorescence may also result from triplet-triplet annihilation, in which two excited triplets collide with each other resulting in the emission of a photon from an excited singlet. Both pathways result in a second lifetime peak with a lifetime that may approach microseconds similar to phosphorescence.

$$\tau = \frac{1}{\Gamma + k}$$

Equation 7. Fluorescence lifetime equation

The last major basic characteristic of fluorescence spectroscopy is the relation between fluorescence intensity and concentration. This relationship is highly useful to analytical chemists since fluorescence spectroscopy has superior detection limits compared to absorption spectroscopy. The equation is shown below where Φ is the quantum yield, I_0 is the incident radiant power, ε is the molar absorptivity, b is the path length of the cell and c is the molar concentration.

$$F = \Phi I_0 \left(1 \text{ - } e^{-\varepsilon bc}\right)$$

Equation 8. Relationship between fluorescence and concentration

2.3.2 General Review of FRET

Fluorescence resonance energy transfer (FRET) has been thoroughly studied in synthetic polymer systems [119-122] and many of the principles have been applied to biological macromolecules including proteins [123-125] and DNA [126]. As mentioned previously, the basic premise of the phenomenon involves non-radiative energy transfer from a donor molecule to an acceptor molecule via a long range electrostatic interaction over distances between 10-100 Å. There are several parameters that are necessary for FRET to occur and which dictate the degree to which the energy transfer occurs. Förster used the simplified Equation 9 below to relate the factors that contribute to the Coulombic energy transfer [127].

$$k_{DA} = k\frac{\kappa^2 k_D^o}{R_{DA}^6} J(\varepsilon_A)$$

Equation 9. Förster equation for non-radiative energy transfer

Thus, the rate of energy transfer is dependent on k, a constant dependent on the solvent index of refraction and the concentration. The κ^2 term is known as the orientation factor and takes into account the orientation of the two oscillating dipoles in space. For a random distribution of dipoles, this factor reduces to 2/3. The k_D term is the emissive rate constant of the donor molecule. The R^6 factor is the distance between the donor and acceptor and it has been shown experimentally that the inverse sixth power distance dependence is highly

sensitive. The last important factor is the spectral overlap integral, $J(\varepsilon_A)$, which is the overlap of the donor emission spectrum and the acceptor absorption spectrum [123]. The impact of spectral overlap on FRET has been determined experimentally by Haugland *et al*, whereby the donor and acceptor chromophores were linked to a rigid steroid spacer and the solvent was changed to alter the spectral overlap because the donor emission spectra was dependent on the solvent [128].

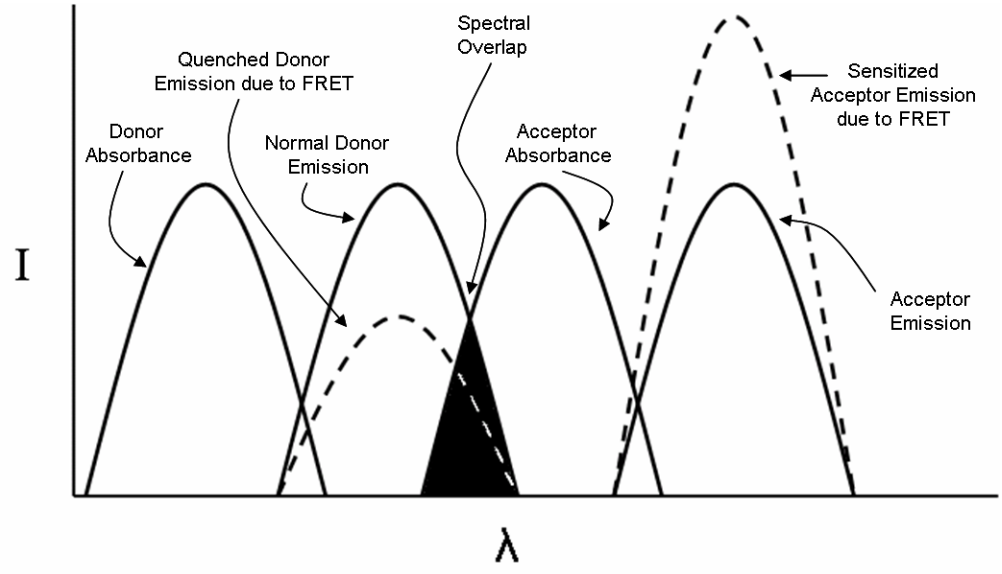

Figure 24. Diagram of characteristic FRET spectra

Donor and acceptor excitation and emission spectra with spectral overlap. Adapted from Herman [129].

The necessary requirement for spectral overlap introduces an interesting problem – so-called 'trivial' energy transfer. Trivial energy transfer is simply a radiative energy transfer that consists of the emission of a photon of light by one molecule followed by absorption of the photon by the acceptor molecule. Clearly, spectral overlap plays a strong role in this process also, which essentially amounts to self-absorption. At high chromophore concentrations, trivial energy

transfer may interfere with FRET, but can be neglected at low concentrations. It can be identified if the emission spectrum varies by changing the path length of the cell [130].

FRET has been used for numerous applications, primarily as a kind of molecular ruler [131]. Labelling of synthetic polymer molecules and biomolecules with known donor-acceptor pairs allows for the measurement of distances between certain groups or binding sites and the measurement of dynamic conformational properties and structural fluctuations of macromolecules in solution [132, 133]. The more specific version of the simplified FRET equation, where the parameters contributing to *k* and the spectral overlap integral, $J(\varepsilon_A) = \int_0^\infty F_D(\nu)\varepsilon_A(\nu)\frac{d\nu}{\nu^4}$ are shown is:

$$k_{D^*\to A} = \frac{9000(\ln 10)\kappa^2\phi_D}{128\pi^5 n^4 N R^6 \tau_D}\int_0^\infty F_D(\nu)\varepsilon_A(\nu)\frac{d\nu}{\nu^4}$$

Equation 10. Alternate version of Förster's equation

If the donor-acceptor pair is well defined, then the Förster distance for the pair, R_0, where energy transfer is one half of maximum is established. This further simplifies to the equation shown below:

$$R_0^6 = \frac{9000(\ln 10)\kappa^2\phi_D}{128\pi^5 n^4 N}\int_0^\infty \frac{F_D(\bar{\nu})\varepsilon_A(\bar{\nu})d\bar{\nu}}{\bar{\nu}^{-4}}d\bar{\nu}$$

Equation 11. Expression for Förster distance

When Equation 11 and 12 are combined you can see that the rate of energy transfer can given by

$$k_{DA} = \frac{1}{\tau_d}\left(\frac{R_0}{r}\right)^6$$

Equation 12. Non-radiative energy transfer rate expressed in terms of Förster distance

A major assumption used in this derivation is that the donor-acceptor distance is fixed and these expressions will not apply to a system with a random distribution of donors and acceptors [116]. A more complex treatment is required for a distribution of distances and in most cases involves an averaging of the transfer rates [133]. For a fixed distance the observed fluorescence decay can be fitted with a single exponential curve and therefore, a more complex system will not have a single exponential dependence. It is also useful to note that the current treatment described here can be used regardless of the fluorescent properties of the acceptor molecule, as emission of the acceptor is not a prerequisite for energy transfer. Thus it can be used to examine situations in which the overall outcome of the process is either radiative or non-radiative.

2.3.3 FRET in Polymers and Interfaces

The distance dependence of FRET is a very useful tool for looking at the microstructure of polymers and interfaces. However investigation of such systems usually requires the labelling of separate molecules with donor and acceptor fluorophores. Essentially this becomes a system that has a single

donor interacting with multiple acceptors. Depending on the structure of the system, the donor will be surrounded by multiple acceptors in two or three dimensions. Furthermore, if the acceptor distribution is assumed to be random, each donor molecules will experience a different spatial distribution of acceptors, thus yielding an ensemble averaged signal. As mentioned in Section 2.3.2, this situation becomes much more difficult to model in rigorous terms.

The situation involving random homogeneous solutions of donor and acceptor molecules has been described [134]. This can be expressed as:

$$\frac{F_{DA}}{F_D} = 1 - \sqrt{\pi}\exp\left(\gamma^2\right)\left[1 - erf\left(\gamma\right)\right] \quad (13a)$$

Where

$$\gamma = \frac{\sqrt{\pi}}{2}\frac{A}{A_0} \quad (13b)$$

Equation 13. Equations for FRET in random homogeneous solutions

In which A is the acceptor concentration and A_0 is the critical acceptor concentration that gives 76% energy transfer and is related to the Förster distance by $A_0 = 447/R_0^3$, where R_0 is in units of angstroms. So A/A_0 is the number of acceptor molecules in a sphere with a radius equal to the Forster distance, R_0. The concentration of acceptors is now important because the donor and acceptor are decoupled. The error function is defined as:

$$erf(\gamma) = \frac{2}{\sqrt{\pi}} \int_0^{\gamma} \exp\left(-x^2\right) dx$$

Equation 14. Error function for FRET in random solutions

Shiah and Morawetz were the first to use FRET to examine self diffusion of polymers [135]. They examined the self diffusion of polyethyl methacrylate (PEMA) and polybutyl methacrylate (PBMA) with steady state FRET via heating lyophilized mixtures of the labelled polymers above their glass transition temperatures to induce diffusion. Recently, Van Drooge *et al.* used a similar approach to examine the distribution of lipophilic drug molecules in solid hydrophilic matrices for the development of controlled drug delivery [136]. Winnik *et al* have employed time resolved measurements of fluorescence resonance energy transfer to study the structure of polymer colloids such as latex for the better part of two decades [119-121, 137, 138].

Pekcan *et al.* studied the development of interpenetrating networks of graft copolymers and homopolymers using covalently linked donors and free acceptors absorbed into one phase of the films [120]. Pekcan *et al.* also examined the coalescence and film formation of polymethyl methacrylate (PMMA) latexes using a similar method [122]. In this case the donor and acceptor were covalently linked to PMMA latex particles in separate batches and then the particles were mixed and heated above the glass transition which led to coalescence and film formation. Since the donor fluorescence decay can be split

into two components: one due to energy transfer and a second exponential term due to normal relaxation pathways, they identified coalescence by the deviation from an exponential fit.

Winnik's group has replicated this methodology combined with Fickian diffusion models to determine apparent diffusion coefficients for several different latex formulations [139-141]. They have also examined the effect of temperature [140, 142], molecular weight [143], moisture [144] and plasticizers [143] on polymer diffusion in latex films. The paper by Feng *et al.* investigating the impact of moisture on polymer diffusion in latexes has interesting implications to the cellulosic fibre bond [144]. They observed that moisture had little impact on hydrophobic polymers such as PMMA or PBMA, but did find that water increased the diffusion by a factor of five for hydrophilic co-polymers of PBMA that included 5 wt% of methacrylic acid. They also discovered that deprotonation of COOH groups with NH_3 or NaOH led to increased diffusion rates in the wet state. Although the polymers investigated are quite different from the natural polymers that comprise a fibre bond, Winnik has demonstrated that FRET is capable of providing information about film formation and the basic concepts of diffusion are likely to hold true at the fibre-fibre interface.

Various other interfacial systems have been studied using FRET that could be considered analogous to the fibre-fibre interface. These include the study of the core-shell interface of environmentally responsive hydrogel particles [145-147],

and phospholipid bilayer membrane interfaces [148-152]. In the case of near planar systems such as lipid membranes, Kuhn developed a mathematical approach for FRET between a donor molecule and a plane of acceptors [153], where the RET rate constant of the donor is:

$$k_t = \frac{\sigma \pi R_0^6}{2\tau_D z^4}$$

Equation 15. Kuhn's model for FRET between a donor and a plane of acceptors

Where σ is the acceptor density (molecules/area), τ_D is the lifetime of the donor in the absence of acceptor and z is the separation between the two planes. The geometry is shown below in Figure 25. Niles *et al* used a variation of this approach to image the interaction between phospholipid vesicles and a planar phospholipid membrane [152]. However, since lipid bilayers usually involve head group labelling, Niles *et al* also had to include the additional distance caused by the thickness of the bilayer because the labels could be on either leaflet of the membrane. Wong and Groves used a very similar approach to image and measure the size of membrane bound proteins at cell-cell junctions. They also labelled lipid membrane head groups and measured the topography of the membrane "blisters" caused by the proteins. This allowed them to measure the size of the proteins directly labelling them.

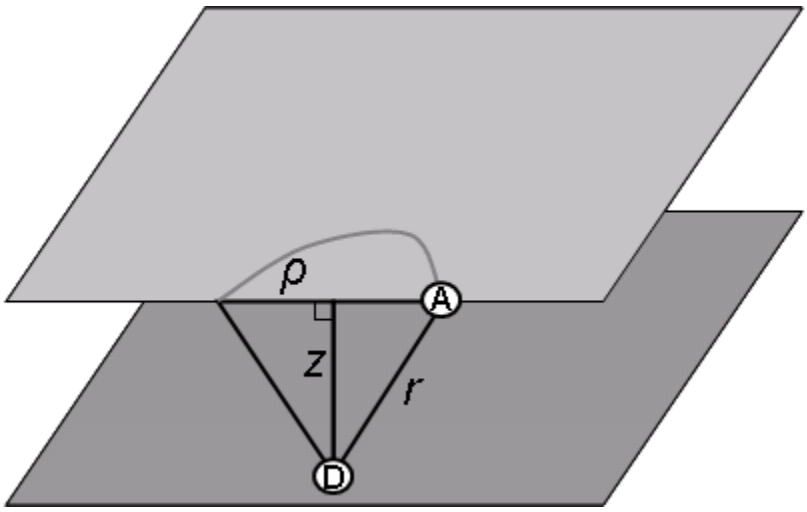

Figure 25. Geometry of FRET between a donor and a plane of acceptors

Where z is the separation between planes, r is the D-A distance and ρ is the in-plane radial coordinate [151, 152].

2.3.4 FRET Imaging

The concepts of FRET are also readily incorporated into imaging experiments. Combining FRET with optical microscopy enables the researcher to investigate processes and structural details far beyond the resolution of the microscope alone. In principle the two are easily coupled; all that is required is an experimental sample containing a FRET pair, a microscope equipped with a strong light source, fluorescence filter sets that match the excitation and emission properties of the FRET pair in use and sensitive CCD cameras for image acquisition. Reflected light (epifluorescence) microscopes, confocal microscopes and fluorescence lifetime imaging microscopes can be setup to execute FRET experiments. Given the relative ease of the adaptation to imaging, it is no surprise that a wide range of applications have been pursued [154].

The most common approach uses epifluorescence microscopes equipped with at least two filter cubes to image steady state FRET [155]. The filter cube contains an excitation bandpass filter, a dichroic mirror and an emission filter (bandpass or longpass). FRET is then calculated based on the ratio of acceptor intensity and donor intensity. This can be achieved either by two-channel detection or by taking two separate images after switching cubes. However, there are a variety of other challenges with this approach beyond the requirements for FRET.

The division of images in the ratio method requires that the two images are projected to the camera with the exact same x-y position. This is called image registered sub-pixel resolution and most thin film interference filter manufacturers are capable of constructing cubes within these tolerances [156]. The ratio method also requires that the intensity observed when the acceptor cube is in place, is only due to acceptor fluorescence. The same holds true for the donor fluorescence. Thus the main issue in steady state FRET imaging is overlapping spectra. Although spectral overlap is a requirement for FRET, too much overlap can cause problems when filters are relied upon for wavelength selection. This problem is commonly referred to in the literature as “cross-talk.” Cross-talk can arise from overlap between donor and acceptor excitation spectra, which results in direct excitation of the acceptor as shown on the left hand side of Figure 26. It can also be an issue when the donor emission spectrum has a long tail that extends into the peak wavelengths of the acceptor emission. There are also

more rare circumstances where acceptor emission appears in the donor emission filter window [157].

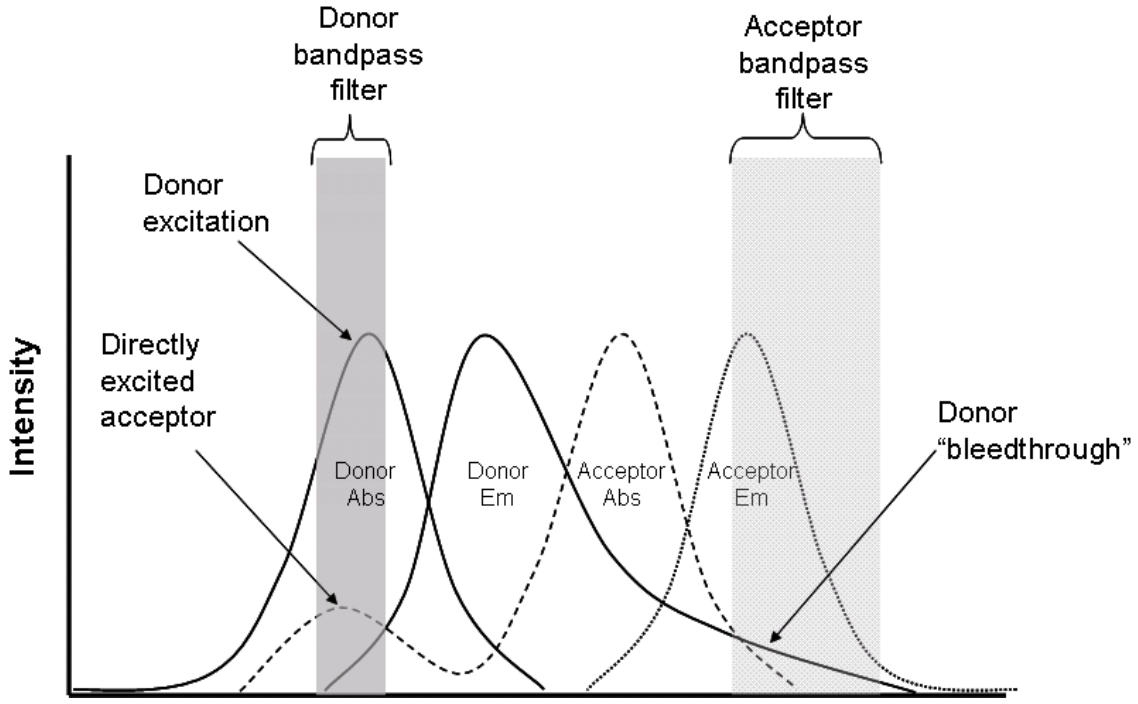

Figure 26. Spectral overlap problems with FRET microscopy

There are a variety of approaches for dealing with the problem of crosstalk between filter sets in FRET microscopy [154, 157-159]. The most thorough treatment of the problem has been by Gordon *et al*. They identified the problem of crosstalk in three filter set FRET microscopy approaches. Where filter sets are labelled D, A and F: the D filter set consists of donor excitation and emission filters; the A filter set has an acceptor excitation and emission filter; and the F filter set has donor excitation and acceptor emission filters. They described the problem with the following basic equations:

$$Df = Dfd + Dfa$$
$$Ff = Ffd + Ffa$$
$$Af = Afd + Afa$$

Equation 16. Terms used in FRETN algorithm

Where the capital letter (D, F, A) refers to the filter set, the second lower case letter refers to the fluorochromes present (f has both donor and acceptor present) in the image, and the third letter refers to the signal coming from one fluorochrome. In the above equations, Dfa, Ffd and Afd are crosstalk terms. Ultimately, Gordon *et al* derived an algorithm to calculate an adjusted FRET value that accounts for all of the crosstalk terms. The system of equations is:

$$\overline{Afa} = \frac{Af - (Ad/Fd)Ff}{1 - (Fa/Aa)(Ad/Fd)}$$

$$FRET1 = \frac{Ff - (Fa/Aa)Df - \overline{Afa}[(Fa/Aa) - (Fd/Dd)(Da/Aa)]}{G[1 - (Da/Fa)(Fd/Dd)]}$$

$$\overline{Dfd} = Df + FRET1[1 - G(Da/Aa)] - \overline{Afa}(Da/Aa)$$

$$FRETN = \frac{FRET1}{\overline{Dfd} \cdot \overline{Afa}}$$

Equation 17. Primary system of equations in FRETN algorithm

Where FRETN is the fully corrected measure of FRET derived from three different images. G is:

$$G = \frac{QY_A}{QY_D}\frac{\phi_A}{\phi_D}\frac{T_F}{T_D}$$

Equation 18. Definition of G in FRETN algorithm

Where: QY is the quantum yield of the donor and acceptor; φ is the fraction of fluorochrome fluorescence transmitted by the respective emission filter; and T is the percent transmission of the respective filter set.

An alternative to elaborate ratio algorithms is to use a method called acceptor photobleaching [148, 155, 160]. Since the occurrence of FRET is characterized by donor quenching, it is possible to calculate FRET by measuring the donor emission signal from a sample labelled with both donor and acceptor dye, before and after photobleaching the acceptor by exposing the sample to the acceptor excitation wavelength. Before photobleaching, the acceptor should quench the donor fluorescence and give a lower donor signal. After photobleaching, the removal of acceptor should result in a higher donor signal. Obviously, this approach can be limited because it can require a considerable amount of time depending on the acceptor's resistance to photobleaching. This approach is often not acceptable for highly fluid systems where fluorescence recovery after photobleaching (FRAP) is relatively rapid.

FRET microscopy has been used to image a wide variety of processes and structures including membranes [150-152], DNA [134], single cells [161], protein binding [159, 160] and many other applications [154]. The aforementioned work

by Wong and Groves (Section 2.3.3) on the topography of phospholipid bilayers is especially relevant to the fibre-fibre bond [150, 151]. Wong and Groves were able to image and identify voids and intimate contact areas between the two bilayers at the nanoscale level, which is very similar to what is needed to elucidate the structure of fibre bonds.

Chapter 3: Problem Analysis and Objectives

The primary goal of this research is to develop a method that provides more information about the structure of cellulosic fibre bonds. Ideally, it would be to develop a method capable of approximating both the actual fibre-fibre contact as well as the relative strength of the fibre-fibre interaction. A summary of the literature reveals that there are three main prerequisites for developing improved methodology for the examination of fibre bonds. These demands should be viewed as opportunities for a novel method to make a significant contribution to the understanding of fibre bonding.

The first critical requirement is that the measurement should be in situ, such that fibre bonds are studied under conditions which are similar to those that exist for common uses of fibre network products. Some of the current methods such as light scattering or standard optical microscopy are capable of meeting this requirement. However, higher resolution methods such as nitrogen gas adsorption and scanning electron microscopy require extensive sample preparation. Scanning electron microscopy or transmission electron microscopy of cellulosic materials requires that the fibres are either first coated with a conductive material prior to imaging or stained with a metal colloid [59, 60, 97, 162, 163]. Furthermore, microtome sectioning of fibre intersections either results in considerable physical alteration of the fibre bond or requires pre-treatment under harsh conditions as described by Nanko *et al* [162]. Nitrogen gas adsorption requires an extensive degassing protocol that results in a very low

moisture content that is not representative of typical ambient conditions [70, 76, 78, 79, 164].

The second critical requirement is that the method should either provide evidence of molecular interactions or yield spatial information about the interface that is on the length scale relevant to molecular interactions. It would be preferable to identify molecular interactions, but a method that is able to determine nanoscale distances between fibre components would be very useful circumstantial evidence that would allow researchers to infer that molecular interactions are occurring. Based on the original work of Tabor [94] and more recent work by Notley *et al* [97] and Bergstrom [96], it seems likely that distances between cellulose surfaces of less than 20 nanometres can result in significant attractive van der Waals forces. Stronger interactions such as hydrogen bonding would place a more stringent requirement of less than 1 nanometre [84]. Thus a technique capable of measuring interfibre distances of 1-20 nanometres would allow reasonable inferences about molecular interactions between fibre bonds.

Current methods such as nitrogen gas adsorption are capable of probing interfaces using the necessary spatial resolution, but are subject to mass transport limitations [71] and Barber and Dietrich have raised questions about their applicability to cellulosics [78, 79]. Most workers agree that light scattering and optical microscopy are not capable of providing sufficient resolution and are

likely further limited by requirements for regular surfaces [45, 52, 53, 69, 71, 165, 166].

The third critical requirement is that any new method of significance should be capable of handling the widely heterogeneous morphology of fibre network structures. Fibre networks, particularly those composed of natural fibres consist of a complex system of voids, free surfaces of varying roughness and interfaces. Thus it is imperative to consider the environment in which fibre bonds are created. Given the variance in natural fibre dimensions, fibre surface structure, and pore size distributions it is likely that any system dependent on a certain geometry is inappropriate.

Given these requirements, the primary hypothesis of this work is that fluorescence resonance energy transfer is an appropriate method for gathering additional information about the structure and development of fibre-fibre interfaces. More specifically, the combination of FRET and epi-fluorescence microscopy should provide a robust technique for imaging cellulosic fibre interfaces in ambient conditions with relatively little perturbation of the surface nanostructure or surface chemistry. It is believed that FRET microscopy is appropriate because it yields a signal that is proportional to intermolecular distance in the length scale of interest. FRET is most commonly employed to study systems in ambient conditions and is not constrained by geometrical or morphological limitations.

The major objectives of this research are as follows:

- Develop a protocol to functionalize cellulosic fibres with a suitable FRET pair.
- Investigate FRET response in fibre mats using steady state fluorescence spectroscopy.
- Develop a method to image fibre-fibre interfaces using FRET microscopy.
- Evaluate the impact of different traditional papermaking process variables on the fibre-fibre interface as probed by FRET.

The methods used to achieve these objectives are described in Chapter 4. Subsequent chapters are written so that they may be read independently of the rest of the document. Chapter 5 describes the protocol developed to dye cellulosic fibres and explores the absorption and emission spectra of fibre sheets. Chapter 6 describes the imaging of natural and regenerated cellulosic fibre interfaces using FRET microscopy. Chapter 7 further explores the changes in natural cellulose fibre interfaces caused by classical papermaking processes. Chapter 8 investigates the development of fibre interfaces as water is removed via drying. Chapter 9 consists of the development of cellulose and xylan model systems as well as FRET microscopy experiments designed to help explain the results observed in Chapters 5-7. Finally, some overall conclusions and recommendations for future work complete the document.

Chapter 4: Materials and Procedures

4.1 Fibres

Natural and regenerated cellulose fibres were employed in this study. Mill produced, never dried white spruce (*Picea glauca*) kraft pulp was provided by Alberta Pacific (Boyle, Alberta, Canada). The pulps were either post-chlorine dioxide stage (D_0) or fully bleached with a OD(E+O+P)DED pulps. The received pulps were screened using a Valley Screen as per TAPPI Standard Method T 278 sp-04 and then washed by diluting 200 oven-dry gram batches with four litres of deionized water followed by dewatering with a Buchner funnel. This process was repeated ten times. The D_0 pulp was further bleached with a DED bleaching sequence in the laboratory and exhaustively washed yielding a final ISO brightness of 90. Viscose staple fibre (39 mm length, 1.2 denier) was supplied by Lenzing AG (Austria). The fibre was manually cut to an average fibre length of 1.9 mm, washed and then air dried before use.

4.2 Chemicals

The two fluorescent dyes used in this work, 7-diethylaminocoumarin-3-carboxylic acid hydrazide (DCCH), and fluorescein-5-thiosemicarbazide (FTSC), were purchased from Invitrogen (Carlsbad, CA, USA) and used without further purification. All other chemicals in this research were purchased from Sigma-Aldrich, VWR, or Fisher Chemicals and used as described below.

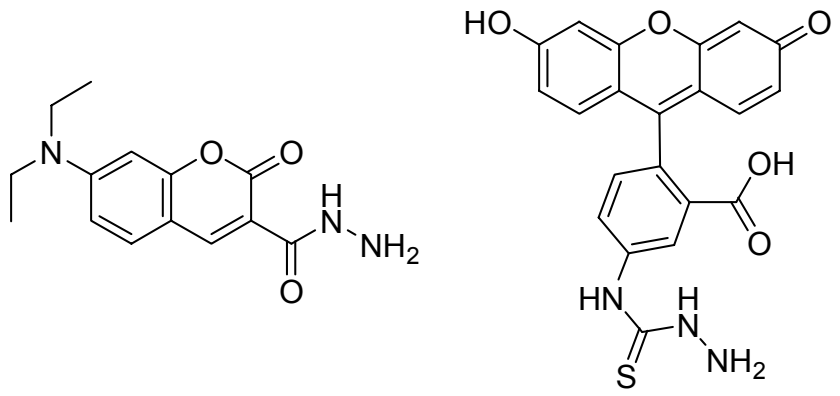

Figure 27. Structures of fluorescent hydrazide dyes

DCCH (left) and FTSC (right).

4.3 Standard Procedures

4.3.1 Laboratory Pulp Refining

All laboratory pulp refining in this work was executed by Rob Lowe using a standard PFI mill following the TAPPI Standard Method T 248 sp-00. Pulps were refined to between 300 and 3000 revolutions using a beating gap of 0.2 mm.

4.3.2 Fibre Quality Analysis and Fibre Coarseness

Fibre length and coarseness was determined using the fiber quality analyzer developed by OpTest Equipment, Inc (Hawkesbury, Ontario, Canada). Procedures described in the operation manual, Fiber Quality Analyzer, Code LDA96 were used to determine average fibre length and coarseness. Average fibre length was determined optically for a dilute fibre suspension (~0.0008% consistency) using a proprietary internal image analysis program. Fibre length is reported in mm as a length weighted average of 5000 fibres and fibre coarseness is reported in mg/100m. Results were considered to be satisfactory if two tests

yield results within 5.0%. If the two samples did not agree, another sample was analyzed until the relative error was within 5.0%.

4.3.3 Fibre Fractionation

Refined pulp samples were fractionated in the Bauer-McNett fibre classifier to remove fines and short fibres. The screens shown in Table 16 were used. The majority of fibres were retained on an R14 screen and this fraction was labelled "medium-long." The medium long fraction was used for all experiments unless otherwise indicated.

Table 16. Table of fibre fractions and corresponding screens used

Fraction	Screen
Long	R12
Medium Long	R14
Medium Short	R28
Short	R35

4.4 Dyeing Cellulosic Materials

The hydrazide dyes were applied to the fibres using a method adapted from Anderson [167]. A 2% suspension of cellulose fibre (oven dry basis) in the appropriate solvent (FTSC: N,N,-dimethylformamide, DCCH: methanol), containing 1.6 mmol/L of dye, and 1.8 mmol/L of HCl was magnetically stirred in the dark overnight at room temperature. The resultant dyed fibres were briefly washed with their respective solvents and then subjected to a mild sodium borohydride reduction (1.3 mmol/L $NaBH_4$). The fibres were briefly rinsed with DMF to remove excess $NaBH_4$. Finally, to assure that only covalently linked dye remained on the fibres; they were Soxhlet extracted with acetonitrile overnight.

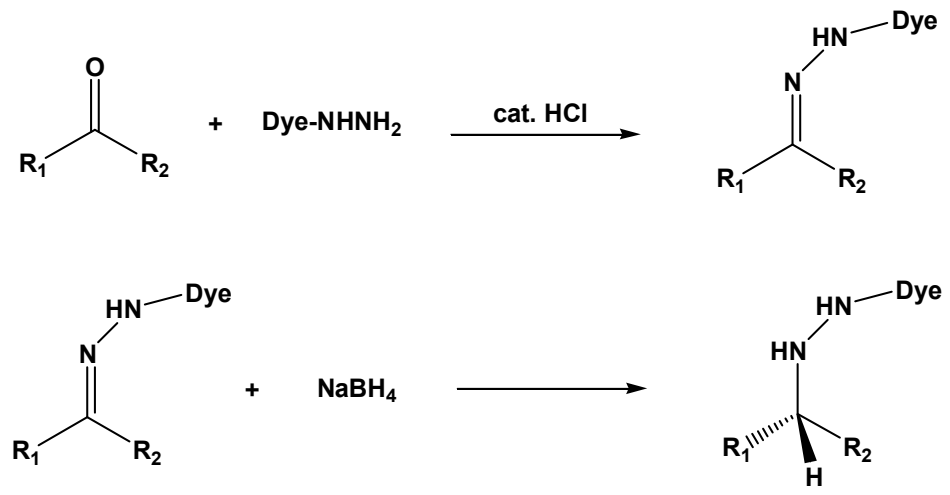

Figure 28. Functionalization of cellulosics with fluorescent hydrazides

4.5 Sample Preparation for Fibre Sheets

Small viscose sheets were prepared from various mixtures of dyed viscose and periodate viscose in a filtration apparatus. The filtration apparatus consisted of a fritted glass disk, filter paper and a polytetrafluoroethylene (PTFE) mesh screen. The fibre mixture was suspended in 300mL of 0.005M sodium tetraborate buffer (pH 9), poured into the filtration apparatus, allowed to calm, and then rapidly dewatered using a vacuum flask attached to a water aspirator. The sheets were formed at pH 9 because the emission properties of fluorescein change dramatically at pH<7 [168]. The wet fibre mat on the PTFE screen was then transferred to blotters and pressed at various pressures using an automated pneumatic press with heated platens at 80°C for six minutes. The sheets were then air-dried overnight in a blotter sandwich prior to testing.

4.6 Time-of-Flight Secondary Ion Mass Spectrometry

Time-of-flight secondary ion mass spectrometry (TOF-SIMS) analysis was performed by James Gibson at Evans PHI (Chanhassan, MN) to verify the coverage and even distribution of dye on the fibre surfaces. Fibre mats were prepared from blank viscose fibres or exhaustively solvent extracted dyed fibres and then were submitted for time-of-flight secondary ion mass spectrometric (TOF-SIMS) analysis. The dyed fibre mats were composed of 100% dyed fibre. Positive and negative ion mode TOF-SIMS data was collected from 350μm X 350μm regions using a Physical Electronics TRIFT III instrument employing a ^{69}Ga LMIG primary ion beam. Nitrogen species were the main focus for determination of dye presence.

4.7 Diffuse Reflectance Spectroscopy

Ultraviolet-visible (UV/vis) absorption spectra were collected using a Perkin-Elmer Lambda 900 UV/vis spectrometer (Perkin Elmer, Waltham, MA, USA) equipped with a PELA-1000 (Labsphere, North Sutton, NH) diffuse reflectance integrating sphere accessory. The accessory includes double beam optics, a six-inch diameter integrating sphere and its own detector. Background corrections were recorded using a pressed PTFE powder disc standard from Labsphere (SRS-99-020). Reflectance data were measured over a low reflectance standard and a high reflectance standard with known reflectance values. An average of three measurements was used to calculate light scattering (s) and absorption (k)

coefficients. The coefficients were calculated in an Excel spreadsheet using Equations 19a-c from Kubelka-Munk and Scallan-Borch theory:

$$k = \frac{s(1-R_\infty)^2}{2R_\infty} \quad (19a)$$

$$s = \frac{1}{g(1/R_\infty - R_\infty)} \ln \frac{(1-R_W R_\infty)(R_\infty - R_{wb})}{(1-R_{wb}R_\infty)(R_\infty - R_W)} \quad (19b)$$

$$\frac{1}{R_\infty} + R_\infty = \frac{(R_{wb} - R_{bb})(1+R_W R_B) - (R_W - R_B)(1+R_{wb}R_{bb})}{R_B R_{wb} - R_W R_{wb}} \quad (19c)$$

Equation 19. Detailed Scallan-Borch equations for paper absorption and scattering coefficients

Where R_∞ is the reflectance of an optically thick sample, k is the absorption coefficient (m^2/kg), s is the scattering coefficient (m^2/kg), R_{wb} is the reflectance of the white background, R_{bb} is the reflectance of the black background, R_W is the reflectance of a single sample sheet over the white background, R_B is the reflectance of a single sample sheet over the black background and g is the sheet basis weight (kg/m^2). Spectra were collected from 400 to 600 nm with a 1 nm step size.

Since wavelength selection in the Lambda 900/PELA-1000 instrument occurs prior to the sample, highly fluorescent samples were prone to overestimated reflectance values. This occurs because the spectrophotometer records the

scattered light as well as the emitted light. Thus Equations 19a-c will result in overestimation of the scattering coefficient and underestimation of the absorption coefficient. This was mediated by placing custom-sized short pass thin film interference filters from Omega Optical (Brattleboro, VT) at the bottom of the sphere in front of the detector as shown in Figure 29. This is a similar approach to that of Mirenda *et al.* [169].

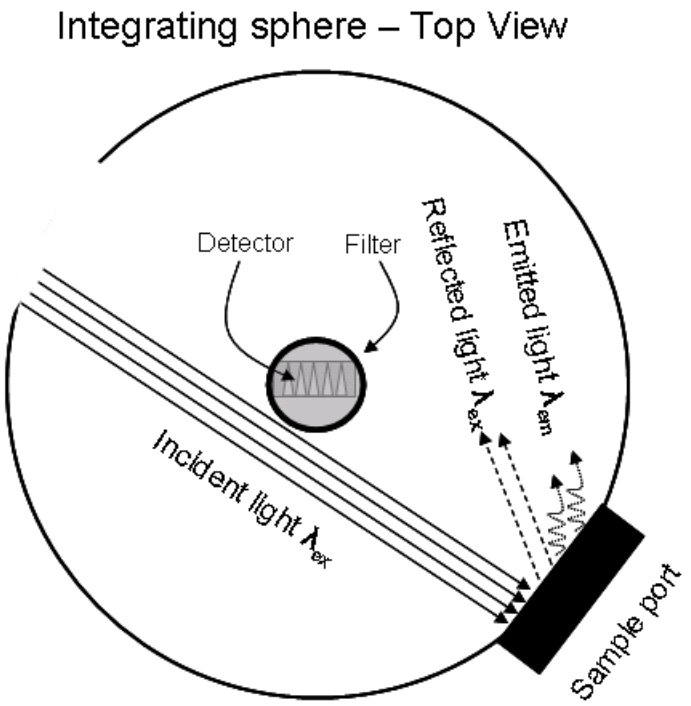

Figure 29. Top view of integrating sphere with fluorescence filter correction

A 460 nm short pass filter was used for samples containing DCCH and a 500 nm short pass filter was used for samples containing FTSC. These filters were carefully lowered down into the integrating sphere and placed on top of the detector port. Background and sample spectra were collected with and without each of the filters. The transmittance profiles of the two filters are shown in Figure 30.

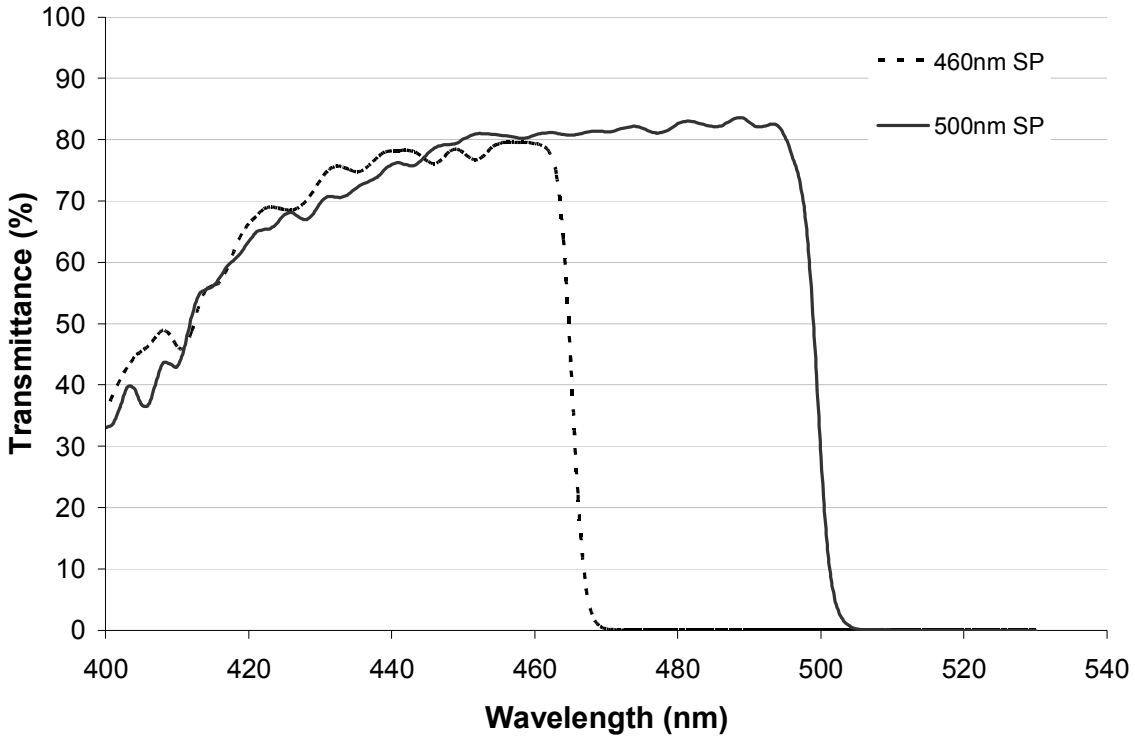

Figure 30. Transmittance profile of custom-sized short pass filters

4.8 Steady State Fluorescence Spectroscopy

Fluorescence spectra were collected under ambient conditions using an ISS PC-1 steady-state fluorescence spectrophotometer equipped with a 300W xenon arc lamp and a R928 PMT (Hamamatsu) photon-counting detector. The excitation and emission monochromator slits were set to achieve 8nm and 4nm spectral bandwidths respectively and the front-face sample holder was set to an angle of 22.5°. Spectra were collected using a step size of 1 nm and a 1 second integration time.

4.9 Sample Preparation for Microscopy

Single fibre samples were prepared according to methodology developed by Lowe *et al* [170] with several modifications. A suspension containing an equal mixture of DCCH and FTSC dyed fibres was prepared by diluting 25 mg of each dyed pulp to 1 L with 0.025 N sodium tetraborate buffer solution. Fluorescein based dyes such as FTSC are pH dependent [168] and therefore, a sodium tetraborate buffer solution (0.025 N) was used to maintain pH 9 during the slide making process. Fibre crossings were prepared by diluting 10 mL of the fibre suspension to 500 mL with deionized water and then draining onto a 34 mm diameter 70 mesh PTFE screen (Spectrum Labs, Rancho Dominguez, USA). The fibres were transferred to glass slides with couching and then wet pressed at different loads between wet blotter papers. Slides were allowed to dry and condition at 50% relative humidity and 23°C. Images were also acquired under these conditions.

4.10 Fluorescence Microscopy for FRET

A Leica inverted reflected light microscope, a 50 watt metal halide lamp, and a Hamamatsu ORCA-ER digital camera were used to acquire 1.0 megapixel images. The microscope was equipped with a fluorescence disc allowing a quick change of the filter sets without disturbing the sample. Exposure time was held constant between filter set changes and varied from 0.15 – 0.5 seconds depending on the initial sample intensity. During image acquisition, fibre crossings were minimally exposed to excitation light to prevent photobleaching.

Each fibre crossing was analyzed by collecting three fluorescence micrographs using three different custom filter sets manufactured by Chroma Technology Corp. (Rockingham, VT). Each custom filter set was designed to capture a distinct signal from the fibre crossing: the donor emission (D), the directly excited acceptor emission (A), and the acceptor emission due to FRET (F). Table 17 describes each filter set and Figures 31-33 show the transmission spectra for each filter set.

Table 17. Excitation and emission specifications for the custom filter sets

Filter Set	Excitation	Emission
Donor	440 ± 5 nm	485±5 nm
Acceptor	500 ± 5 nm	535 nm LP
FRET	440 ± 5 nm	535 nm LP

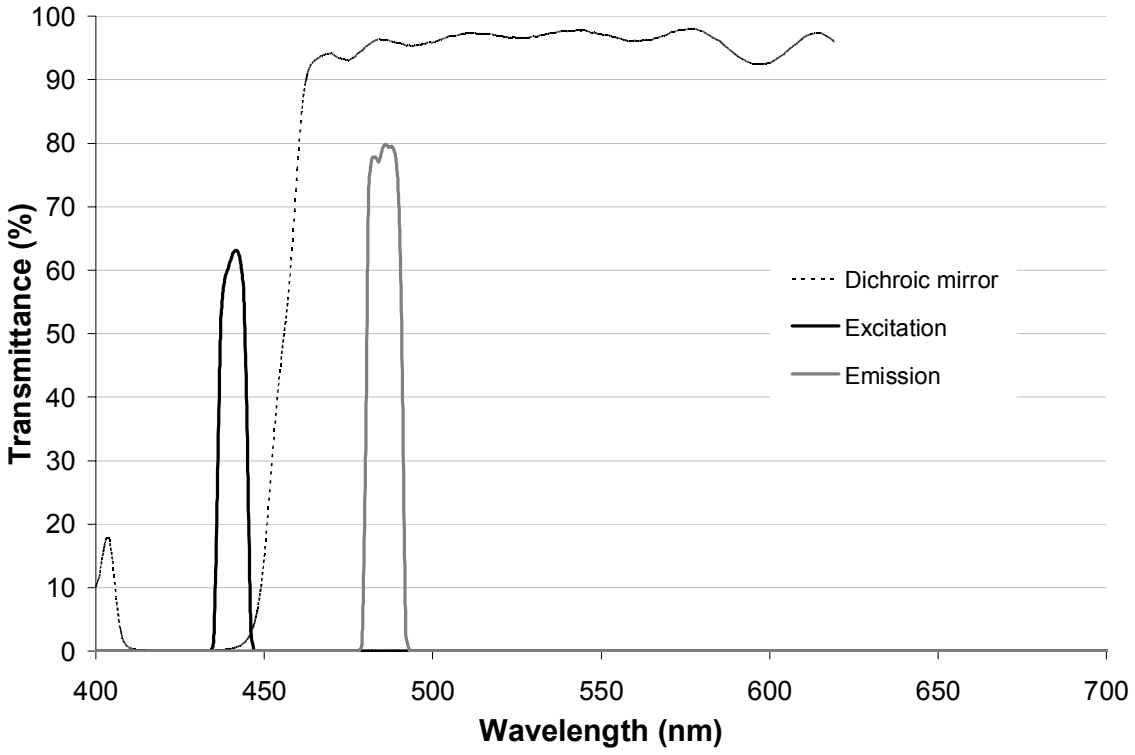

Figure 31. Transmittance specifications for "Donor" filter set

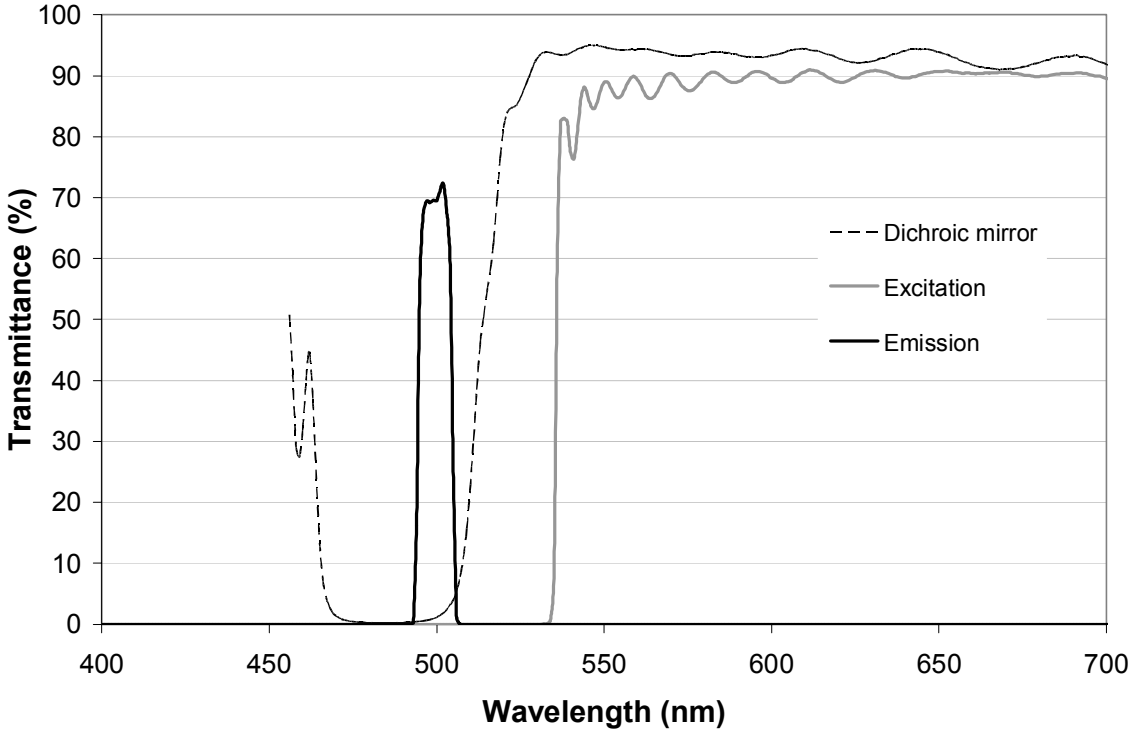

Figure 32. Transmittance specifications for "Acceptor" filter set

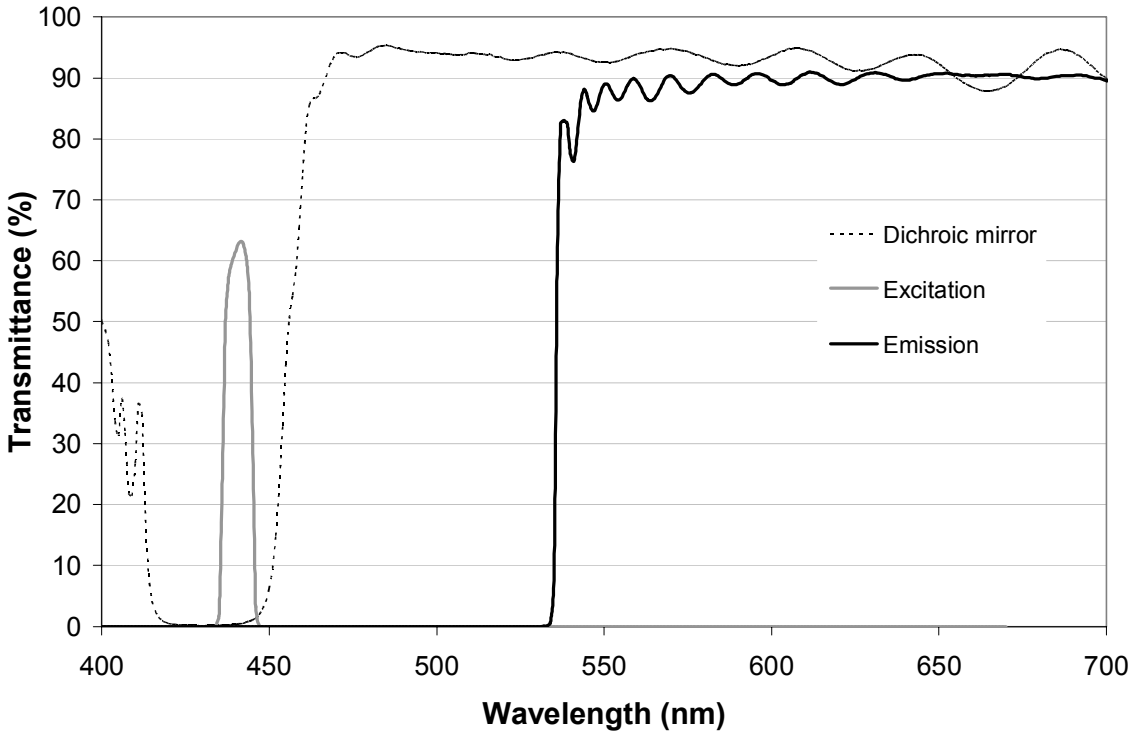

Figure 33. Transmittance specifications for "FRET" filter set

4.11 Image Analysis for FRET Microscopy

The measurement of FRET can be complicated by local dye concentration changes and inefficiencies in the microscope filter sets. The recent FRETN algorithm developed by Gordon [157] was employed in this work to correct the signal at each pixel. Twenty crossings were analyzed for each condition and each fibre crossing was analyzed by the collection of three fluorescence micrographs using three different filter sets. The FRETN correction method described below requires values for samples containing exclusively donor or acceptor dye. That requirement is met by obtaining average gray scale intensities from non-crossing regions on each of the fibres using three filter sets as shown in Figure 34.

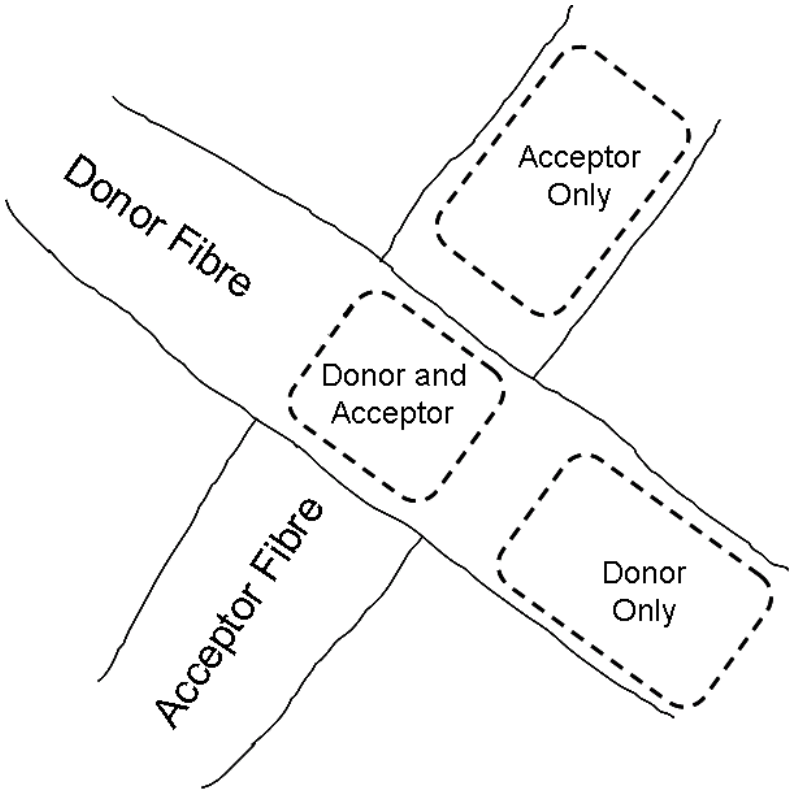

Figure 34. Sketch of a fibre crossing showing regions of interest

Donor only, acceptor only, and both donor and acceptor conditions are measured with each of the three filter sets giving a total of nine values for the analysis. These nine values are then used to calculate the corrected FRETN value at each pixel in the crossing using MATLAB and the MATLAB Image Analysis Toolpak. Equations 20 and 21 below are adapted from Gordon *et al.* and used to calculate FRETN for fibre crossings. The first (capitalized) letter in each term refers to the Filter set employed – FRET, Donor, or Acceptor. The second letter refers to the section of the picture where the value was collected: the acceptor fibre,"a;" the donor fibre, "d;" or the fibre crossing, "x;" For example, "Dx" refers to the signal from the fibre crossing using the donor filter set in the microscope.

$$G = \frac{QY_A}{QY_D}\frac{\phi_A}{\phi_D}\frac{T_F}{T_D}$$

Equation 20. Expression for G used in FRETN algorithm

Where QY_A and QY_D are the quantum yields of the two dyes. Φ_A refers to the fraction of acceptor fluorescence transmitted by the acceptor cube. Φ_D is the fraction for the donor fluorescence transmitted by the donor cube. T_F and T_D are the percent transmissions of the neutral density filters in the FRET and Donor filter sets respectively. Literature values were used for the quantum yields and the other factors were obtained from the filter set spectra given to us by Chroma Technology.

$$\overline{Axa} = \frac{Ax - (Ad/Fd)Fx}{1 - (Fa/Aa)(Ad/Fd)} \quad \text{(21a)}$$

$$FRET1 = \frac{Fx - (Fa/Aa)Dx - \overline{Axa}[(Fa/Aa) - (Fd/Dd)(Da/Aa)]}{G[1 - (Da/Fa)(Fd/Dd)]} \quad (21b)$$

$$\overline{Dxd} = Dx + FRET1[1 - G(Da/Aa)] - \overline{Axa}(Da/Aa) \quad (21c)$$

$$FRETN = \frac{FRET1}{\overline{Dxd} \cdot \overline{Axa}} \quad (21d)$$

Equation 21. Adapted system of equations used for FRETN algorithm

The projected crossing area is calculated planimetrically in MATLAB from each fibre crossing in the reflected light image. This normalization for crossing area is necessary in order to account for the inherent variation in the dimensions of the natural fibres and to provide a basis for the comparison of the two fibre sources.

4.12 Preparation of Dialdehyde Cellulose

In the event that the films derived from microcrystalline cellulose starting material did not yield sufficient fluorescent signal, the cellulose was subjected to periodate oxidation using the method of Varma and Kulkarni [171]. Four grams of Avicel PH-101 (Fluka) was suspended in 45- 60 mL deionized water in a round bottom flask with a magnetic stirbar in a water bath at 45°C. Sodium metaperiodate was dissolved in 15-30 mL deionized water and added dropwise to the cellulose suspension with an addition funnel for 60 minutes. After periodate addition had finished, the reaction mixture was further stirred at 45°C for an additional 2-10 hours. Reaction times ranged from 3-10 hours and periodate charges were between 0.5 and 3 grams. Upon completion, the mixtures were filtered and then

thoroughly washed with approximately one litre of deionized water. The samples were then frozen and lyophilized for 48hrs to remove water.

4.13 Preparation of Cellulosic Trimethylsilyl Derivatives

Trimethylsilylcellulose (TMSC) and Trimethylsilyl dialdehyde cellulose (TMS-DAC) were prepared using a modified procedure from Kontturi *et al.* [172-175]. 0.5 grams of cellulose or dialdehyde cellulose was dissolved in 50 mL of 9% (w/w) lithium chloride (LiCl) in N,N-dimethylacetamide (DMAc) by stirring in a 100 mL three-neck round bottom flask in a water bath at 60°C for 3 hours. This method is modified slightly from McCormick *et al.* dissolution of cellulose in LiCl/DMAc [176]. After the dissolution was complete and the solution was totally clear, the water bath was heated up to 80°C and 20mL of hexamethyldisilazane was added dropwise for 1 hour while flushing with nitrogen gas. The mixture was then allowed to cool for 1 hour and then 10 mL methanol was added to induce precipitation of TMS-DAC which was left overnight. The precipitate was collected by filtration and then purified by dissolving in 20 mL tetrahydrofuran and then filtering that solution into 500 mL of methanol. The re-precipitated dyed TMS-DAC was then collected by filtration and allowed to air dry. The product was fully soluble in toluene at concentrations up to 80 g/L.

4.14 Solvent Casting of Carbohydrate Films

Xylan films were prepared using a modified method from Grondahl *et al.* and Gabrielli *et al.* [177, 178]. Mixtures of 0.23 g dyed xylan, 0.14g undyed xylan and

0.09 g were dissolved in 12 mL of deionized water and 4 mL of pH 11 buffer (prepared from a 1:1 mixture of 0.05 N NaOH and 0.025 M sodium tetraborate decahydrate) by stirring at 95°C for 15 minutes. After cooling for 10 minutes, the solution was poured into 86 mm diameter polystyrene Petri dishes. The films were allowed to dry at 50% relative humidity and 22°C for 24 hours. This gave 75 g/m^2 xylan films containing 20% xylitol as a plasticizer. The films are easily peeled from the polystyrene dishes and handled.

Cellulose films were prepared by dissolving 25 mg of dyed TMS-DAC and 225 mg blank TMSC in 8.0 mL of toluene. This required vigorous shaking and some heating. The solution was then filtered through some cotton wool to remove any dust particles and poured into a 78 mm polytetrafluoroethylene (PTFE) dish. The toluene evaporated in approximately 30 minutes and then the film was peeled from the dish. The films were desilylated by briefly soaking them in 2 N aqueous HCl for 60 seconds followed by repeated rinsing with deionized water and then soaking in 0.025 M sodium tetraborate buffer for 5 minutes followed by air drying at 50% relative humidity and 22°C for 24 hours.

4.15 Preparation of Film Samples for Microscopy

Strips of DCCH or FTSC dyed cellulose and xylan were cut manually with a razor blade and then arranged into crossings on a clean glass slide. The strips were approximately 10 mm long and 0.5 mm in width. Cellulose crossings were then pressed by placing a PTFE screen down on the crossings along with two wet

blotters followed by pressing either with a 15 lb weight (5 psi) or in the automated press with 900 lb load for 5 minutes or 20 minutes. Xylan crossings were pressed under a glass coverslip using the same conditions without any added water. Unfortunately, it was not possible to wet press the xylan crossings because they are nearly water soluble and deform too easily to be handled when wet.

4.16 Solid State CP/MAS ^{13}C NMR Characterization of Carbohydrates

Solid state CP/MAS ^{13}C NMR spectra of carbohydrate samples were recorded by Dr. Yunqiao Pu at room temperature on a Bruker Advance/DMX-400 instrument operating at 100.06 MHz using a MAS WB CP BB VTN-BL 4 mm probe and ZrO_2 rotors. The MAS spin rate was 5 kHz. Acquisition was performed with a CP pulse sequence using 4.5 μs pulse, 2.0 ms contact pulse and 5.0 s delay between repetitions. 8000 scans were accumulated for each sample.

4.17 Fourier Transform Infrared (FTIR) Spectroscopy

Fourier Transform Infrared (FTIR) transmission spectra were collected for each of the carbohydrate samples in the solid state using a Magna-IR System 550 (Nicolet Instrument Corporation). Pellets were formed by pressing mixtures of 3 mg of dry sample and 500 mg of dry spectroscopy grade potassium bromide (KBr) at 15000 psi for 3 min. under vacuum.

4.18 Molecular Weight Distribution Analysis

Molecular weight distributions of cellulose and xylan starting materials were determined by Dr. Yunqiao Pu.

4.18.1 Cellulose

Avicel PH-101 microcrystalline cellulose samples were thoroughly dried over P_2O_5 under vacuum. The dried samples were derivatized with phenyl isocyanate. About 15 mg of dry cellulose sample was soaked in 4 ml anhydrous pyridine in a 25 ml flask, and 0.5 ml phenyl isocyanate was added. The flask was sealed with Teflon-lined cap. The reaction mixture was stirred magnetically in an oil bath at 65 C for 2 ~ 3 days until the cellulose was completely dissolved. After the reaction completed, the solution was cooled and 1 ml methanol was added to consume unreacted phenyl isocyanate. The mixture was then poured into 100 ml water-methanol (3:7). The precipitated cellulose tricarbanilates were purified through centrifuging at 8000 rpm by repeated washing with water-methanol 3 times, and water 2 times. The cellulose tricarbanilates were then freeze-dried and vacuum dried for analysis.

The molecular weight (MW) and molecular weight distribution analysis of the cellulose tricarbanilates was determined using a Hewlett Packard 1090 series HPLC system consisting of in-line filter and an auto-sampler, a UV detector, and three columns of Styragel HR1, HR3 and HR4 (Waters Inc., USA) linked in series. Tetrahydrofuran (THF) was used as the eluent with a flow rate of 0.8

ml/min at room temperature. The system was calibrated with standard narrow polystyrene samples. The cellulose tricarbanilate samples were dissolved in THF (1 mg/ml) and then filtered with a 0.2 µm filter. The filtered sample (10 µl) was injected into the column system with UV detection at 236 nm. Data were collected with Agilent ChemStation Rev. A.10.01 and analyzed with Agilent GPC Add-on Rev. A.02.02 software. The number-average molecular weight (M_n), weight-average molecular weight (M_w) and polydispersity index were calculated by using the same software.

4.18.2 Xylan

Xylan samples were collected and dried over P_2O_5 under vacuum before size exclusion chromatography (SEC) analysis. The SEC analyses were carried out using a Hewlett Packard 1090 series HPLC system consisting of in-line filter and an auto-sampler, a 1047A Hewlett Packard refractive index (RI) detector, and three columns of Ultrahydrogel 120, 250 and 500 (Waters Inc., USA) linked in series. The RI detector was set at 35° C. The eluent was 0.1 M sodium nitrate containing 0.02% sodium azide and the flow rate was 0.5 ml/min. The xylan samples were dissolved in mobile phase (1 mg/ml) and then filtered with a 0.2 µm filter. The filtered sample (10 µl) was injected into the SEC column system for analysis. Pullulan standard samples were used as narrow calibration standards. The RI detector was connected to a Hewlett Packard 35900C Multichannel Interface and the signal was processed utilizing the Agilent ChemStation Rev. A.10.01 and GPC Addon Rev. A.02.02 software.

Chapter 5: FRET in Fibre Networks

5.1 Introduction

The strength of paper is inherently linked to the ability of pulp fibers to form inter-fibre bonds. A fibre-fibre bond can be defined as an area between two fibers sufficiently close such that molecular interactions can occur between the surfaces of the fibers. Several mechanisms for fibre-fibre bond formation have been proposed; the most generally accepted being hydrogen bonding. While there is evidence that some other types of molecular interactions may help account for fibre-fibre bonding, all these mechanisms must be accompanied by two fibre surfaces within very close proximity of one another (on the order of 1-10 nm) [75, 166]. As the fibre surfaces approach one another, molecular interactions begin to occur and the fibre-fibre bond forms. Ultimately, the bonding density and the nature of the bonding interaction determine the efficacy of the bonded area to transfer load between fibers. This dictates end product quality in terms of paper optical and strength properties.

A method capable of measuring inter-fibre distances *in situ* at the length scale relevant to the aforementioned molecular interactions is necessary to advance the understanding of the contribution of bonding to the material properties of fibre network structures. Fluorescence resonance energy transfer presents a unique opportunity to achieve these results since it is a distance dependent phenomenon that operates over the 1-10 nm length scale that is desired to evaluate bonded areas in paper [123, 127]. Although FRET is typically used in

biological systems for the measurement of macromolecular dynamics [123-125, 134], it has also been applied in the study of the structures of solid state systems including core-shell microgels [145, 146], latexes [119, 121, 122], and phospholipid bilayers [150-152].

The application of FRET to the study of interfibre bonding naturally requires the labelling of cellulosic fibres with a suitable FRET pair. Fluorescent labelling of cellulosic fibres has been pursued to meet a variety of objectives in pulp and paper. Liu *et al.* developed a method to stain pulp fibres with the fluorescent dye acridine orange in order to quantify lignin content and visualize its distribution [179]. Acridine orange appears to preferentially associate with lignin thus providing a possible means for lignin quantification. Li and Reeve were able to confirm these results and use confocal laser scanning microscopy to image lignin distribution across the fibre wall [180]. Mathews *et al.* used similar methodology and non-covalent attachment for the estimation of fibre charge [181]. Although interesting, these methods were complicated by excimer or ground state dimer emitting species and did not employ robust attachment methods.

A covalent approach is preferred for FRET, since dye migration would negatively impact the results. Zhu *et al.* used fluorescence to detect ortho-quinones in lignin containing pulps by making use of the reaction between ortho-quinones and ortho-phenylenediamine to yield fluorescent phenazines. Rohrling *et al.* used hydroxylamine derivatives of carbazole for the determination of carbonyl groups

in cellulosics [182-185]. The reaction of amine containing compounds such as hydrazides and hydroxylamines with various carbonyl compounds is well known [167, 186-188]. Rohrling's approach is of particular interest since carbonyls are present in trace levels in cellulose, lignin and hemicellulose. This would allow for significant fluorescent dye concentrations (10 – 40 µmol/g) while not allowing over-labelling that could significantly impact surface properties.

5.2 Materials and Methods

5.2.1. Fibres

Viscose staple fibre was donated by Lenzing Austria and used as the model cellulose fibre system. The original fibres were 39mm in length and 1.2 denier (1.2 g/9000 m length) but were manually cut to approximately 2 mm in length, washed with deionized water and air-dried prior to use. The viscose was then subjected to a mild periodate oxidation using a ratio of 1.7mmol $NaIO_4$/g viscose in water with stirring in the dark at 38°C for one hour. The periodate-oxidized fibres were thoroughly washed with deionized water and air dried. The periodate oxidation forms carbonyls via the oxidative cleavage of the C_2-C_3 carbon-carbon bond forming the dialdehyde as shown in Figure 35 and was necessary to ensure that the dye loading was significant. The spruce fibre is a never dried bleached white spruce (*Picea glauca*) kraft pulp obtained from Alberta Pacific (Canada). The pulp was lab bleached with chlorine dioxide and fully washed prior to dyeing. The fibre properties were determined using an OpTest Fibre Quality Analyzer. The average fibre length was determined to be 2.5 - 3.0 mm.

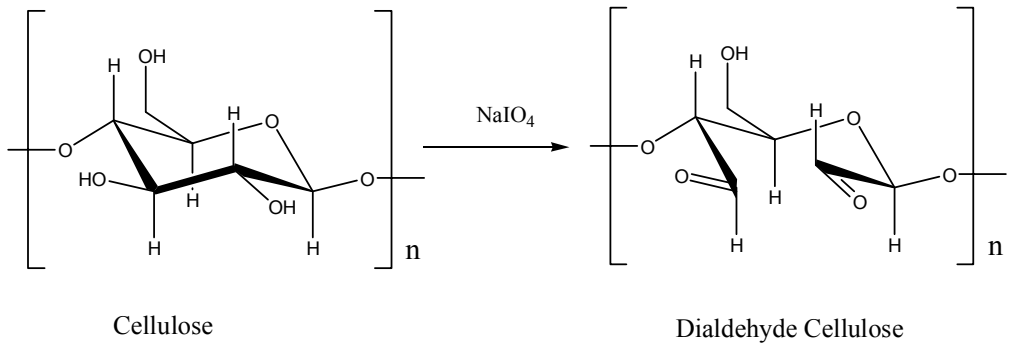

Figure 35. Mild periodate oxidation of cellulose to dialdehyde cellulose

The two fluorescent dyes shown in Figure 36, 7-diethylaminocoumarin-3-carboxylic acid hydrazide (DCCH) and fluorescein-5-thiosemicarbazide (FTSC) were purchased from Invitrogen (Carlsbad, USA) and used as received. These hydrazide derivatives react with carbonyls to form hydrazone linkages as shown in Figure 37. The hydrazide dyes were applied to the fibres using a method adapted from Anderson [167]. A suspension of 0.25 g of air dried fibre in 10mL solvent (DCCH:methanol, FTSC:*N*,*N*,-dimethylformamide) was magnetically stirred overnight in the dark at room temperature in the presence of 25 µmol of dye and 27.5 µmol of aqueous HCl. The resultant dyed fibres were washed thoroughly with water followed by exhaustive washing with hot DMF (90°C) to remove excess dye and finally soxhlet extracted with acetonitrile to remove any trace dye.

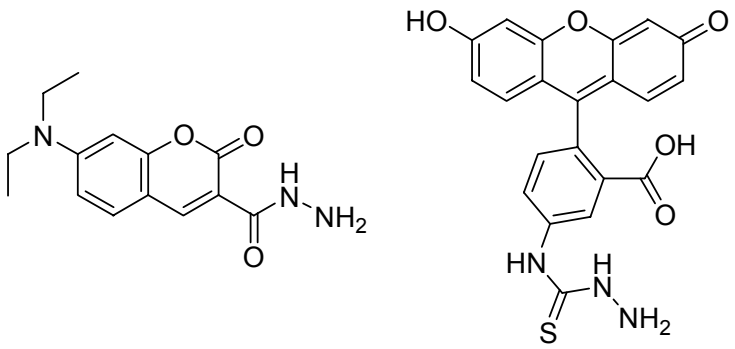

Figure 36. Chemical structures of DCCH (donor) and FTSC (acceptor) dyes

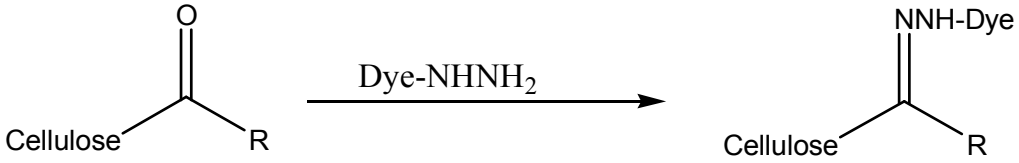

Figure 37. Chemistry for coupling dye hydrazides to cellulose carbonyls via hydrazone linkages

5.2.2. Preparation of Small Fibre Sheets

In order to examine the spectral properties of the resultant fibres it was necessary to form small sheets. Small 34 mm diameter viscose or white spruce sheets were prepared from various mixtures of dyed fibre and blank fibre in a filtration apparatus. The filtration apparatus consisted of a fritted glass disk, filter paper and a polytetrafluoroethylene (PTFE) mesh screen. The fibre mixture was suspended in 300mL of 0.005M sodium tetraborate buffer (pH 9), poured into the filtration apparatus, and then rapidly dewatered using a vacuum flask attached to a water aspirator. The sheets were formed at pH 9 because the emission properties of fluorescein change dramatically at pH<7 [168]. The wet fibre mat

on the PTFE screen was then transferred to blotters and pressed at various pressures using an automated press. White spruce sheets were pressed at ambient temperature but viscose sheets were pressed using heated platens at 80°C for 6min. The sheets were then air-dried overnight in a blotter sandwich prior to testing.

5.2.3. Time of Flight Secondary Ion Mass Spectrometry

Time-of-flight secondary ion mass spectrometry (TOF-SIMS) analysis was performed by Evans PHI (Chanhassan, MN) to verify the coverage and even distribution of dye on the fibre surfaces. Viscose fibre mats were prepared from exhaustively solvent extracted dyed fibres and then submitted for time-of-flight secondary ion mass spectrometric (TOF-SIMS) analysis. Positive and negative ion mode TOF-SIMS data was collected from 350µm X 350µm regions using a Physical Electronics TRIFT III instrument employing a ^{69}Ga LMIG primary ion beam.

5.2.4. UV/Vis Spectra of Fibre Mats

Ultraviolet-visible (UV/vis) absorption spectra were collected using a Perkin-Elmer Lambda 900 UV/vis spectrometer (Perkin Elmer, Waltham, MA, USA) equipped with a PELA-1000 (Labsphere, North Sutton, NH) diffuse reflectance integrating sphere accessory. The accessory includes double beam optics, a six-inch diameter integrating sphere and its own detector. Background corrections were recorded using a pressed PTFE powder disc standard from Labsphere

(SRS-99-020). Reflectance data were measured over a low reflectance standard and a high reflectance standard with known reflectance values. An average of three measurements was used to calculate light scattering (s) and absorption (k) coefficients. The coefficients were calculated in an Excel spreadsheet using the Equations 19a-19c from Kubelka-Munk and Scallan-Borch theory:

Since wavelength selection in the Lambda 900/PELA-1000 instrument is before the sample, highly fluorescent samples were prone to overestimated reflectance values. This occurs because the spectrophotometer records the scattered light as well as the emitted light. This was mediated by placing custom-sized short pass thin film interference filters from Omega Optical (Brattleboro, VT) at the bottom of the sphere in front of the detector. This is a similar approach to that of Mirenda *et al* [169]. A 460 nm short pass filter was used for samples containing DCCH and a 500 nm short pass filter was used for samples containing FTSC. These filters were carefully lowered down into the integrating sphere and placed on top of the detector port. Spectra were collected using the same backgrounds as described above.

5.2.5. Steady State Fluorescence Spectroscopy

Fluorescence spectra of the viscose sheets were collected under ambient conditions using an ISS PC-1 steady-state fluorescence spectrophotometer equipped with a 300W xenon arc lamp, a Hamamatsu R928 PMT photon-counting detector, and a front face sample detector. The excitation and emission

monochromator slits were set to achieve 8nm and 4nm spectral bandwidths respectively and the front-face sample holder was set to an angle of 22.5°. Spectra were collected using a step size of 1 nm and a 1 second integration time. It was determined that 60 g/m^2 basis weights and 11% dyed fibre yielded a strong fluorescent signal.

5.3 Results and Discussion

Two fundamental decisions regarding the linking chemistry and the identity of the dyes were required before the project could commence. Ultimately, further work using fluorescence microscopy is the primary aim of this thesis, so the decision was made to attempt to match the spectral properties of the dyes with the optimal light flux of the Leica microscope 50W metal halide light source and the peak photon counting sensitivity of the Hamamatsu CCD camera in our current microscopy apparatus. Since the majority of this work will be executed on this instrument, this approach will yield maximum fluorescent signal and provide the best opportunity for success.

The X-Cite metal halide light source has continuous emission intensity in the 300-600 nm region of the electromagnetic spectrum with distinct maxima at 320, 370, 410, 450 and 550 nm. The 400-450 nm section of the lamp output has particularly good intensity and thus the donor dye should have its absorption maximum in this region. The Hamamatsu ORCA-ER CCD camera coupled to the microscope has peak sensitivity (quantum efficiency) at approximately 525 nm.

With these spectral parameters defined, 7-diethylaminocoumarin and fluorescein were chosen as the donor and acceptor fluorophores respectively. These two dyes illustrated in Figure 38 below are readily acquired commercially and have been used as a FRET pair on several occasions in the literature [126, 189-191]. The coumarin derivative has an absorption maximum at 440 nm and fluorescein has its emission maximum at 510 nm. Thus their spectral properties match with the constraints imposed by the instrument.

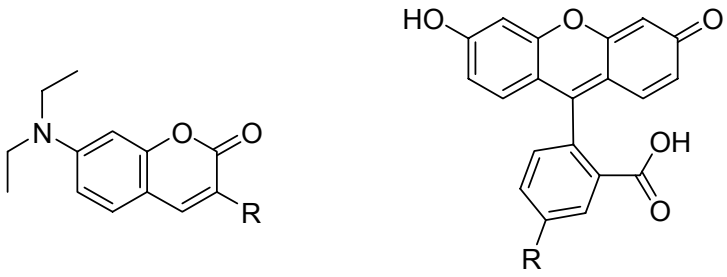

Figure 38. Structures of basic 7-diethylaminocoumarin and fluorescein

The next major question was how to covalently attach the dyes to a cellulosic substrate. Due to the sensitive distance dependence of FRET, it is critical for the dye molecules to be fixed in place on the fibre surface with a covalent bond. This would ensure that dye molecules would be unable to migrate during sheet formation or pressing. Since most carbohydrate chemical functionalities are relatively chemically inert under mild conditions, the decision was made to make use of cellulose carbonyl groups for the linkage. This decision was made easier by the fact that hydrazide derivatives of the two preferred fluorescent dyes are commercially available from Molecular Probes.

Soxhlet extraction with acetonitrile was expected to remove non-specifically bound dye. Fluorescence spectroscopy of the filtrate showed almost no fluorescence from either FTSC or DCCH dyes. However, it was determined that it would be useful to be able to identify the covalent linkage in some manner. This is a difficult problem since the total dye content on the fibre was at trace levels. FTIR spectra of KBr pellets containing blank viscose or DCCH dyed viscose showed no significant differences. It was decided to submit the samples for Time of Flight Secondary Ion Mass Spectrometry (TOF-SIMS) in the hope that some mass fragments containing the hydrazide linkage would remain intact.

There are several interesting results from the TOF-SIMS analysis of the viscose fibres. First of all, it was not possible to generate an identifiable parent ion of either dye that included the hydrazide linkage. The positive ion mode did manage to generate a carbonyl fragment of the DCCH dye with the structure shown in Figure 39. The mass spectra are shown in Figure 40.

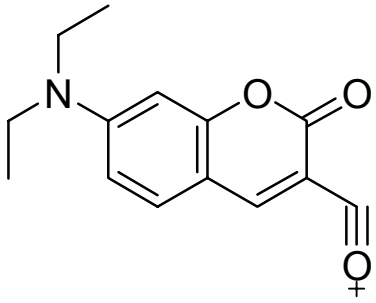

Figure 39. Proposed structure of DCCH fragment ion with 244 m/z

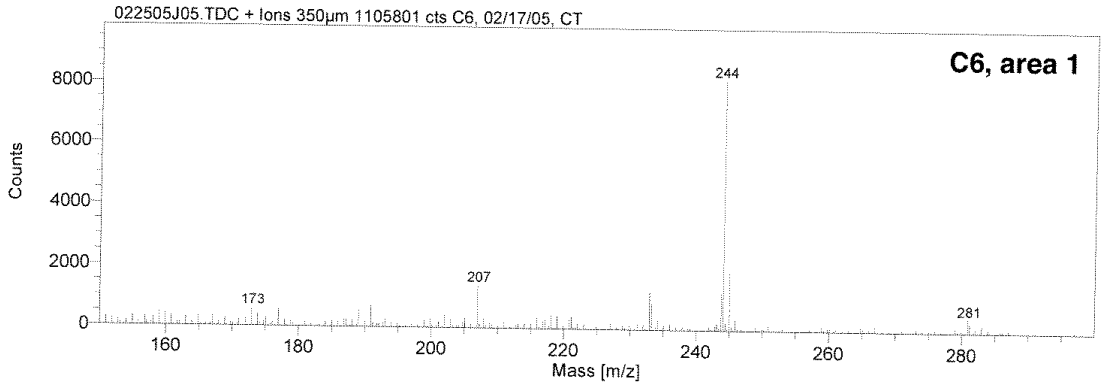

Figure 40. Mass spectra of 244+ m/z ion from coumarin treated sheets

It was possible to identify dye content based on nitrogen containing species, specifically the CN^- and CNO^- mass fragments and it was determined that the FTSC and DCCH dyeing protocols gave equivalent dye concentrations on the surface. Table 18 shows that the nitrogen species are more plentiful in the dyed fibres than in the blank and also shows that the DCCH carbonyl fragment ion (244 m/z) is only present in significant quantities in the DCCH dyed fibre as expected. The nitrogen content is six times higher in the dyed fibres as in the unextracted blank and over two orders of magnitude higher DCCH carbonyl fragment ion in the DCCH dyed fibre versus the FTSC dyed fibre and the blank.

Table 18. TOF-SIMS data for mass fragments relevant to the dyes

Ionic Species	m/z	TOF-SIMS Peak Integrals DCCH (counts)	FTSC (counts)	Blank (counts)
CN^-	26.0	34511	34258	6657
CNO^-	42.0	9753	9782	1526
$C_{14}H_{14}O_3N^+$	244.1	9429	79	71

It was also found that the viscose fibres contained a variety of contaminants related to the spinning process. The viscose rayon manufacturers usually add a variety of surfactants and lubricants to the spinning solution in order to improve fibre quality. This was made obvious by the fact that a mistake was made and the blank viscose fibres were not soxhlet extracted prior to forming the sheet for analysis. The total amount of most of the contaminants decreases substantially for the dyed pulp, which likely indicates that the acetonitrile extraction removes most of the contaminants that are insoluble in water. Table 19 summarizes the contaminant data identified by TOF-SIMS.

Table 19. TOF-SIMS data for contaminants present in dyed viscose fibre

Ionic Species	m/z	TOF SIMS Peak Integrals DCCH (counts)	FTSC (counts)	Blank (counts)
Ethylene glycol monostearate	283.14	2103	1534	19874
Irganox	219.14	4312	2729	17179
BHT	233.20	16891	8088	25540
Palmitate	255.23	1633	2631	5866

It was also necessary to obtain UV/visible absorbance spectra for the sheets. Absorbance spectra were obtained using an integrating sphere attached to a spectrophotometer. Since wavelength selection in the instrument used occurs prior to the sample, highly fluorescent samples will have distorted and reduced absorption spectra due to contamination from emitted photons. This phenomenon is exploited in the paper industry when fluorescent whitening agents are added to high brightness printing papers. This can be compensated for by collecting the spectra with a short pass filter between the sample and the

detector [169]. This strategy prevents the emitted light from reaching the detectors and allows for correct measurement of the absorption scattering coefficients using Scallan-Borch/Kubelka-Munk theory [65-67].

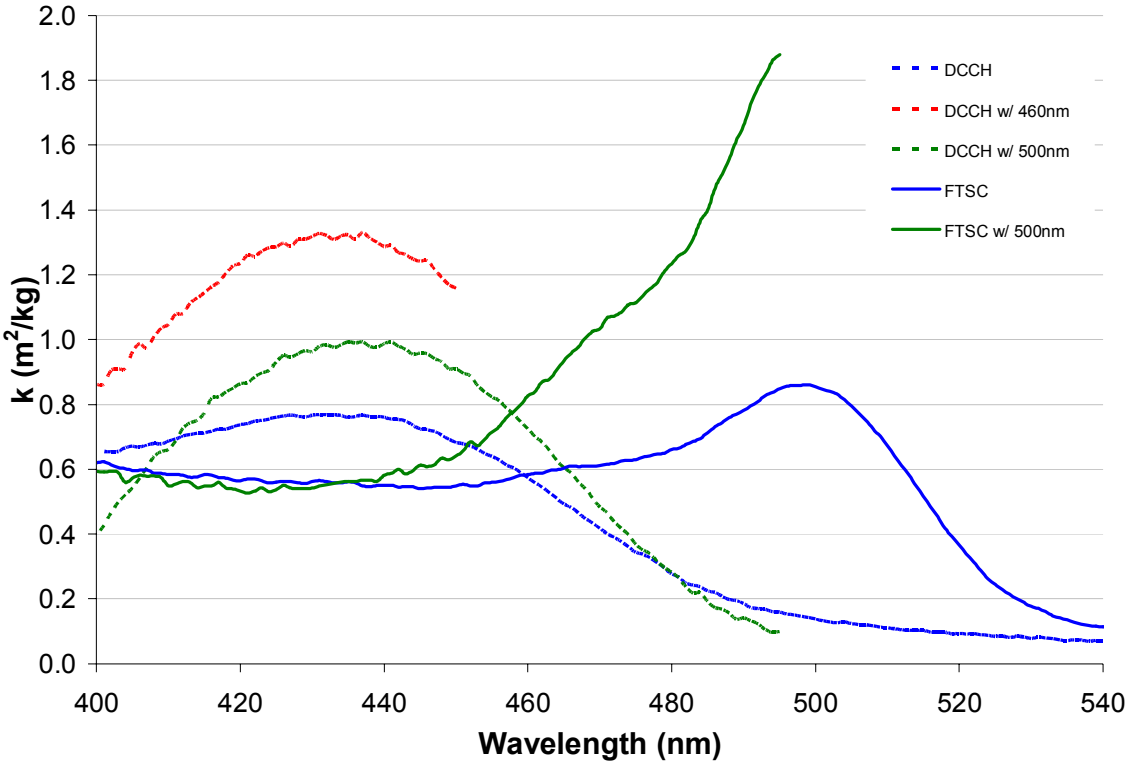

Figure 41. Absorption coefficient spectra for fluorescein and coumarin dyed viscose sheets with short pass filters

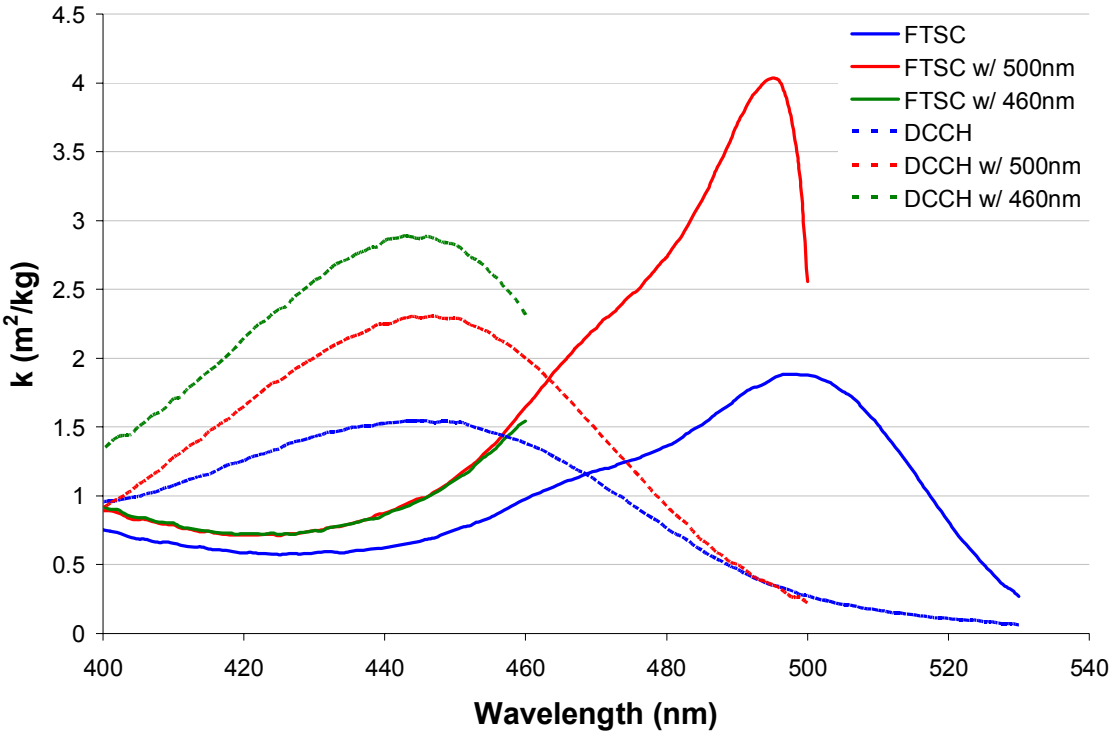

Figure 42. Absorption coefficient spectra for fluorescein and coumarin dyed white spruce sheets with short pass filters

Figures 41 and 42 demonstrate the profound impact that fluorescence has on the absorption spectra of the dyed fibre sheets. The absorption coefficients for the FTSC dyed sheets more than double when a 500 nm short pass filter is used. As could be expected, the 460 nm short pass filter gives very similar results for the FTSC in Figure 42 for the white spruce sheets. Likewise, the DCCH samples also show increased absorption coefficients when short pass filters are used. In the case of the coumarin dye, switching the short pass filter matters because DCCH emits at a shorter wavelengths than the FTSC. It is interesting that the relative increase in the absorption coefficients for the DCCH sheets is less than

that seen for the FTSC. This is likely because FTSC has a higher quantum yield than DCCH in solution [189].

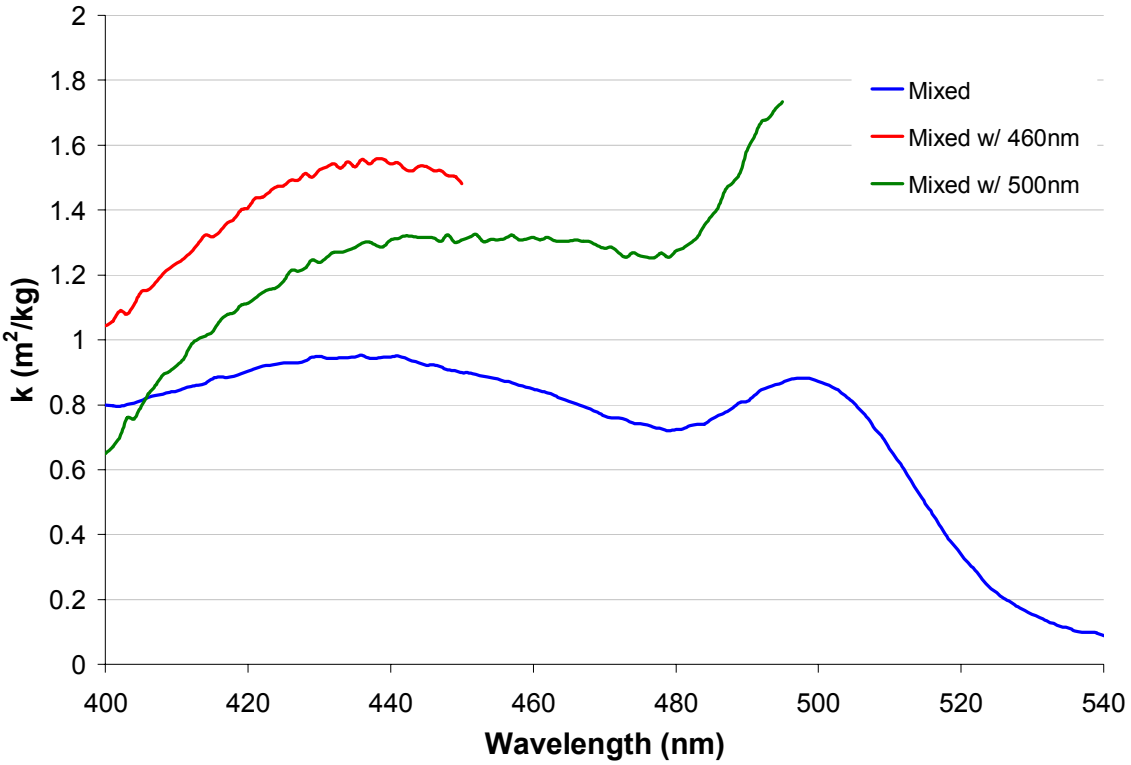

Figure 43. Absorption coefficient spectra for mixed viscose sheets with short pass filters

The spectra for the mixed sheets containing both FTSC and DCCH dyed fibres are shown in Figures 43 and 44. Unfortunately, it is not possible to use a single short pass filter and get meaningful spectra for the mixed sheets. Comparison of the spectra taken with the short pass filters indicates that there is stray DCCH fluorescence present in the more complete spectrum collected with the 500 nm short pass filter in place. It is also interesting to compare the viscose and white spruce absorption coefficients. The white spruce fibres have considerably higher absorption coefficients than the corresponding dyed viscose fibre, which likely

means that the white spruce fibres have higher carbonyl content. This still happened despite the periodate oxidation of the viscose to enhance the carbonyl content. The presence of lower molecular weight hemicellulose in the white spruce is probably responsible because they have more reducing end groups per unit mass than cellulose.

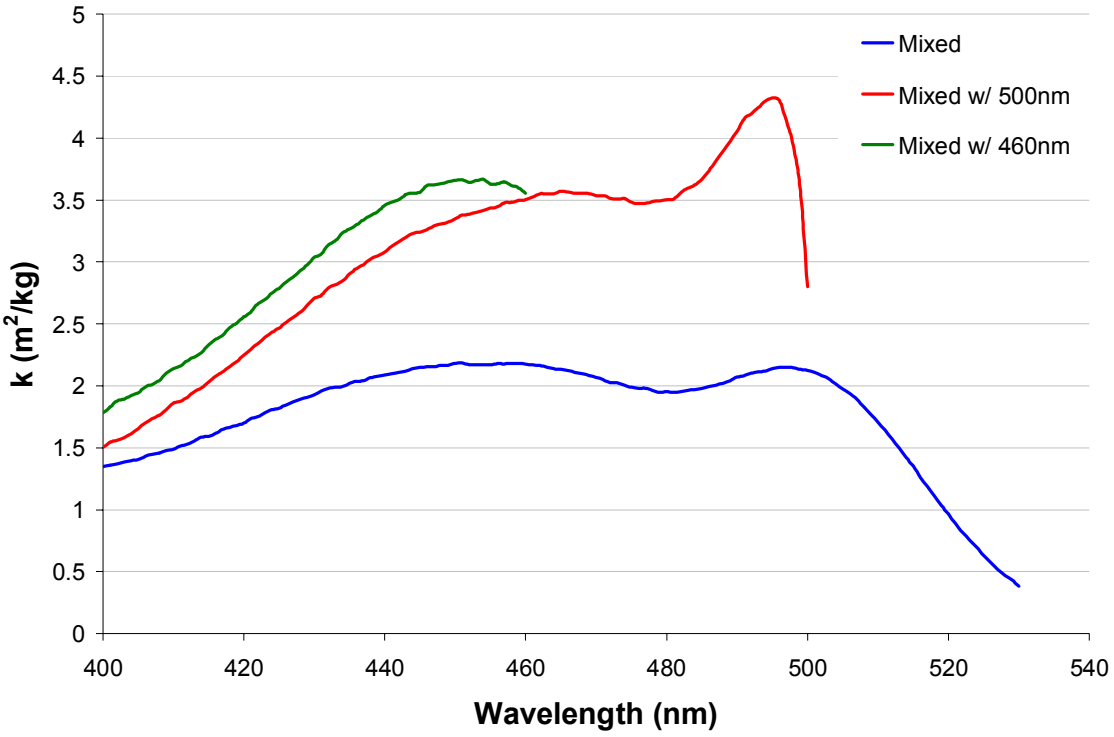

Figure 44. Absorption coefficient spectra for mixed white spruce sheets with short pass filters

The excitation and emission spectra for sheets containing 11% DCCH-dyed viscose fibre or 11% FTSC-dyed viscose fibre are shown in Figure 45. The excitation and emission maxima for the two dyes bound to viscose are slightly red-shifted approximately 20 nm relative to their spectra in DMF. There is good agreement between the excitation maxima in Figure 45 and the absorption maxima in Figure 41. There is a slight difference between the fluorescein

excitation maximum and the absorption maximum, but this is believed to be due largely to the rapid decrease in transmission near 500 nm for the 500 nm short pass filter. The overlap integral between the coumarin emission spectra and fluorescein excitation spectra is quite large thus fulfilling a critical requirement for energy transfer.

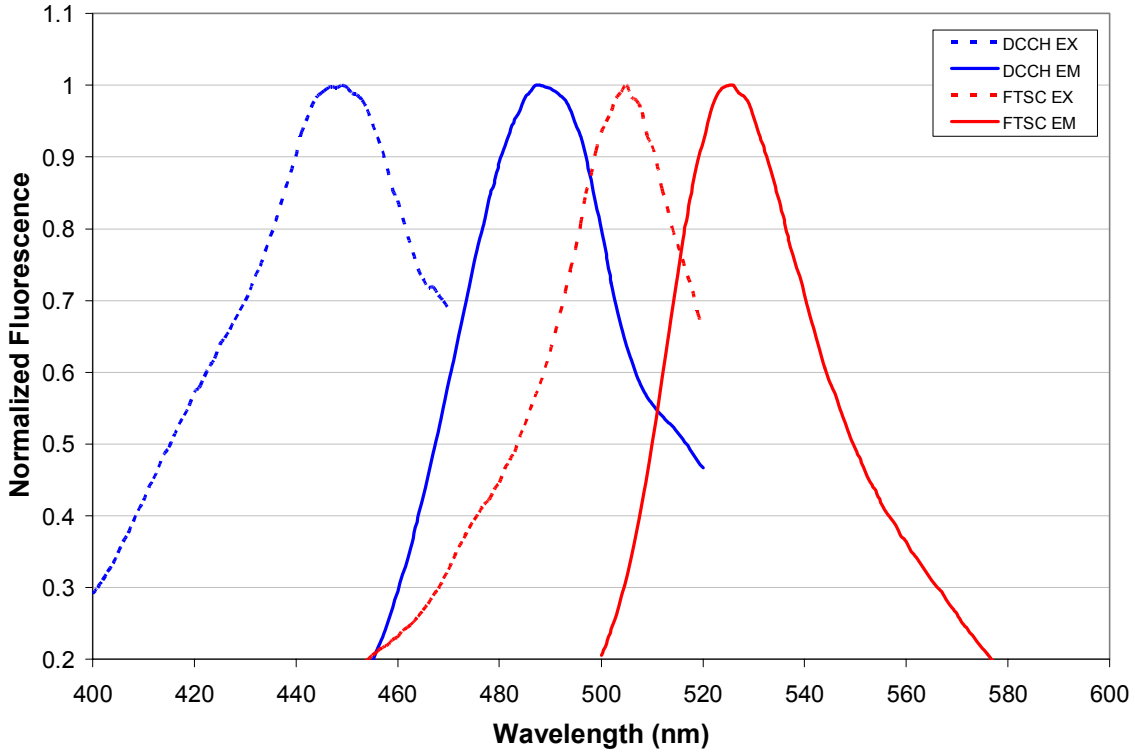

Figure 45. Excitation and emission spectra for viscose sheets containing DCCH-dyed fibre or FTSC dyed fibre

Given this spectral information, emission spectra of the coumarin, fluorescein and mixed sheets containing both coumarin and fluorescein dyed fibre were collected using excitation at 440 nm. This wavelength was selected to give near peak coumarin excitation with minimal direct excitation of the fluorescein chromophores. The emission spectra of sheets containing fluorescein-dyed,

coumarin-dyed, or equal amounts of both dyed fibers (11% DCCH and 11% FTSC) are shown in Figure 46. The mixed sheet emission spectrum demonstrates the characteristic quenching of donor fluorescence and sensitization of acceptor fluorescence that accompanies energy transfer processes. This figure serves as a proof of concept that indicates that it may be possible to measure FRET at the fibre-fibre bond interface. Although this result is not an unequivocal characterization of the mode of energy transfer it does suggest that energy transfer does occur to some degree in this system.

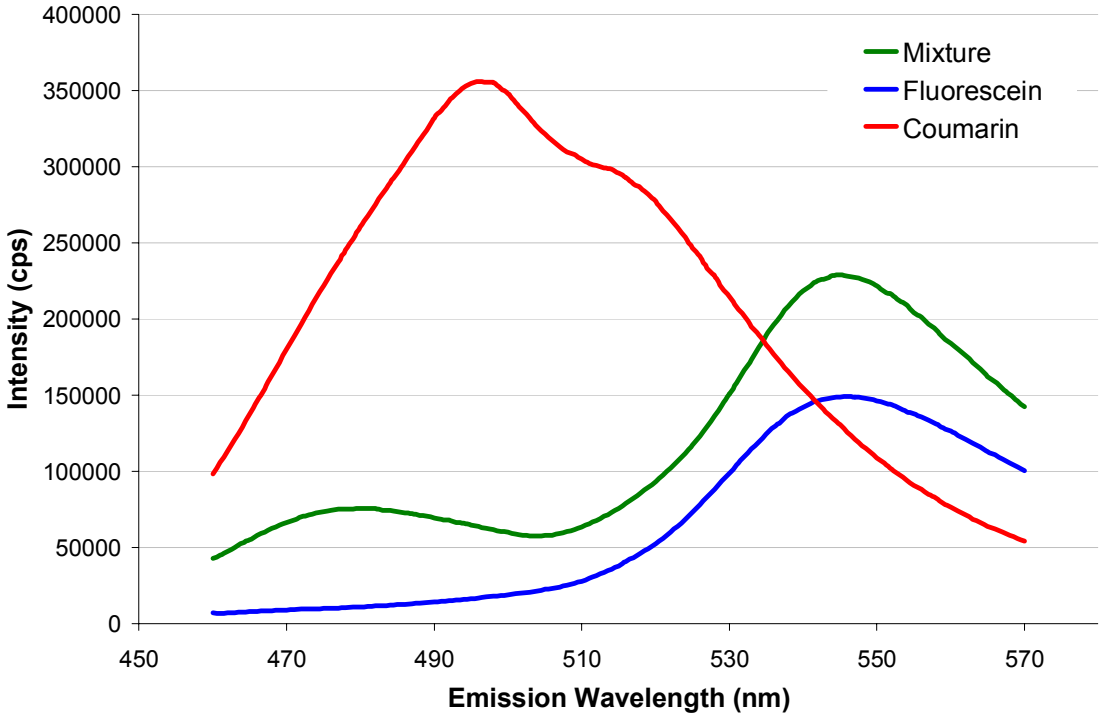

Figure 46. Emission spectra of dyed viscose fibre sheets

DCCH, FTSC and a mixture of both dyed fibres with 440nm excitation

In order to further explore the application of this technique to ensemble averaged measurements of viscose fibre sheets it was decided to manipulate sheet

consolidation through wet pressing. Papermakers routinely use numerous techniques to manipulate bonded area. Wet pressing and refining principally used to increase bonded area. Given the morphology of the viscose fibre system, refining is not an appropriate approach. In fact, refining can drastically change variables such as total surface area, fibre length, shape and conformability; each of which has differing contributions to bonded area. As a result, this work employed different wet pressing pressures to achieve higher levels of sheet consolidation.

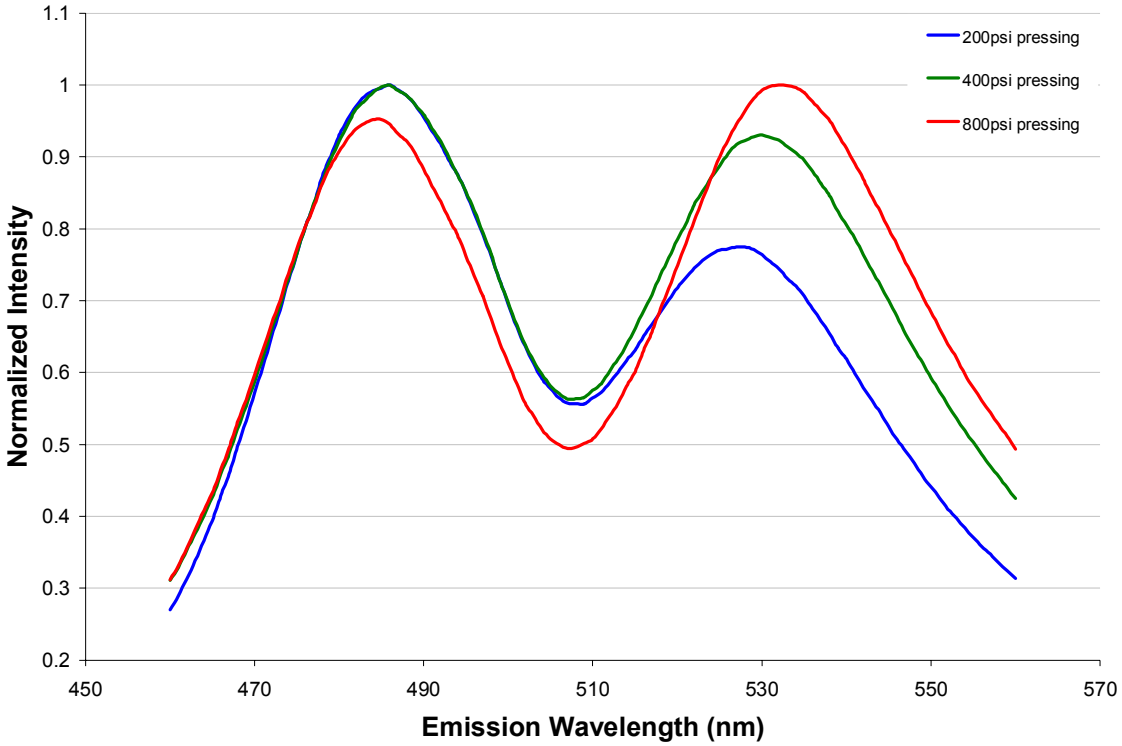

Figure 47. Normalized emission spectra of mixed sheets wet pressed at different levels

Pressed at 200 psi, 400 psi and 800 psi and using 440 nm excitation

Figure 47 shows the normalized emission spectra from sheets containing both types of dyed fibres wet pressed at three different levels. The spectra show

increased emission at 535 nm (acceptor emission) and slightly reduced emission at 485 nm (donor emission) as the wet pressing pressures are increased. The increased wet pressing pressure leads to increased sheet consolidation and by extension, to increased relative bonded area. This piece of evidence further suggests that the energy transfer phenomenon described here is mediated by inter-fibre distances. It is not clear whether the result is primarily a function of increased ET efficiency due to fibres being brought into closer proximity or rather due to new fibre areas being brought close enough together such that ET processes become significant.

Another interesting observation from Figure 47 is the shift of the acceptor emission to longer wavelengths as wet pressing increases. One possible explanation for this observation is that the chemical environment for the dye molecules changes as sheet consolidation is increased. This could be similar to a solvatochromic response in which the energy of the electronic transition is reduced either through destabilization of the ground state or stabilization of the excited state. Coumarin dyes are routinely used as solvatochromic probes [192-196], but solvatochromic behaviour is not normally observed in fluorescein derivatives. However, fluorescein is susceptible to contact quenching [197-199]. It is possible that the observed shift in the spectra is due to some combination of these phenomena.

A simplified approach to steady-state FRET measurements is to take the ratio of the acceptor and donor emission intensity [124, 147]. This ratio was then plotted versus the wet pressing pressure in Figure 48. This graphical representation of the spectra from Figure 47 more clearly shows the relationship between increased wet pressing and the apparent energy transfer. The relationship appears to level off at high pressing pressures. Given the rigid, rod-like structure of the viscose fibres employed in this study it should be expected that the system would have a limited response to increased pressing levels.

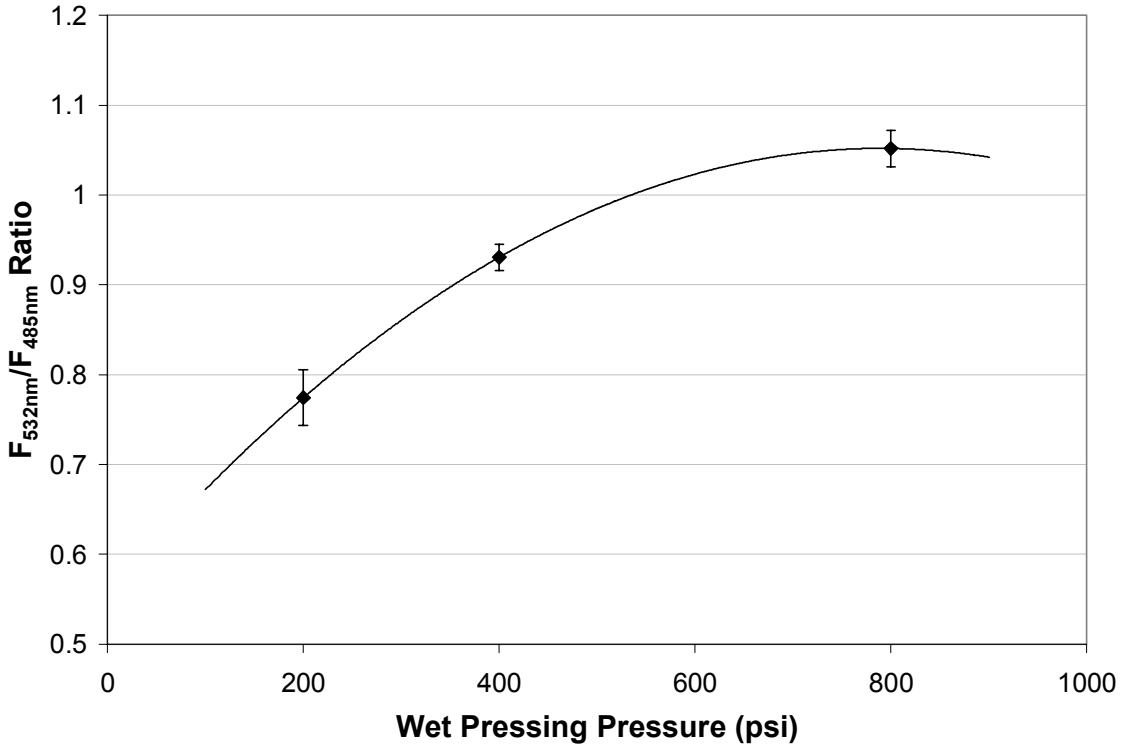

Figure 48. Fluorescence emission intensity ratio versus wet pressing pressure

These results were logical and the next step would be to examine the white spruce sheets and eventually correlate this ensemble averaged FRET signal with

established methods of measuring relative bonded area. However, a key flaw in the technique was discovered shortly into the study. This flaw is illustrated in Figure 49 below, which was generated by looking at stacks of viscose sheets in the ISS PC-1 spectrofluorometer.

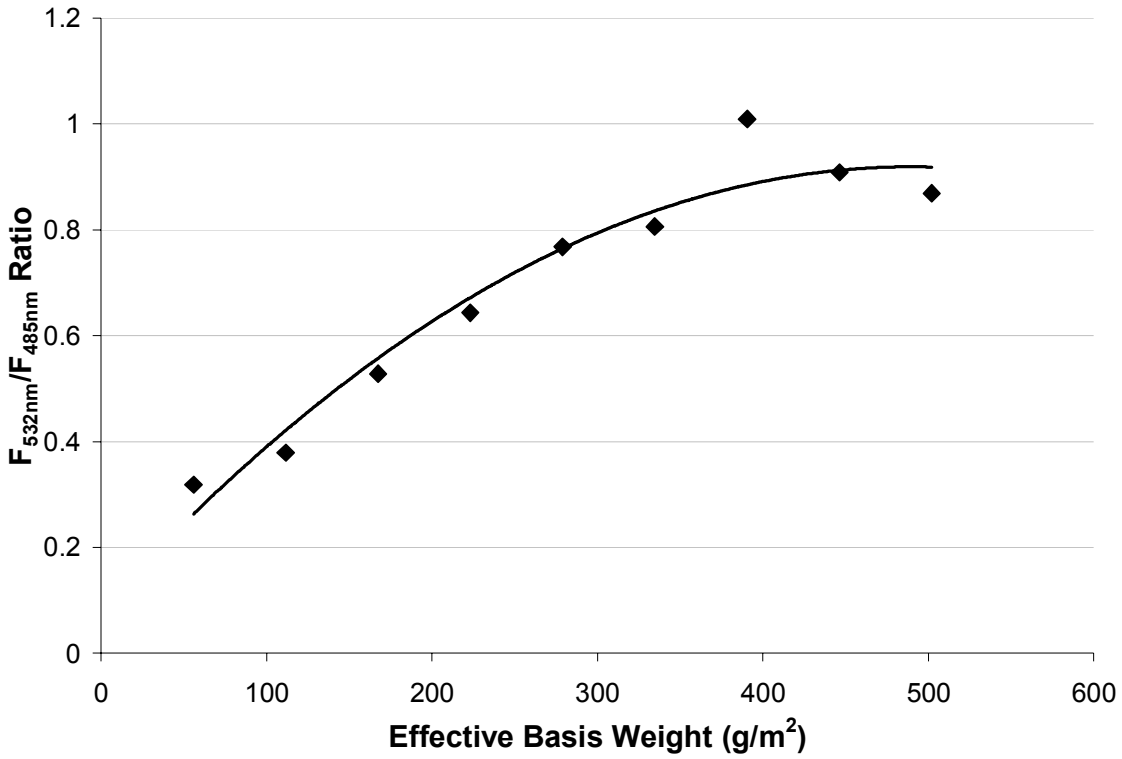

Figure 49. Fluorescence emission ratio versus effective basis weight

It shows that the 532nm/485nm ratio previously used to indicate the development of fibre bonding in a viscose fibre sheet is actually highly dependent on basis weight. This indicates that the FRET signal is dependent on beam path length and thus also related to scattering. The end result is that the change in apparent FRET signal with basis weight is likely a result of radiative energy transfer, also known as trivial energy transfer, which arises from the simple emission,

absorption and re-emission of photons. This result can be identified in solution by increasing the path length of the sample. This result is further compounded for solid samples by light scattering. Thick samples will have less transmitted light, thus more photons are available for the absorption, emission, re-absorption, re-emission cycle of radiative energy transfer. This finding precludes further study into the efficacy of ensemble averaged FRET measurements.

5.4 Conclusions

Despite the disappointing result for the fibre sheets, much of this work was necessary in order to proceed with the main objective of the project which is to image fibre-fibre interface topography with nanometre resolution. The dyed fibres that were generated and characterized are critical for the subsequent microscope work. It would not be possible to select proper filters for the fluorescence microscope without determining the absorptive and emissive properties of these dyes tethered to fibres. Fortunately, the problems that were encountered in the measurement of FRET in a paper sheet do not apply to the investigation of single fibre crossings. In retrospect it was likely far too ambitious to expect that it would be possible to determine a reliable FRET signal for a system as complicated as a fibre sheet. This serves as a reminder that setting up a FRET system is not a trivial task.

Chapter 6: Imaging Cellulosic Fibre Bonds with FRET Microscopy

The following chapter is reproduced with the kind permission of Elsevier Ltd.[1]

6.1 Introduction

The development of biomass-derived materials is receiving increased focus primarily due to the need for sustainable green chemistry processes and materials [200-202]. Cellulose fibres are particularly attractive for incorporation into advanced materials due to their ubiquitous renewable production, facile isolation and strength properties. Cellulose fibres have been extensively investigated for potentially unique applications in composites [203, 204], nanocomposites [205, 206], and as scaffolds in tissue engineering [207]. A fundamental understanding of fibre-fibre interfaces is critical to the design and fabrication of networked structures such as composites because stress transfer between load bearing fibres operates through fibre-fibre and fibre-matrix interfaces. For composites with high fibre/matrix volume ratios, the percentage of fibre specific surface area (m^2/kg) that is close enough to facilitate molecular interactions such as hydrogen bonding or attractive van der Waals forces [97] is of critical importance [45] to their physical performance properties. Fibre-fibre interfaces are also important to composites with low fibre/matrix volume ratios. For example, Dufresne and Favier *et al.* have concluded that the formation of a

[1] This article was published in Carbohydrate Polymers, Vol. 69 (4), Cameron I. Thomson, Robert M. Lowe, and Arthur J. Ragauskas, *Imaging cellulose fibre interfaces with fluorescence microscopy and resonance energy transfer*, pp 799-804, Copyright Elsevier Ltd. (2007).

network of tunicin cellulose whiskers is responsible for the dramatic increase in Young's modulus of composites containing just 5% cellulose whiskers, by volume [208, 209]. Despite the importance of fibre-fibre interfaces to both nano- and macro-scale network structures the need for proper characterization has not been fully addressed.

This study is directed to provide a new approach for characterizing fiber-fiber distance constraints at the interface. Our approach is to functionalize a cellulose fibre system with a pair of fluorescent dyes capable of fluorescence resonance energy transfer (FRET) and then utilize fluorescence microscopy to provide images of relative energy transfer values within fibre-fibre interfaces. These relative energy transfer values are proportional to the distances between labelled fibre surface components that comprise the fibre-fibre interface.

Forster developed a theory for the long range radiationless transfer of energy between chromophores almost sixty years ago [210], now commonly referred to as FRET. FRET occurs when two fluorophores within 1-10 nm have sufficient quantum yields, favourable dipole-dipole orientations, and significant spectral overlap between the donor emission and acceptor absorption spectra. [211] The phenomenon has been used as a powerful tool in biochemistry for the measurement of molecular distances with applications to the investigation of protein dynamics [125] and sensing strategies [191]. Wong and Groves [150,

151] studied an analogous system to that of fibre crossings while imaging the topography of lipid bilayers via intermembrane resonance energy transfer.

6.2 Materials and Methods

6.2.1. Fibres and Chemicals

Viscose staple fibre was acquired from Lenzing AG (Austria). The fibres were 1.2 denier (1.2 g/9000 m length), manually cut to an average length of 1.9 mm, washed thoroughly with deionized water and air-dried prior to dyeing. The spruce fibre is a never dried bleached white spruce (*Picea glauca*) kraft pulp obtained from Alberta Pacific (Canada). The pulp was lab bleached with chlorine dioxide and fully washed prior to dyeing. The fibre properties were determined using an OpTest Fibre Quality Analyzer. The average fibre length is 2.5 - 3.0 mm; the fibre width is 25-75 μm and the cell wall thickness is 1-3μm.

7-Diethylaminocoumarin-3-carboxylic acid hydrazide (DCCH) and fluorescein-5-thiosemicarbazide (FTSC) were obtained from Molecular Probes (Eugene, OR, USA) and used as received. All other chemicals were obtained from Aldrich and used as received.

6.2.2. Instrumentation

Steady state epi-fluorescence micrographs were collected under controlled temperature and humidity (50% relative humidity and 23°C) using a Leica inverted light microscope equipped with a fluorescence disc for fast changes

between filter sets. Custom filter cubes were manufactured by Chroma Technology Corp (Rockingham, VT). The filter sets are chosen to separate three distinct signals (EX/EM): the donor fluorescence (440nm/480nm); the directly excited acceptor fluorescence (500nm/525nm long pass); and the acceptor fluorescence due to FRET (440nm/525nm long pass). Digital images were collected using a Hamamatsu ORCA-ER digital camera.

6.2.3. Functionalizing Fibres with Fluorescent Dyes

The model system in this study consists of natural and regenerated cellulose fibres labelled with a fluorescein/coumarin dye pair via covalent hydrazone linkages as shown in Figure 50. Both fluorescent dyes, DCCH (donor) and FTSC (acceptor) are commercially available from Molecular Probes (Eugene, OR) and have been used for various FRET applications [126, 189, 211].

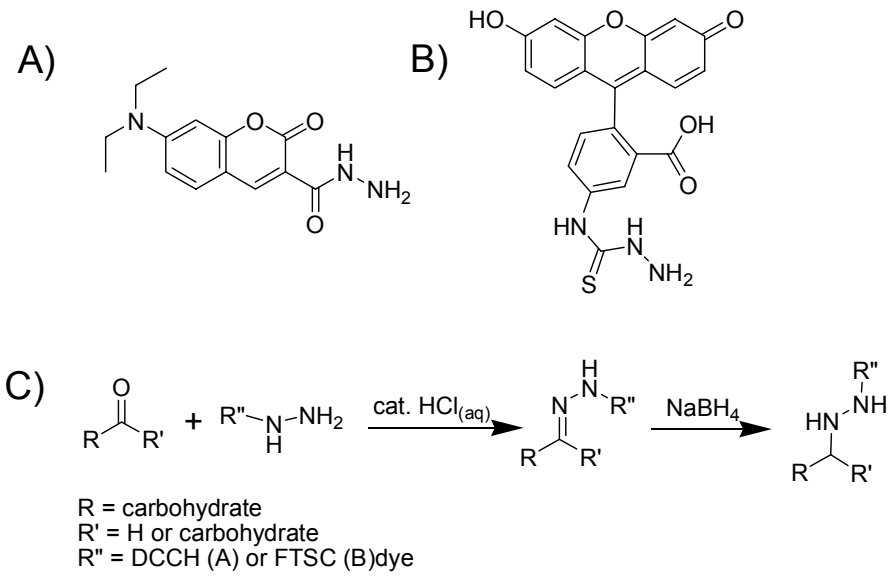

Figure 50. Structures of FRET pair dyes and dye chemistry schematic

A) DCCH; B) FTSC; C) Dye chemistry

The dyes were applied to the fibres using a method adapted from Anderson [167]. Fibre suspensions (3% w/w) were dyed overnight in glass vials containing either 1.6 mmol/L solution of FTSC in 15 mL dimethylformamide or 1.6 mmol/L solution of DCCH in 15 mL methanol. Both systems contained 28 µmol of HCl to catalyze the reaction. After dyeing, the fibres were briefly washed with DMF (50 mL) and then subjected to a mild sodium borohydride (0.50 g fibre and 0.02 mmol $NaBH_4$) treatment in DMF (15 ml) for one hour. The fibres were again washed with DMF (50 mL), placed in cellulose extraction thimbles, then Soxhlet extracted with acetonitrile overnight to remove any excess dye. Precautions were taken throughout the process to minimize sample exposure to light.

6.2.4. Preparation of Fibre Crossings

Dilute suspensions (50 mg/L) of mixed fluorescein-dyed and coumarin-dyed fibres were prepared in deionized water and adjusted to pH 9 with 0.0005 mol/L sodium tetraborate decahydrate buffer. Fibre intersections as shown in Figure 51 were prepared on glass slides by first filtering the suspension onto filter paper. The fibres were then transferred to glass slides with light pressing followed by air-drying at 50% relative humidity and 23°C in a controlled temperature and humidity room for at least 6 h.

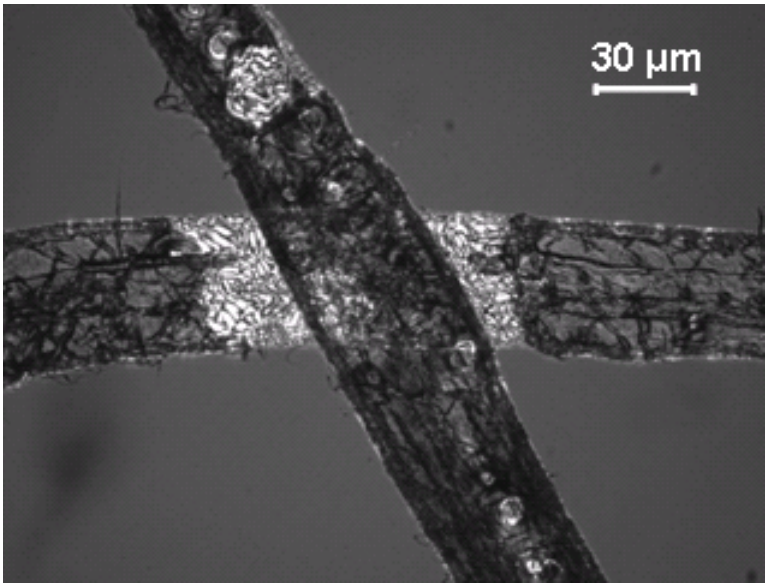

Figure 51. Micrograph of white spruce fibre crossing on glass slide

Reflected light image with 600X magnification

6.2.5. Image Analysis

The measurement of FRET can be complicated by local dye concentration changes and inefficiencies in the microscope filter sets. The FRETN algorithm developed by Gordon [157] was employed in this work to correct the signal at each pixel. Twenty crossings were analyzed for each condition and each fibre crossing was analyzed by the collection of three fluorescence micrographs using three different filter sets. Examples of fluorescent micrographs of white spruce and viscose fibre crossings captured with the FRET filter set are shown in Figures 52 and 53 respectively.

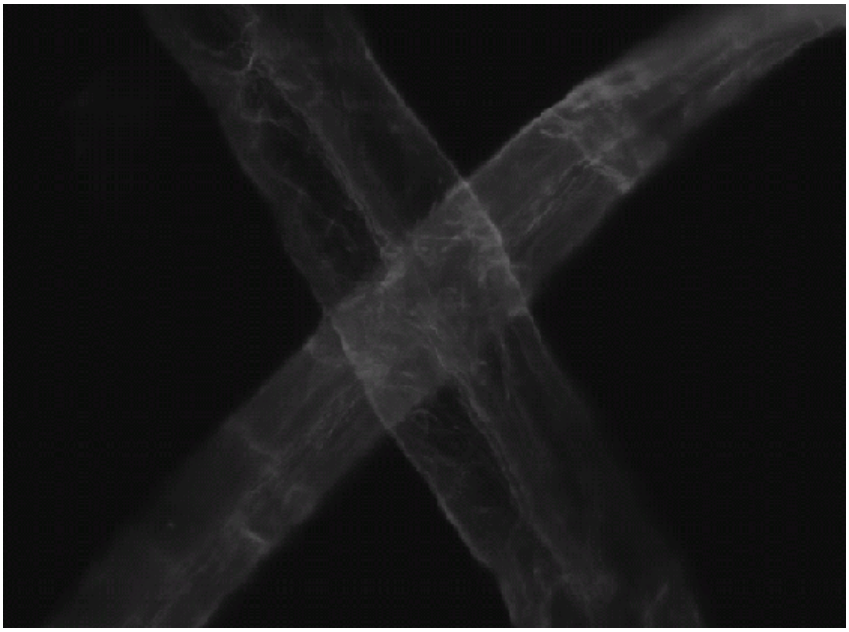

Figure 52. Fluorescent micrograph of dyed white spruce crossing

Using FRET filter set and 600X magnification

The FRETN correction method described below requires values for samples containing exclusively donor or acceptor dye. That requirement is met by obtaining average gray scale intensities from non-crossing regions on each of the fibres using three filter sets. Donor only, acceptor only, and both donor and acceptor conditions are measured with each of the three filter sets giving a total of nine values for the analysis. These nine values are then used to calculate the corrected FRETN value at each pixel in the crossing using MATLAB and the MATLAB Image Analysis Toolpak. Equations 20 and 21 from Chapter 4.11 were adapted from Gordon *et al.* and used to calculate FRETN for fibre crossings. The first (capitalized) letter in each term refers to the Filter set employed – FRET, Donor, or Acceptor. The second letter refers to the section of the picture where the value was collected: the acceptor fibre,"a;" the donor fibre, "d;" or the fibre crossing, "x;" For example, "Dx" refers to the signal from the fibre crossing using

the donor filter set in the microscope. Literature values were used for the quantum yields and the other factors were obtained from the filter set spectra given to us by Chroma Technology.

The projected crossing area is calculated planimetrically in MatLab from each fibre crossing in the reflected light image. This normalization for crossing area is necessary in order to account for the inherent variation in the dimensions of the natural fibres and to provide a basis for the comparison of the two fibre sources. A comparison of white spruce in Figure 52 and viscose in Figure 53 clearly shows that the viscose fibres are considerably smaller. The image data from MATLAB was then exported to Excel for further analysis.

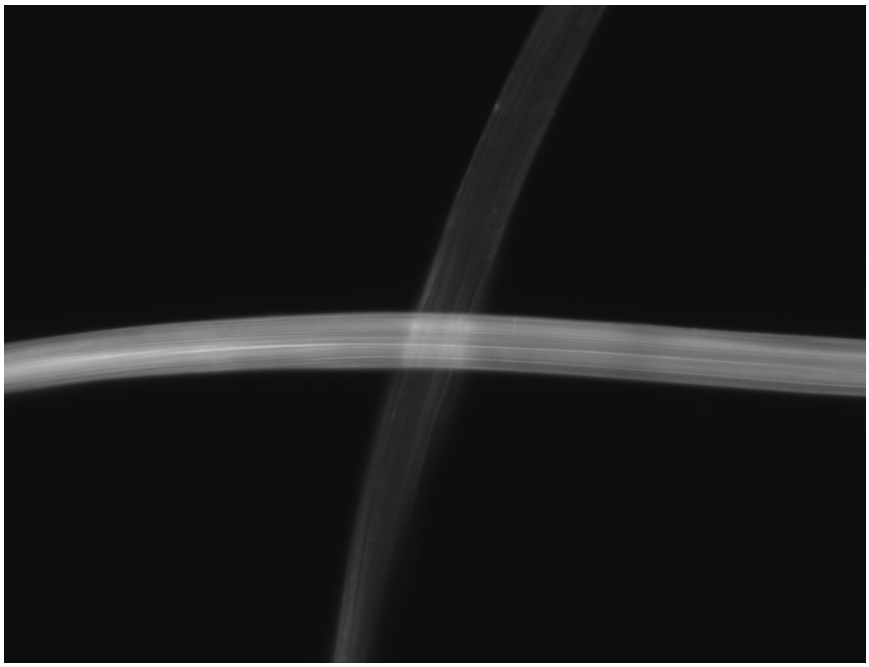

Figure 53. Fluorescent micrograph of viscose fibre crossing
600X magnification using FRET filter set

6.3 Results and Discussion

The primary region of interest in Figures 52 and 53 is the fibre crossing area where both donor and acceptor dyes are present and FRET can occur. Figure 54a shows a representative FRETN surface plot from a viscose fibre crossing. Striations on the viscose fibres manifest themselves as a 'waffle like' pattern in the FRETN surface. It stands to reason that this type of response is the result of the high ridges on each fibre contacting each other. There are no regions in the viscose fibre interface with high levels of energy transfer. Figure 54b shows the FRETN surface for a crossing consisting of natural wood (*Picea glauca*) fibres. This interface is significantly different from that of the more regular viscose fibres. It possesses none of the regularity seen for the viscose crossing and appears to be an irregular interface. The white spruce FRETN surface also demonstrates area of closer contact as shown by the color coded FRETN legend that was not present in the viscose crossings.

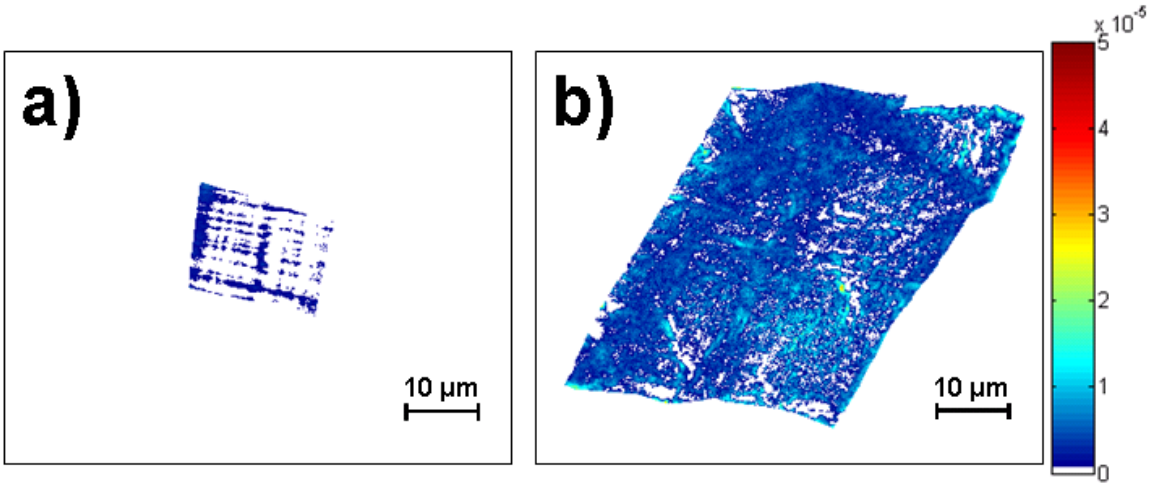

Figure 54. Comparison of FRETN images of viscose and white spruce fibre crossings

Images calculated in MATLAB from 600X magnification fluorescent micrographs: a) viscose crossing and b) white spruce crossing

Figure 55 compares the pixel distributions of spruce and viscose fibre intersections. This histogram is composed of all FRETN pixels for all crossings in each condition and is normalized for the total projected crossing area of those crossings. The viscose crossings have a tight distribution of pixels with low FRETN values, while the spruce fibres have a more broad distribution with a greater population of pixels with high FRETN values.

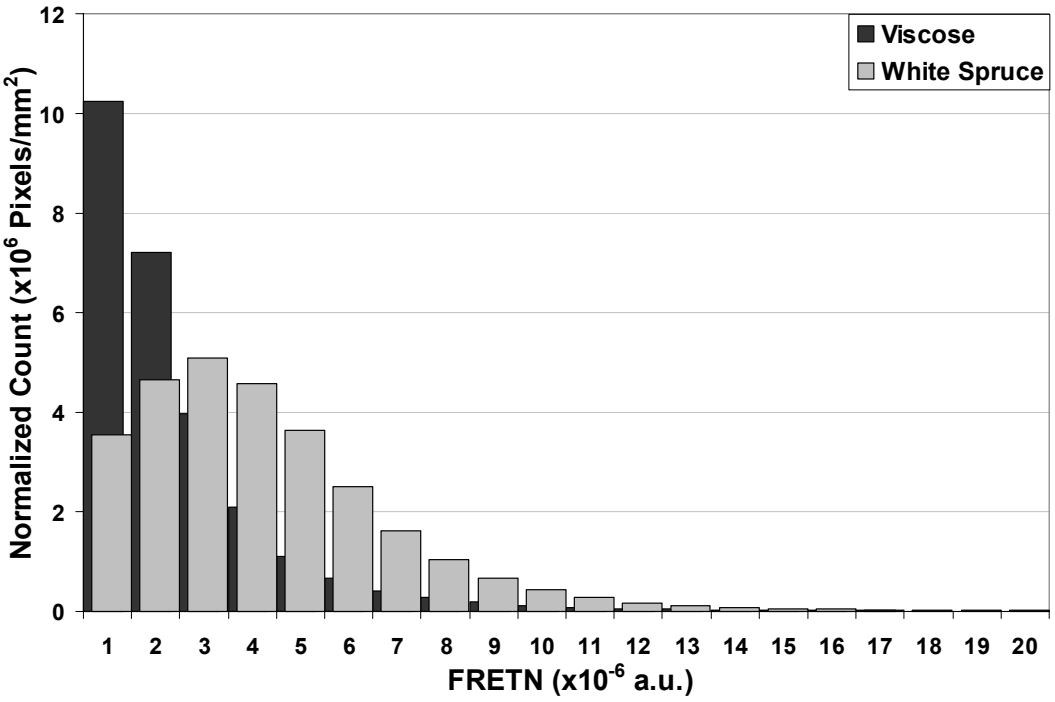

Figure 55. Histogram of FRETN pixels normalized for the total crossing area

For viscose and white spruce fibres

These results suggest that spruce pulp fibres will have a higher degree of bonding than viscose fibres. This result is supported by measurements of the ultimate strength of individual fibre-fibre joints in the literature. McIntosh and Leopold observed that fibre-fibre bonds were nearly seven times stronger than

fibre-cellophane bonds [212]. Likewise, it has been observed that untreated rayon fibres [213, 214] demonstrate lower joint strengths as compared to wood fibers. There is evidence that natural fibres have several advantages over viscose fibres that can lead to superior performance in cellulose fibre composites [215, 216]. However, the advantages of natural fibers are not limited to fibre-fibre bonding and thus the findings from this study may not fully explain the benefits of natural fibres incorporated into cellulose reinforced composites.

Recent observations of the surfaces of natural wood fibres in the wet state with atomic force microscopy indicate that these surfaces are highly fibrillar in nature [105-107]. Several researchers have also observed that these fibrils are extended in solution [107, 108]. Furthermore, microindentation methods have indicated that natural wood fibre surfaces are highly compliant to depths of 200-800 nm into the cell wall [108]. Unlike regenerated cellulose, the surfaces of wood fibres contain amorphous low molecular weight polysaccharides [217] which may be capable of interdiffusion thus leading to adhesion at the fibre-fibre bond [75]. These low molecular weight components have lower glass transition points than pure cellulose and are likely to deform considerably under ambient conditions [218]. The viscose fibres used in this study had smooth ridges running parallel to the fibre axis that were not amenable to the formation of large areas of intimate fibre-fibre contact. The results obtained in this study reflect the differences in surface morphology and topochemistry for natural and regenerated cellulose fibres.

Furthermore, a FRET response due to interdiffusion has been observed by Winnik *et al.* for the coalescence and film formation of various latex particles in aqueous and non-aqueous dispersions [119, 122, 140, 142]. Although their studies did not include imaging, the latex systems studied bear an analogy to the cellulosic fibre interfaces in this work. Thus, the entanglement of compliant fibrils combined with the intermixing of lower molecular weight polysaccharides may be contributing to the increased areas of closer contact for wood fibres as measured by FRETN. It may be possible to combine both approaches which would provide dynamic topographical information as well as mechanistic and kinetic details of cellulosic interface development using FRET.

6.4 Conclusions

For the first time, cellulose fibre interfaces are imaged using FRET and fluorescence microscopy. Steady-state epi-fluorescence microscopy suggests that energy transfer from coumarin dyed fibers to fluorescein dyed fibres is occurring. This is also the first known observation of non-radiative energy transfer occurring between objects of this scale. The FRET response for spruce fibre interfaces is distinctly different from that observed in viscose fibre. The fibrillar structure of spruce fibre surfaces and the presence of low molecular weight hemicelluloses is likely responsible for this difference.

Chapter 7: Determining the Impact of Process Variables on Fibre-Fibre Bonds with FRET Microscopy

7.1 Introduction

Fibre-fibre bonding is widely regarded as one of the most important properties for the papermaker because it is principally responsible for the internal cohesion of a paper sheet [219]. Bonding is traditionally defined using two independent factors: bonded area and specific bond strength (bond strength per unit bond area) [220]. There is significant industrial importance in decoupling these two factors because bonded area is directly related to both optical and strength properties, while specific bond strength has little impact on the optical properties.

Refining and wet pressing are traditional papermaking tools that have a direct impact on bonded area [56, 221, 222], and thus they manipulate both strength and optical properties. This trade-off can be overcome by directing research efforts toward enhancing specific bond strength leading to significant benefits for many paper grades. The determination of specific bond strength requires that a true bonded area between fibres be measured. Current methods may not accurately deconvolute the contributions of molecular interactions between fibres from the surface area over which they operate.

Given its importance, the structure and mechanism of formation of the fibre bond has been a key subject for the paper physics community. Numerous researchers

have collected information and developed theories about the fibre bond based on either the direct observation of individual fibre crossings or inference from various ensemble averaged measurements of paper sheet properties. In tandem, these two strategies have given the paper industry a great deal of practical information regarding the development of fibre bonds in paper.

Currently, there is no definitive method capable of probing the structure of the fibre-fibre interface. Although the direct and indirect methods summarized here have been able to describe much of the material behaviour of paper they have various limitations which prevent them from gaining further information about the fine structure of bonded cellulose interfaces. A new, preferably *in situ,* method that is capable of studying paper fibres in ambient conditions is desired.

Further understanding of fibre-fibre interfaces and improved definitions of specific bond strength and relative bonded area clearly demand the application of novel experimental techniques. New methods need to circumvent the limitations of light scattering, conventional microscopy and BET gas adsorption in order to probe the topography of the fibre-fibre interface. The photophysical phenomenon known as fluorescence resonance energy transfer (FRET) provides an opportunity for the modern paper physicist to study the fibre-fibre interaction on a molecular level.

FRET is widely used in medical and biochemical research as a tool to determine distances and global structural alterations in proteins and DNA on the 10-100Å

scale [125, 161, 223]. FRET gains new applications daily in a variety of fields, particularly material science. The technique is useful because it can be used in imaging applications when a fluorescence microscope is employed [157, 159, 161]. To the authors' knowledge, FRET has not been utilized in the study of pulp and paper and more specifically has not been used to probe the nature of the fibre-fibre bond.

FRET could be applied to a paper system in the following manner. Two fibres, independently dyed with the donor and acceptor dyes, are brought into close proximity via capillary forces and wet pressing. When illuminated with the appropriate wavelength of light to excite the donor dye molecule, acceptor fluorescence can be detected if the two molecules are within 100 Å. Variations in the intensity of acceptor and donor fluorescence provide the ability to use FRET as a "spectroscopic ruler" to provide spatial information about the fibre-fibre interface.

7.2 Materials and Methods

7.2.1. Fibre and Sample Preparation

Both natural and regenerated cellulose fibres were prepared for this study. A never dried white spruce (*Picea glauca*) pulp, provided by Alberta Pacific (Canada), was bleached with chlorine dioxide and exhaustively washed yielding a final ISO brightness of 90. The bleached white spruce fibres were PFI refined to 300 or 2000 revolutions and then fractionated in a Bauer-McNett classifier.

The medium long (R14) and short (R35) fibre fractions were reserved for dyeing. Viscose staple fibre (39 mm length, 1.2 denier) was supplied by Lenzing AG (Austria). The fibre was manually cut to an average fibre length of 1.9 mm, washed and then air dried before use.

Two fluorescent dyes were purchased from Molecular Probes (Eugene, OR, USA). The donor, 7-diethylaminocoumarin-3-carboxylic acid hydrazide (DCCH), and acceptor, fluorescein-5-thiosemicarbazide (FTSC), were chosen because they are an extensively used and well characterized FRET pair [126, 189]. The hydrazide dyes were applied to the fibres using a method adapted from Anderson [167]. A 2% suspension of cellulose fibre (oven dry basis) in the appropriate solvent (FTSC: N,N,-dimethylformamide, DCCH: methanol), containing 1.6 mmol/L of dye, and 1.8 mmol/L of HCl was magnetically stirred in the dark overnight at room temperature. The resultant dyed fibres were briefly washed with their respective solvents and then subjected to a mild sodium borohydride reduction (1.3 mmol/L $NaBH_4$). Finally, the fibres were Soxhlet extracted with acetonitrile overnight to insure that only covalently linked dye remained.

Single fibre crossing samples were prepared according to a methodology developed by Lowe *et al* [170]. The FTSC dye is pH dependent, therefore, a sodium tetraborate buffer solution (0.025 N) was used to maintain pH 9 during the slide making process [168]. A 50/50 mixture of DCCH and FTSC dyed fibres

were diluted to volume in a standard handsheet mold and drained onto a filter paper. The fibres were couched onto glass slides and then wet pressed as described in Table 20. Slides were allowed to dry and condition at 50% relative humidity and 23°C before being imaged.

Table 20. Wet pressing conditions for viscose and white spruce samples

Sample	Load (kPa)	Time (min)	Temperature (°C)
Viscose	7	1	25
	3450	5	80
White spruce	7	1	25
	345	5	25
	2070	5	25

7.2.2. Fluorescence Microscopy and Image Analysis

A Leica inverted reflected light microscope, a 50 watt metal halide lamp, and a Hamamatsu ORCA-ER digital camera were used to acquire 1.0 megapixel images. The microscope was equipped with a fluorescence disc allowing a quick change of the filter sets without disturbing the sample. Exposure time was held constant between filter set changes and varied from 0.15 – 0.5 seconds depending on the initial sample intensity. During image acquisition, fibre crossings were minimally exposed to excitation light to prevent photobleaching. It was found that better fluorescence micrographs were acquired by imaging the top surface of the fibre crossing with a black background placed on the opposite side of the glass slide. Intensity data was analyzed using a MATLAB program coupled with the MATLAB Image Analysis Toolpack to calculate a normalized FRET (FRETN) value at each image pixel in the fibre-fibre interface.

Each fibre crossing was analyzed by collecting three fluorescence micrographs using three different custom filter sets manufactured by Chroma Technology Corp. (Rockingham, VT). Each custom filter set was designed to capture a distinct signal from the fibre crossing: the donor emission (D), the directly excited acceptor emission (A), and the acceptor emission due to FRET (F). Table II describes each filter set.

Table 21. Excitation and emission specifications for filter sets

Filter Set	Description	Excitation	Emission
D	Donor Excitation and Donor Emission	440 ± 5 nm	485 ± 5 nm
A	Acceptor Excitation and Acceptor Emission	500 ± 5 nm	535 nm LP
F	Donor Excitation and Acceptor Emission	440 ± 5 nm	535 nm LP

7.2.3. Factorial Experimental Design

A full 2^3 factorial experiment was executed using high and low values for pressing, refining and fibre fraction as shown in Table 22. The experiment utilized fully bleached white spruce kraft pulps donated by Alberta Pacific. The spruce fibres were refined to a given level and then fractionated in a Bauer-McNett fibre classifier to give a short fraction and a long fraction at each refining level. These fibres were then dyed using the previously described protocol. Fibre intersections were then prepared using the previously described method with wet pressing at two different levels. Twenty intersections were analyzed per condition and average FRETN/projected bond area (PBA) values were obtained

from the image analysis in MATLAB. Viscose fibre crossings were also prepared and wet pressed to different levels to compare the pressing response of the two fibre types.

Table 22. 2^3 factorial screening experimental design

Condition	Pressing Load (kPa)	PFI Refining (revolutions)	Fibre Fraction
1	7	300	short
2	7	300	med. long
3	7	2000	short
4	7	2000	med. long
5	2070	300	short
6	2070	300	med. long
7	2070	2000	short
8	2070	2000	med. long

7.3 Results and Discussion

The main region of interest is the fibre crossing area in which FRET can occur. However, use of the FRETN correction algorithm proposed by Gordon *et al*. [157] to normalize the FRET signal requires data collection from several other regions in the image. Figure 56 shows a representation of a fibre crossing and indicates the areas of interest: the fibre crossing, an area where only donor exists, a region where only acceptor exists, and a region to determine the background signal. Gray scale images using each of the filter sets were acquired and saved for image analysis.

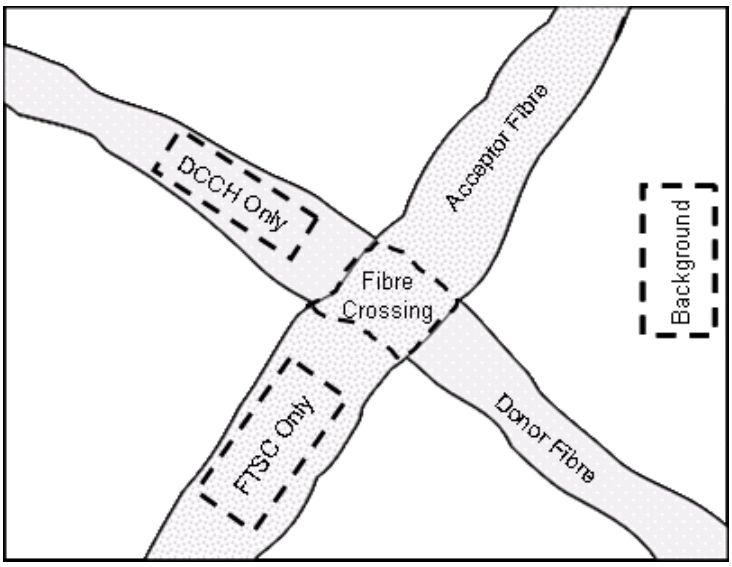

Figure 56. Sketch of fibre crossing indicating regions of interest for FRETN analysis

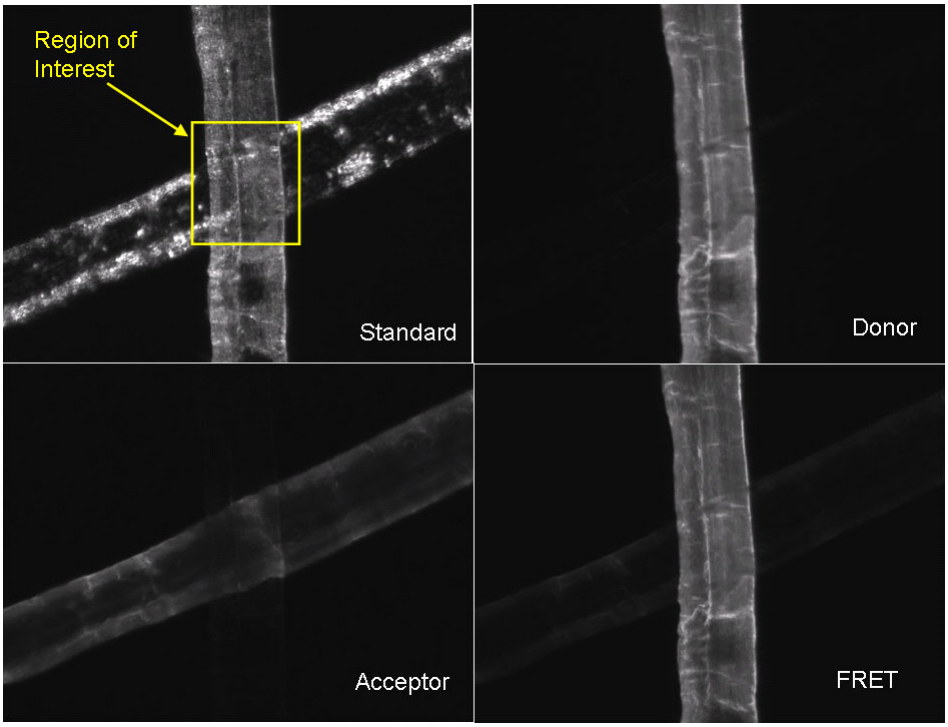

Figure 57. Grayscale images of fibre crossings used for FRETN analysis

Figure 57 shows representative gray scale images of the same fibre crossing in polarized reflected light (Standard) and each of the three fluorescence filter sets.

The normalization method requires donor only, acceptor only, and donor/acceptor values. An average gray scale value for each of these regions using each filter set was collected as shown in Figure 57. This gives a total of nine values that are used to calculate the FRETN value at each image pixel in the fibre crossing.

The wet pressing pressure was varied for the white spruce and viscose fibre samples. Figures 58-62 show representative FRETN surfaces from the fibre-fibre interfaces of viscose and white spruce fibres that have been wet pressed with different loads. The X and Y axes indicate the pixel location while the magnitude of the FRETN value is specified by the colour. Red, orange, and yellow indicate areas with a higher FRETN value and hence a shorter distance between the material on different fibres.

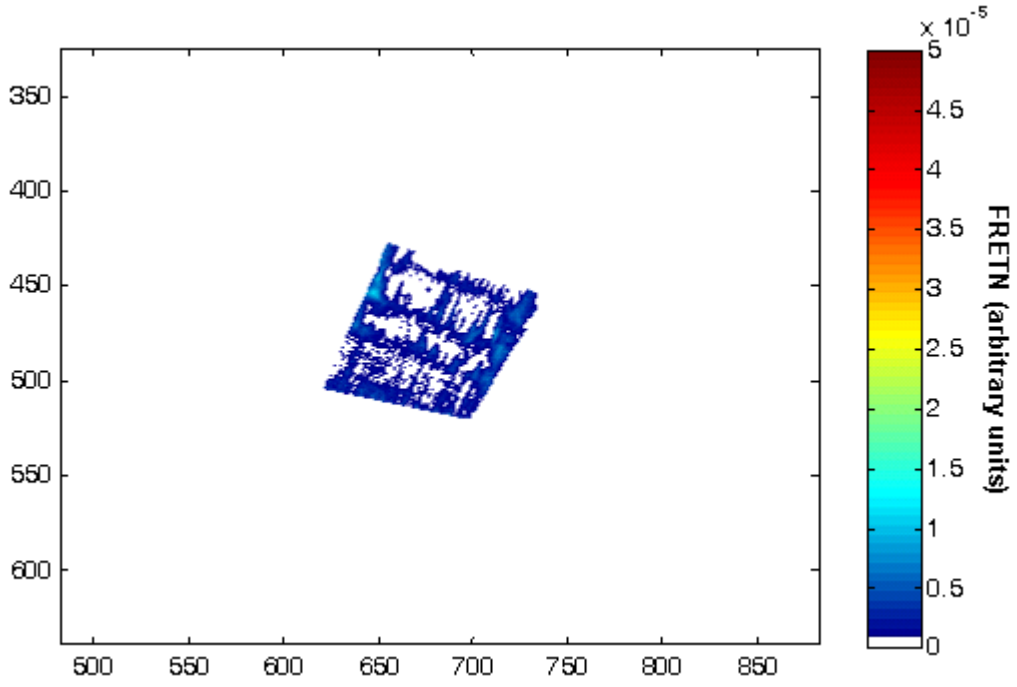

Figure 58. FRETN surface plot of a couched viscose fibre crossing

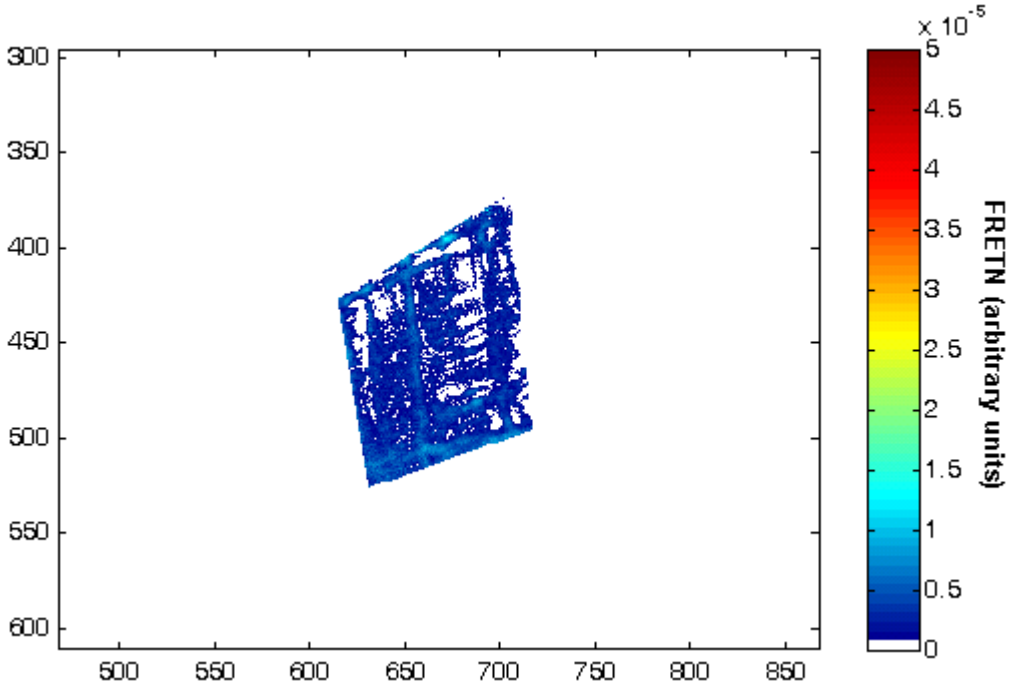

Figure 59. FRETN surface plot of viscose pressed at 3400 kPa

With increased pressing, the two fibre sources behave quite differently. There is virtually no change in the viscose fibres as shown in the representative FRETN surfaces in Figures 58-59. Wet pressing does not appear to lead to shorter distances between dyes attached to viscose fibres. The waffle like pattern visible in the viscose samples arises from ridges on the fibre surface created by the manufacturing process.

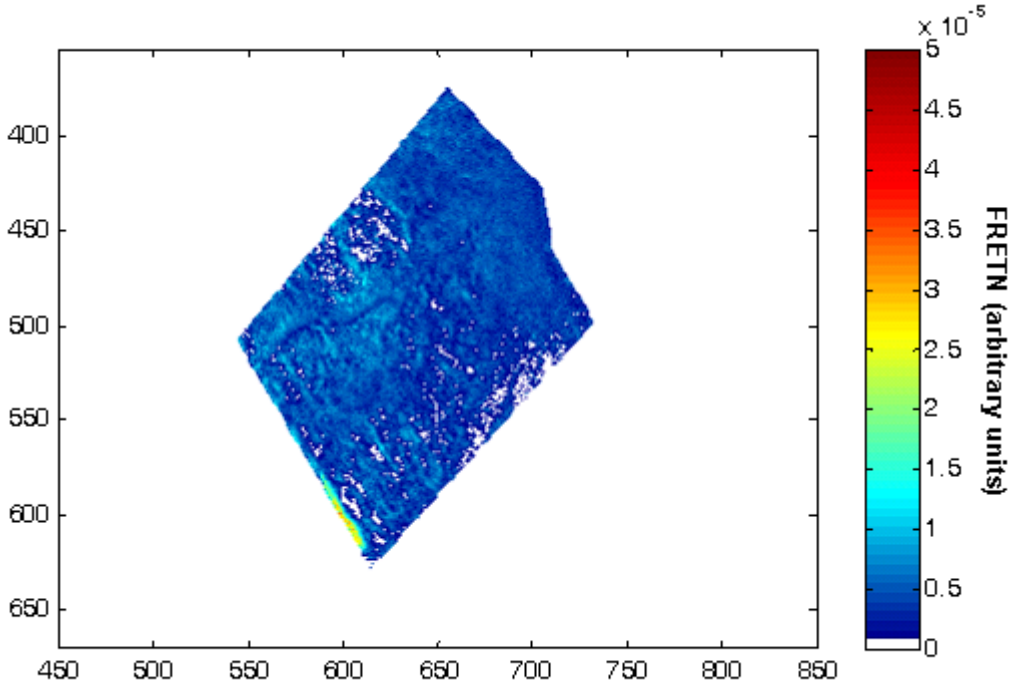

Figure 60. FRETN surface plot of a couched white spruce fibre crossing

Conversely, for white spruce in Figures 60-62, the FRETN surfaces change considerably upon wet pressing. The colour coded FRETN surfaces show an increased number of pixels with large FRETN values in the pressed samples. Higher wet pressing of white spruce fibres results in an increased number of pixels with high FRETN values as well as a decrease in the number of low FRETN pixels. These observations are a net result of the dye pair distance being reduced. The pattern or distribution of non-FRETN areas does appear to change with wet pressing, but there is no change in the overall average number of FRETN pixels per unit crossing area.

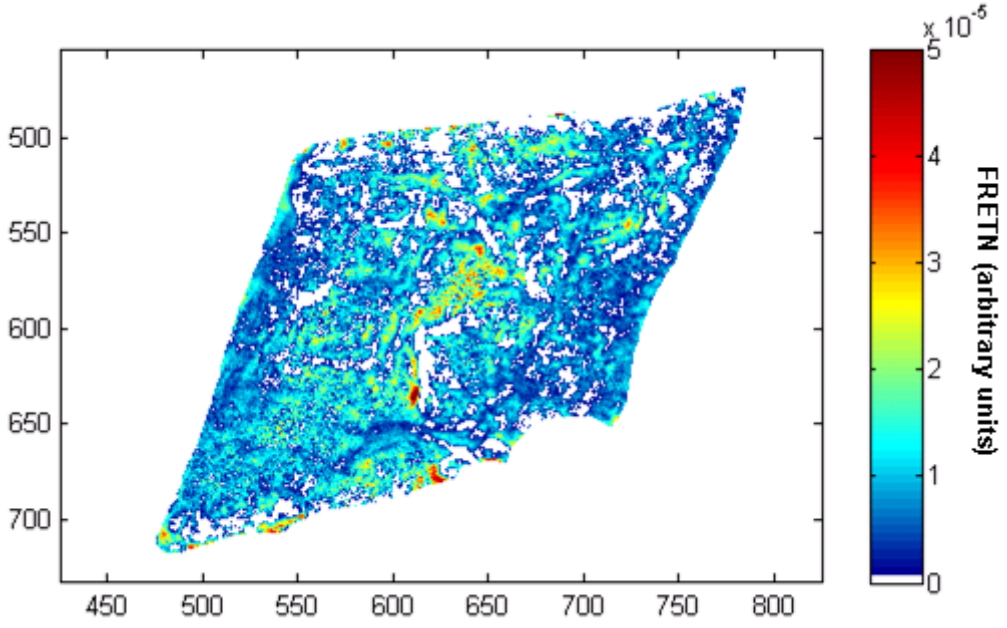

Figure 61. FRETN surface plot of white spruce pressed at 350 kPa

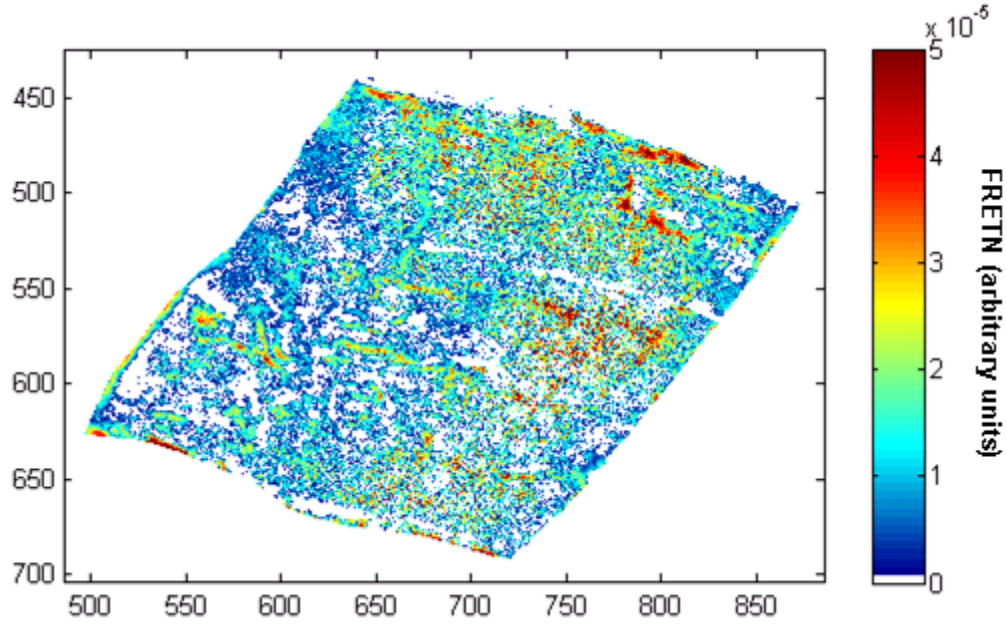

Figure 62. FRETN surface plot of white spruce pressed at 2100 kPa

Morphological and topochemical differences between viscose and natural wood fibres are likely responsible for the different responses. Even at high wet

pressing pressures, the rigid structure of the viscose prevents fibre material from coming into close enough contact to allow molecular interactions. The viscose fibres employed here are rod like and have neither a fibrillar surface nor a collapsible lumen like the white spruce fibres. Also, natural wood fibres will retain hemicellulose and oxidized residual lignin through the pulping and bleaching process. As Goring observed [218], these components are lower molecular weight amorphous polymers with low glass transition temperatures relative to cellulose and thus can contribute to deformability and bonding in natural wood fibres, but are not present in viscose.

The aforementioned ultrastructure and topochemical differences are critical to the consideration of fibre-fibre bonds as polyelectrolyte gel layers formed by the diffusion controlled adhesion of polymers [224-227]. These theories are partially supported by the observation of compliant fibrillar layers at the surface of fibres by atomic force microscopy [228, 229] and would favour the spruce fibre with respect to forming a bonded region. Furthermore, Voyutskii's diffusion theory of adhesion postulates a direct relationship between pressing pressure and the resultant strength of the bond [225]. Figure 63 illustrates how this phenomenon would lead to increased FRET signal in this system. Although the data presented does not consider the ultimate joint strength of these interfaces, our results are in agreement with increased diffusion of surface polymers in a gel-like surface layer.

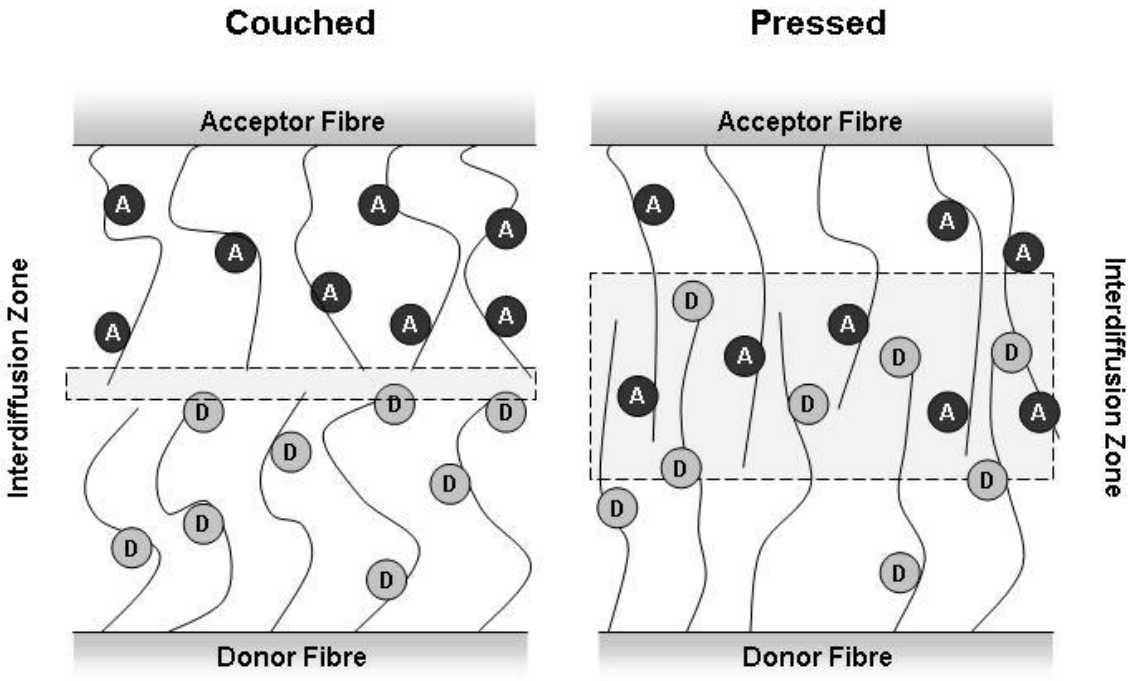

Figure 63. Interdiffusion mechanism during wet pressing at the fibre interface

While images are useful tools for demonstrating how individual fibre interfaces appear, the variation in natural pulp fibres makes it difficult to get quantitative information by comparing single images. A more useful data analysis incorporates the FRETN data from many fibre-fibre crossings into histograms. The FRETN values from every pixel in all fibre crossings for a given condition are divided into bins and then normalized for the crossing area. The crossing area is calculated planimetrically and is necessary in order to help account for the natural variation of fibre dimensions as well as the large size difference between the viscose and white spruce fibres.

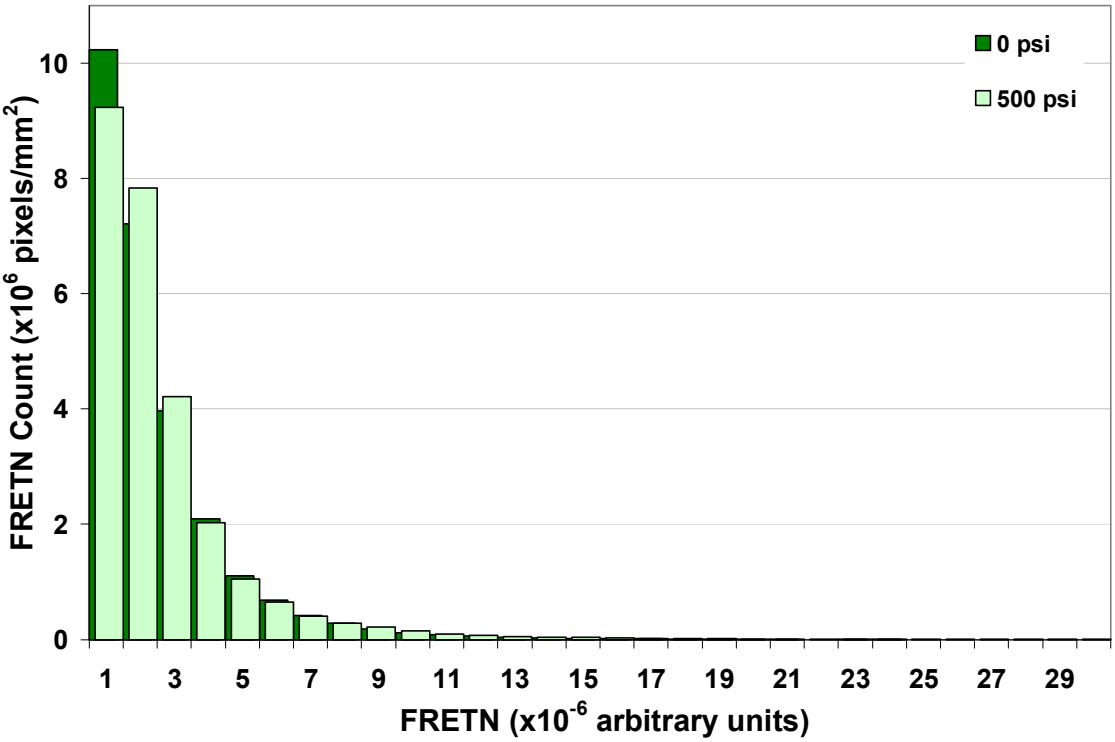

Figure 64. Image histogram for pressed viscose fibre crossings

The response to wet pressing is shown as a histogram for the viscose fibres in Figure 64 and for the white spruce fibres in Figure 65. The viscose histogram confirms the observation from comparing the images and shows almost no difference in the FRETN pixel distribution between low and high wet pressing values. Meanwhile, increased wet pressing for the white spruce fibres shifts the FRETN pixel distribution towards higher FRETN values. The number of FRETN pixels with lower values decreases while the number of higher value FRETN pixels increases. This suggests that the material from the two fibres that comprises the interface is in closer proximity.

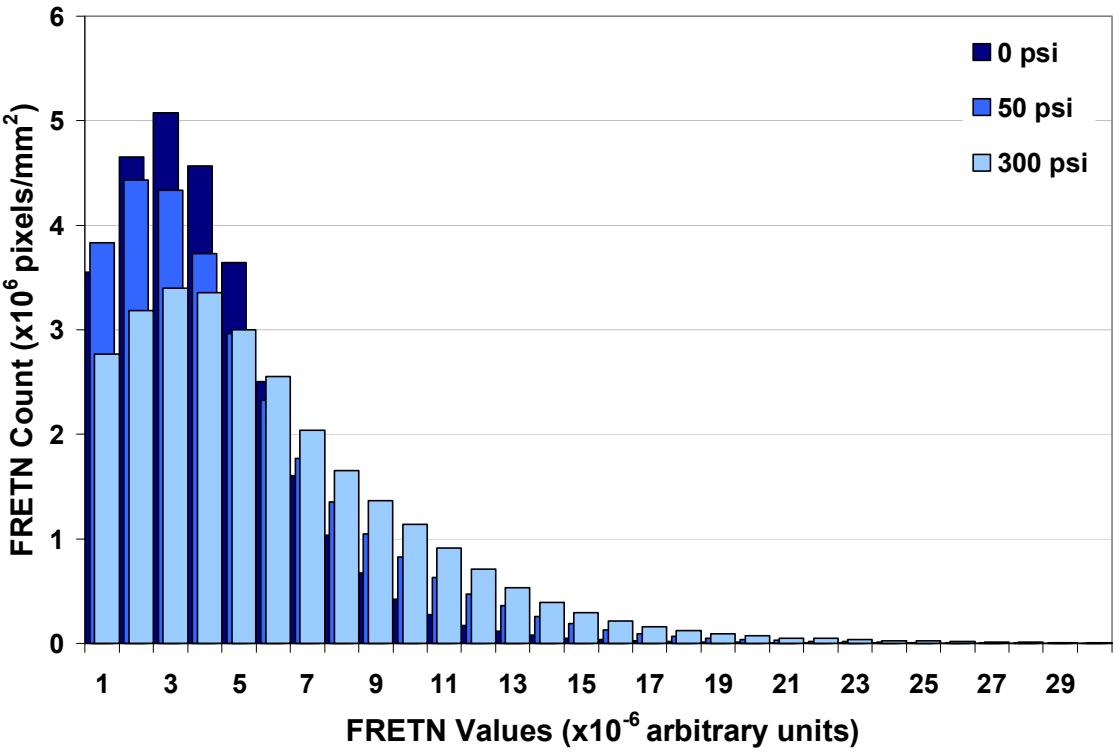

Figure 65. Image histogram of FRETN pixels for pressed white spruce fibres

Viscose images generally had large areas of very low FRETN values even at high pressing levels. However, the author has observed that sheets formed of viscose fibres had very little structural coherence indicating that low FRETN values are not relevant to inter-fibre bonding. This corroborates with other studies showing little bonding between unmodified regenerated cellulose fibres [214, 230]. McIntosh and Leopold [212] observed that fibre-shive joints had bond strengths that were seven times higher than those exhibited by fibre-cellophane strip joints, suggesting that fibres had much higher bonding capacity with each other than with cellophane. Mohlin [231] later observed higher bond strengths for

fibre-fibre joints versus fibre-cellophane joints as well, but not to the same degree. She postulated that McIntosh and Leopold may have used once dried cellophane with less bonding capability than the never-dried cellophane she had prepared in the laboratory.

These observations by Mohlin and McIntosh tangentially support the findings in this work that natural lignocellulosic fibres have increased bonding over regenerated cellulose fibres. The most likely explanation is due to their capability for increased interdiffusion of lower molecular weight components. The large FRETN values observed in spruce fibre interfaces likely result from areas of increased interdiffusion and are likely to contribute greatly to the ultimate strength of the joint. In this study, all values greater than $1x10^{-5}$ FRETN arbitrary units were considered to be close enough for significant molecular interaction.

A 2^3 factorial screening experiment was also executed to determine whether common papermaking variables have a statistically significant effect on whatever the FRETN signal is actually measuring. Fibre fraction, wet pressing and refining were chosen as the variables to analyze. Each of these variables can be relatively easily manipulated by the papermaker. The Bauer McNett fibre classifier fractionates pulp fibres primarily by fibre length using several adjustable mesh screens. While fibre length itself would not be expected to matter to fibre bonding, fibre length does generally correlate with cell wall thickness and fibre coarseness [232, 233]. Fibre coarseness is a bulk measurement defined as the

mass of fibres per unit fibre length with units of mg/100m. Therefore fibre coarseness is related to cell wall thickness and cell wall density. The impact of wet pressing has already been discussed and explored to a certain degree. Lastly, refining is often used in tandem with wet pressing to improve the bonding strength in many paper grades. Refining introduces mechanical energy into the fibre which results in a wide variety of desired effects including fibre straightening, external fibrillation and internal fibrillation or delamination. Unfortunately it can also reduce fibre length via cutting and introduce a number of different modes of fibre damage.

The experiment was designed by JMP statistical analysis software and then the results were analyzed using the same program. Eight different conditions using high and low values of each of the three variables were prepared and analyzed in a randomized order determined by the software. Twenty crossings were analyzed per condition with MATLAB. The average FRETN/crossing area values from Excel were then input into JMP for linear regression analysis. Table 23 shows the results of this analysis. The JMP software deems a variable to be significant at the 95% confidence level if the probability>|t| is less than 0.05. By this criterion, both wet pressing and fibre fraction had a significant effect on the area normalized average FRETN value for the white spruce fibre crossing. This is certainly an expected result for wet pressing given the previous results but perhaps less so for the fibre fraction. Increased fibre length led to decreased

FRETN values which suggests that the thicker cell wall and higher coarseness that accompanies fibre length is likely responsible.

Table 23. Screening experiment results

Effect	Average FRET/area Probability >|t|	Significant
Wet Pressing	0.02	Yes
Refining	0.30	No
Fibre Fraction	0.01	Yes

It is surprising that refining did not have a statistically significant effect on average FRETN values. Previous unpublished experiments suggested that the impact of refining on FRETN was actually slightly negative. Although this experiment suggests these results are not statistically significant, that result was essentially replicated in the screening experiment. Refining is a very complicated process that affects many different fibre properties, but it is possible that refining improves fibre bonding almost strictly through increased relative bonded area. Furthermore, given the fact that FRETN area/crossing area is relatively invariant, this increased relative bonded area is achieved by generating more conformable fibres capable of forming more bonds per fibre rather than more bonded area per crossing.

It should be noted that these results seem to contradict Page's recent interpretation of Nordman bond strength [234]. Page speculated that specific bond strength remains constant with wet pressing, but that it must increase with increased beating. There are a variety of possible explanations for this lack of agreement. While it is likely that higher FRETN signal is proportional to a

reduced distance between dyed materials on each fibre, it is not necessarily the case that this will always lead to higher joint strength. For example, it is possible that wet pressing also introduces stress concentrations into the joint which reduces the ultimate shear strength of the joint. This does not preclude utility of the technique but rather suggests some limitations on the interpretation of the results. It is also possible that the classical problems surrounding bonded area determination by light scattering prevent proper explanation of Nordman bond strength.

7.4 Conclusions

Further verification of the FRET microscopy technique was achieved in this work via the application to wet pressing. Image analysis of fluorescence micrographs of both natural and regenerated cellulose indicates a FRET signal is being produced at fibre crossings and that it can be manipulated with wet pressing load. The distribution of image pixels shifts towards larger FRETN values with increased wet pressing for bleached white spruce fibres. The pressing response observed in this work combined with consideration of the material behaviour of viscose fibres indicates that low FRETN values may not be relevant to bonding. The screening experiment indicated that the effects of wet pressing and fibre fraction on FRETN signal are statistically significant, but that the effect of refining is not significant.

Chapter 8: Cellulosic Fibre Interface Development during Drying

8.1 Introduction

Fibre bonding is critical to the material properties of a finished sheet of paper. Although the properties of the fibres themselves dictate the potential ultimate strength of paper, the realization of that potential is determined by the network's ability to distribute stresses efficiently. Fibre-fibre bonds are solely responsible for distributing stresses in paper and thus their physical and chemical properties have justifiably been the focus of many researchers both past and present [45, 52, 53, 71, 166, 212, 217, 231, 235].

Although water is obviously important to the formation of a wet-laid fibre network, the use and presence of water also has a distinct impact on the final properties of a paper sheet. Campbell first noted that fibers were drawn together by the surface tension forces caused by the capillary action of receding water droplets during water removal [236]. Barkas later calculated these forces to be on the order of 7.1 MPa [58] and several researchers have shown that web forming and drying with alternative solvents results in lower levels of fibre bonding [92]. Besides drawing fibre surfaces close together, water has also been implicated in fibre conformability, plasticization of fibre components [218], as well as an active participant in interfibre hydrogen bonding [57]. The overall importance of water to interfibre bonding is well summarized in McKenzie's application of Voyutskii's [113] diffusion theory of adhesion to fibre bonding [75]. The presence of water should aid in enhancing diffusion of fibre surface components due to

plasticization and improved mobility of fibrils and low molecular weight surface polymers such as hemicellulose.

The result of interdiffusion of fibre components can be measured on the 1-10 nanometre scale using fluorescence resonance energy transfer (FRET) [237]. FRET can be described as a long range dipole-dipole interaction between two fluorescing dye molecules that results in a non-radiative transfer of excitation energy from a donor dye to an acceptor dye [210]. When two fluorophores are within 1-10 nm of each other and have sufficient overlap of the donor emission spectra and the acceptor absorbance spectra, FRET manifests itself as emission at the characteristic wavelength of the acceptor with excitation of the donor. The distance dependence of the phenomenon is due to the fact that the dipole-dipole interaction shows a characteristic inverse sixth power relationship between the energy transfer efficiency and the donor-acceptor distance [134].

The rate of energy transfer is also highly dependent on the overlap of the donor emission and acceptor excitation spectra. The solvent index of refraction and the dye concentration, and the orientation of the two oscillating dipoles in space are also contributing factors. This phenomenon has been used extensively in biochemistry to study the dynamics of proteins and other biomacromolecules [134].

FRET can be applied to cellulosic fibre interfaces via covalent labelling of fibre carbonyls with hydrazide derivatives of an appropriate fluorescent dye pair. The distance dependent interaction between the dye pair can be imaged with fluorescence microscopy when a fibre crossing is constructed from fibres containing the donor and acceptor dye. Our previous work utilized fluorescence resonance energy transfer (FRET) to investigate the response of viscose rayon and bleached kraft pulp fibre crossings to wet pressing [237]. These results lead us to conclude that cellulosic fibre bonds are well explained by the diffusion theory of adhesion.

8.2 Materials and Methods

8.2.1. Fibres and Chemicals

Mill produced, OD(E+O+P)DED bleached, never dried white spruce (*Picea glauca*) kraft pulp was provided by Alberta Pacific (Boyle, Canada). The pulp was screened using a Valley Screen as per TAPPI Standard Method T 278 sp-04. The pulp (200 oven-dry grams) was then washed in a Buchner funnel with deionized water (10 x 4 L). The processed pulp brightness was ISO 88.2. Samples were then PFI refined 300 revolutions and then fractionated in the Bauer-McNett fibre classifier to remove fines and short fibres. The fibres retained on an R14 screen were used for this study with a length weighted average fibre length of 3.10 mm as determined by the Fibre Quality Analyzer (OpTest Equipment, Hawkesbury, Canada).

The two fluorescent dyes used in this work, 7-diethylaminocoumarin-3-carboxylic acid hydrazide (DCCH), and fluorescein-5-thiosemicarbazide (FTSC), were purchased from Invitrogen (Carlsbad, CA, USA) and used without further purification. All other chemicals in this research were purchased from Sigma-Aldrich, and used as described below.

8.2.2. Preparation of Dyed Fibre

The hydrazide dyes were applied to the fibres using a method adapted from Anderson [167]. A 2% suspension of cellulose fibre (oven dry weight basis) in the appropriate solvent (i.e. FTSC: N,N,-dimethylformamide, DCCH: methanol), containing 1.6 mmol/L of dye, and 1.8 mmol/L of HCl was magnetically stirred in the dark overnight at room temperature. After dyeing, the fibres were briefly washed with their respective solvents and then subjected to a mild sodium borohydride reduction (1.3 mmol/L $NaBH_4$ in DMF) for 60 min at room temperature. The dyed pulp was rinsed with DMF and then Soxhlet extracted with acetonitrile overnight to insure that non-specifically bound dye was removed.

8.2.3. Preparation of Fibre Crossings

Single fibre samples were prepared according to methodology developed by Lowe *et al* [170] with several modifications. A suspension containing an equal mixture of DCCH and FTSC dyed fibres was prepared by diluting 25 mg of each dyed pulp to 1 L with 0.025 N sodium tetraborate buffer solution. Fluorescein based dyes such as FTSC are pH dependent [168] and therefore, a sodium

tetraborate buffer solution (0.025 N) was used to maintain pH 9 during the slide making process. Fibre crossings were prepared by diluting 10 mL of the fibre suspension to 500 mL with deionized water and then draining onto a 34 mm diameter 70 mesh PTFE screen (Spectrum Labs, Rancho Dominguez, USA). The fibres were transferred to glass slides with couching and then wet pressed at different loads between wet blotter papers. Slides were allowed to dry and condition at 50% relative humidity and 23°C. Images were also acquired under these conditions.

8.2.4. Fluorescence Microscopy

Fluorescence micrographs of fibre crossings were collected using an inverted reflected light microscope system. The microscope was equipped with a fluorescence disc that allows quick changing of three different filter sets without disturbing the sample, a 50 watt metal halide light source, and a Hamamatsu ORCA-ER digital camera. Exposure time was held constant between filter set changes and fibre crossings were minimally exposed to excitation light to prevent photobleaching. Each fibre crossing was analyzed by collecting three fluorescence micrographs using three different custom filter sets manufactured by Chroma Technology Corp. (Brattleboro, VT). The custom filter sets are designed to capture three separate signals from each fibre crossing: the donor emission (D), the directly excited acceptor emission (A), and the acceptor emission due to FRET (F).

8.2.5. Image Analysis

The three fluorescent micrographs of the fibre crossing are analyzed using Gordon's 1997 FRETN algorithm [157]. The FRETN correction method requires values for samples containing exclusively donor or acceptor dye. These values are obtained using average gray scale intensities from adjacent non-crossing regions on each of the fibres using three filter sets. Donor only, acceptor only, and both donor and acceptor conditions are measured with each of the three filter sets giving a total of nine values for the analysis. These nine values are then used to calculate the corrected FRETN value at each pixel in the crossing as described in Chapter 4.11.

8.2.6. Collecting Images of Single Fibre Crossings During Drying

Fibre crossings were prepared as described above with some key modifications. After wet pressing, the sandwich of glass slide, fibres, PTFE screen and wet blotters is transferred glass slide down onto the microscope stage. Once an appropriate crossing containing an FTSC-dyed fibre and a DCCH dyed fibre is identified, the PTFE screen and wet blotters are removed and the timer is started. The sample is refocused and three fluorescent micrographs are collected with each of the three filter sets. This procedure is repeated at various time intervals.

8.2.7. Collecting Images for Rewetting and Pressing

Slides of fibre crossings were first prepared as above with only couching followed by drying and conditioning overnight at 50% relative humidity and 23°C. After

fluorescence micrographs of these crossings were obtained as described above, the slides were covered with the PTFE screen and two wet blotters and pressed to either 340 kPa or 2070 kPa for 5 minutes at 25°C. After drying and conditioning overnight, the same crossings were found again using distinguishing features such as the fibre shape, orientation, location of pits, cell wall damage or kinks. Once identified, images of the crossings were collected for comparison.

8.3 Results and Discussion

8.3.1. Development of Fibre Bonds with Drying

Although the authors have observed water coursing through fibre lumens in the seconds immediately following blotter removal using standard microscope optics, the fibre crossings typically have little or no free water present after wet pressing regardless of press load. It is likely that the measurements are taken after the Campbell effect when the fibres on the slide have an estimated solids content of 40-50%. Thus the water removed is limited to what is contained within fibre walls and within the fibre interface. Since wet fibres are swollen, it should be expected that drying will result in the contraction of fibre material in the interface during drying. This shrinking combined with the interdiffusion of cell wall polymers should bring the dye pairs closer together on average and give higher energy transfer values with time.

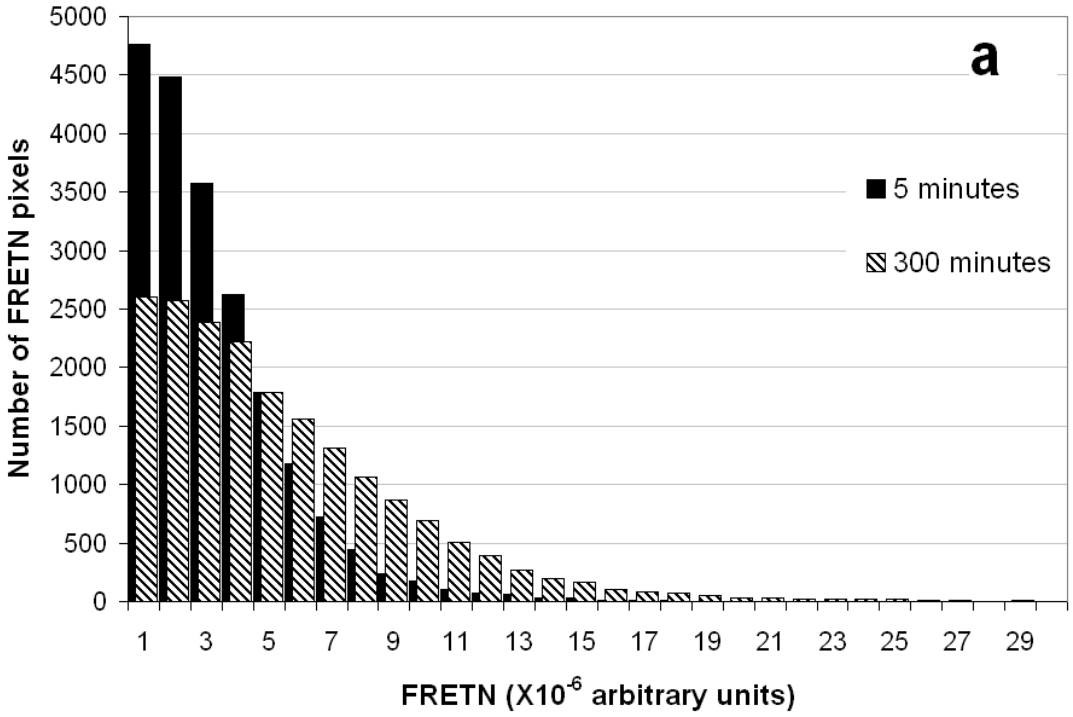

Figure 66. Image histogram of FRETN pixels for a single crossing

After 5 minutes and 300 minutes drying time

The image histogram in Figure 66 expresses the images taken at two different times of a single fibre crossing as a distribution of pixel values. After five minutes drying time, there are a large number of low value FRETN pixels. However, as drying progresses, the average value clearly increases as the distribution flattens out and the number of pixels with higher FRETN values increases after drying for 300 minutes. This indicates that the average distance between dye molecules on each fibre is decreasing as water is removed from the fibres by evaporation.

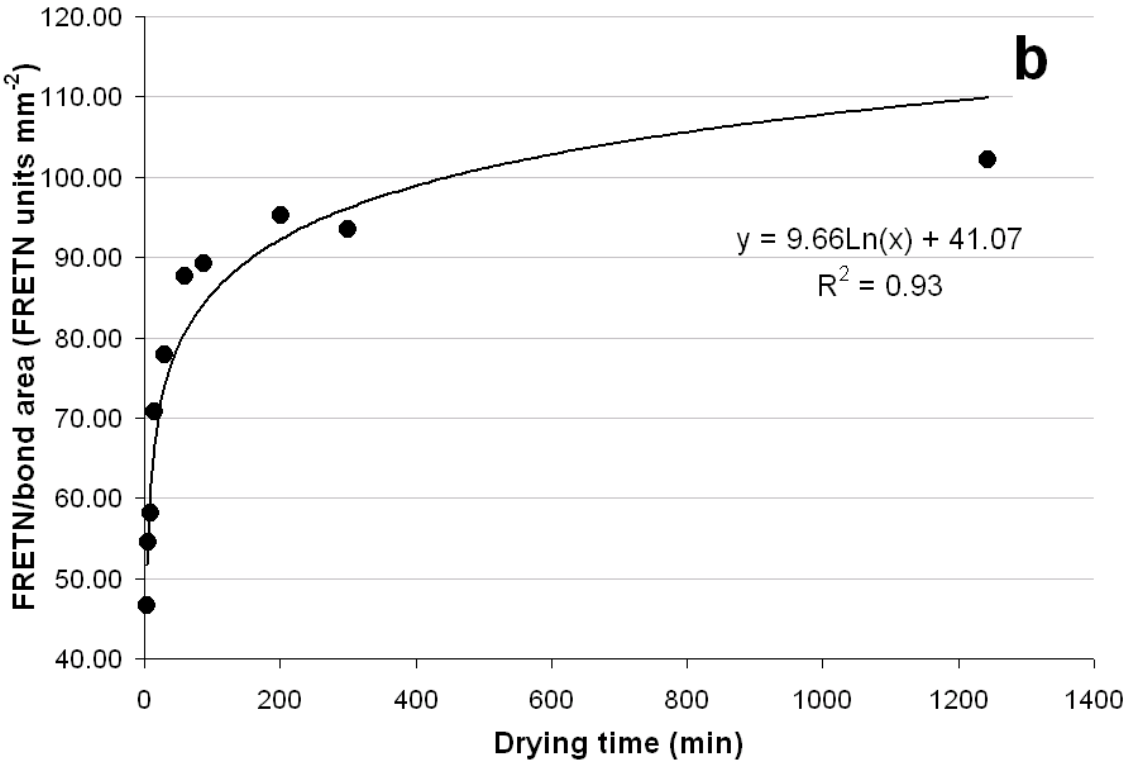

Figure 67. Total FRETN/bond area versus drying time for a single crossing

The graph in Figure 67 shows the total FRETN value normalized for the projected bond area for the same fibre crossing. There is a strong logarithmic relationship between the FRETN signal and drying time for the first 300 minutes. After that point, the FRETN value reaches a plateau and thus begins to deviates from a logarithmic relationship. Figure 68 shows the same relationship for fibre crossings pressed to three different levels. The logarithmic relationship appears to hold regardless of wet pressing load.

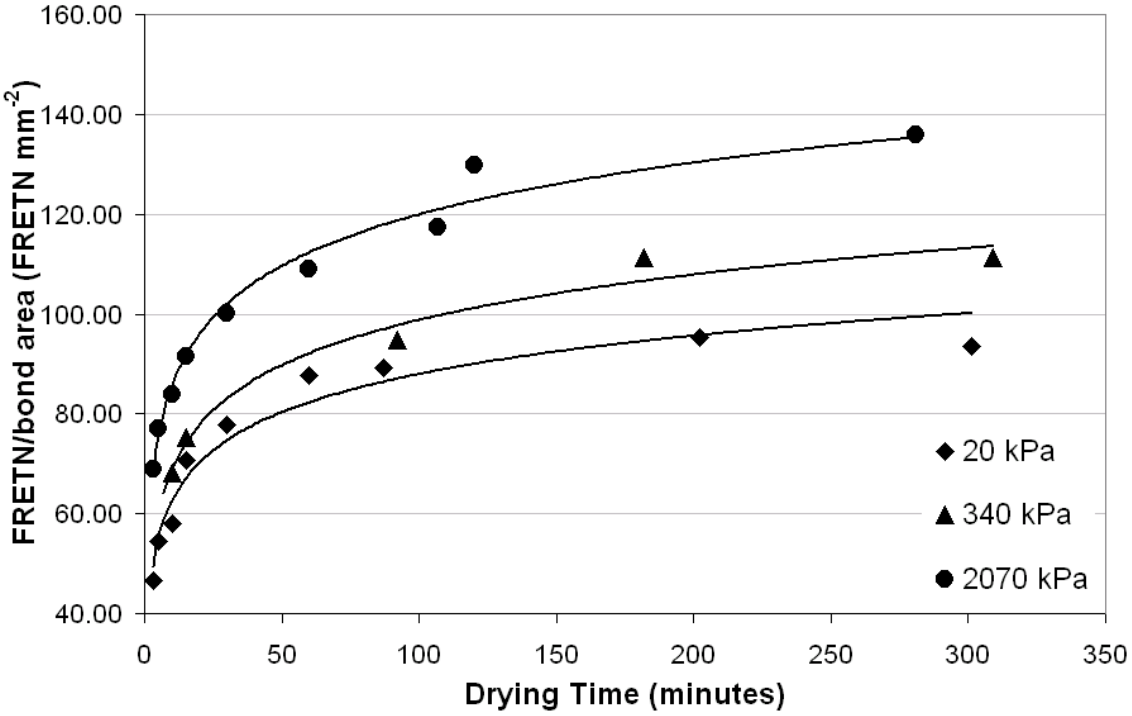

Figure 68. FRETN response with drying time for single fibre crossings

Samples were wet pressed with three different loads

8.3.2. Response of Fibre Bonds to Rewetting and Pressing

Several authors have noted that the fibre-fibre joint strength of chemical pulps decreases after being once dried [238-240]. Gurnagul *et al* (2001) attributed this decrease in bonding to the reduced ability of surface molecules to interdiffuse after a drying cycle. Figure 69 shows representative histograms for a single fibre crossing before and after rewetting and wet pressing at 340 kPa. Even after a crossing is once dried, there is a dramatic change in the fibre bond upon rewetting and wet pressing as expressed by the shift in the distribution of FRETN pixels. Figure 70 shows the average relative increase in FRETN normalized for the bond area for fibre crossings that were rewetted and pressed at 340 kPa and

2070 kPa. The FRETN/bond area increases significantly for both pressing loads, but the higher pressing load results in a greater relative increase.

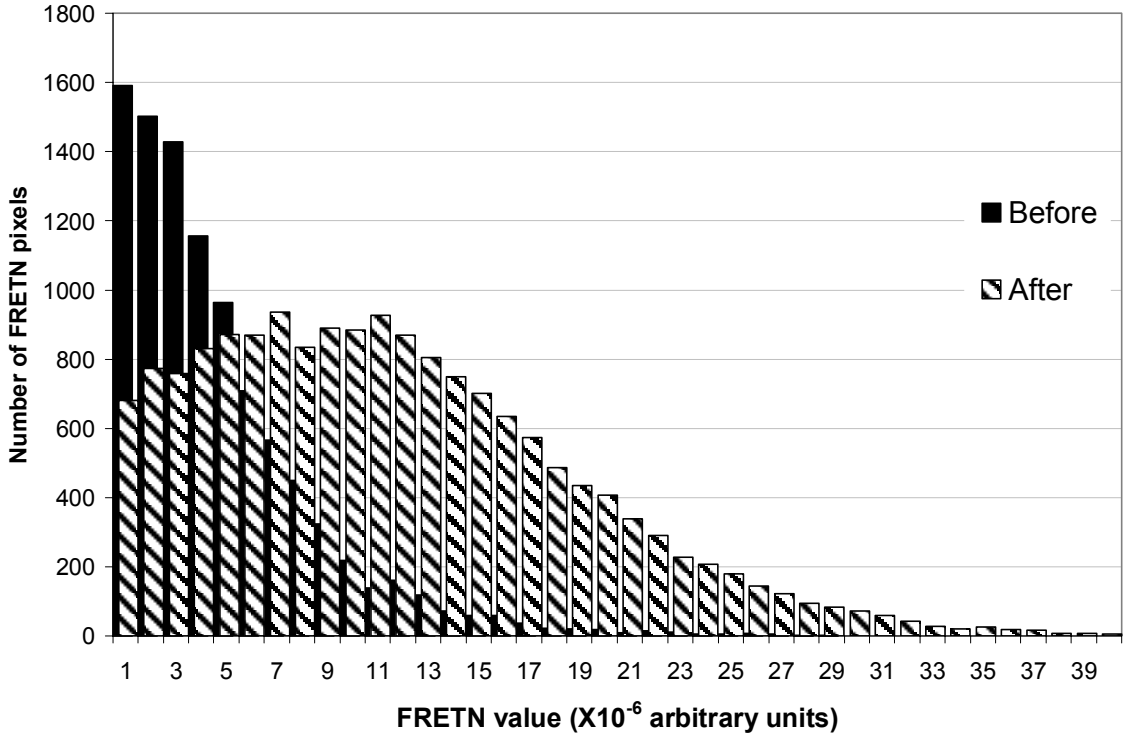

Figure 69. Image histograms of a single fibre crossing before and after rewetting and wet pressing at 2070 kPa

This data indicates that the cell wall components in the fibre interface are still mobile and susceptible to swelling upon rewetting even after air drying at 50% relative humidity. It is interesting to note that Torgnysdotter and Wagberg were able to mitigate the effects of drying on fibre/fibre joint strength using polyelectrolyte multilayers of adsorbed polyallylamine hydrochloride and polyacrylic acid [240]. Other work from this group has suggested that these films are water-rich and thus more capable of retaining interdiffusion capability than natural fibre surface polymers [241].

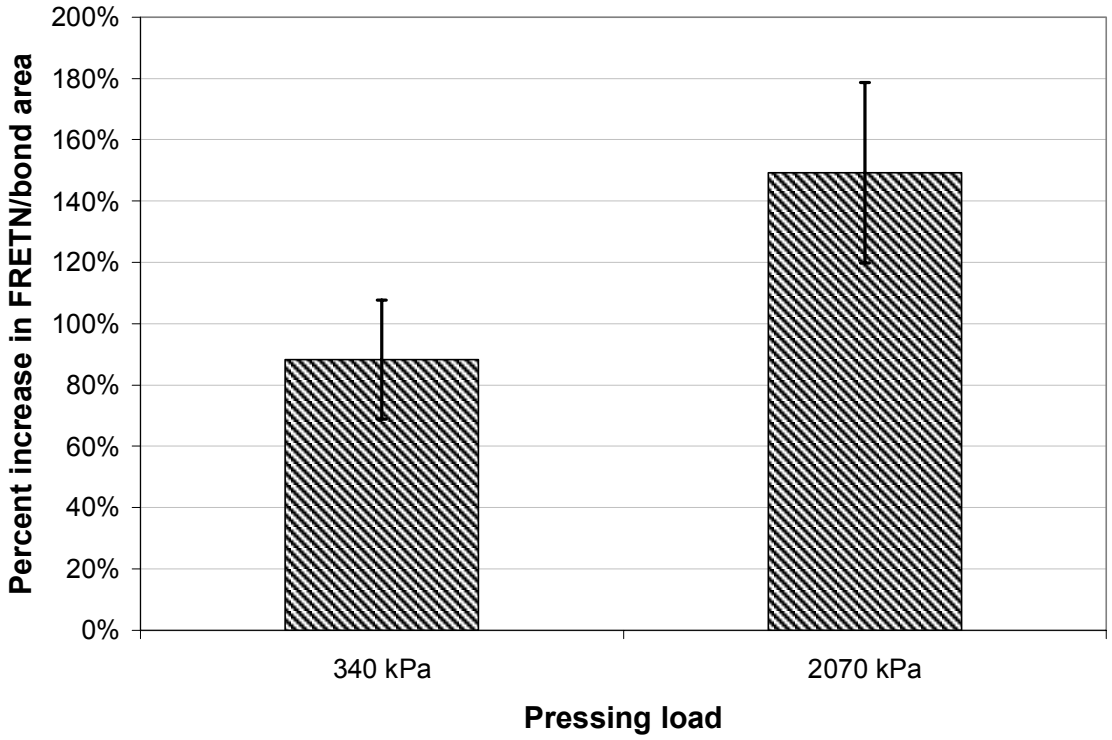

Figure 70. Increase in FRETN/bond area after rewetting and wet pressing.

The standard error bars are calculated from the raw data for all fibre crossings in a given condition. Ten crossings for 2070 kPa and 18 crossings for 340 kPa.

It is useful to consider these results in the context of paper recycling. The presence of water in the fibre interface of air dried fibre crossing may prevent hornification at the fibre surface which otherwise reduces fibre bond strength in recycled papers. In recycled papers, the original paper is fully re-slushed and thus only a small percentage of fibre crossings in the reformed sheet will involve formerly bonded areas that were essentially “protected” from hornification within bonds.

8.4 Conclusions

The results of this study give valuable information about the structure and behaviour of the fibre bond. FRET microscopy provides evidence that there is considerable fibre bond development after wet pressing and that FRET is capable of observing coalescence of the fibre-fibre interface during drying. Furthermore it appears that the coalescence of the interface has a logarithmic relationship with drying time. The FRET signal from once-dried fibre crossings increases dramatically after rewetting and wet pressing for a second time. This indicates that the material within the fibre bonds is still compliant after a single drying cycle and that the interactions between fibre components are likely different from those observed in hornification. These results serve as further evidence that FRET is occurring in this system as measured.

Chapter 9: Investigating Adhesion in Xylan and Cellulose Films with FRET Microscopy

9.1 Introduction

There are several potential explanations for the observed difference between the morphologies of viscose and wood fibre crossings as measured by FRET microscopy in previous chapters. Perhaps the most appealing explanation is that the surfaces of wood fibres contain higher levels of lower molecular weight hemicellulose that is susceptible to interdiffusion. This interdiffusion of cell wall components leads to shorter distances between the FRET dye pair and thus a higher FRETN signal is observed for natural fibre crossings versus regenerated cellulose fibres.

The importance of hemicellulose to the fibre-fibre bond has been observed by numerous researchers [69, 75, 212, 217, 242]. In all cases higher levels of hemicellulose correlate with higher bond strength for both paper manufactured from natural wood fibres and for individual fibre joints. McIntosh found that the bonding strength of kraft fibres decreased as the cook progressed. He also observed that holocellulose fibres from the same pulps, which retain almost all of the native hemicellulose, had very high bond strength as shown in Table 24. Touchette and Jenness found that papers formed from holocellulose fibres had almost four times the bond strength as that of unbeaten kraft fibres [243].

Table 24. Bonding strength of kraft fibres with different cooking times

Peracetic acid delignified loblolly pine summerwood kraft pulps from McIntosh [242]

Kraft Cooking Time (min)	Load at Bond Failure (g)
Holocellulose (0)	26.5
10	9.9
41	5.4
85	3.4
150	2.8
240	4.1
455	2.5

More evidence for this theory can be derived from observations of the joint strength of regenerated cellulose fibres. Sheets formed from regenerated in our laboratory were observed to have very little structural coherence and other studies have discovered low bonding levels between unmodified regenerated cellulose fibres [214, 230]. McIntosh and Leopold [212] observed that fibre-shive joints had bond strengths that were seven times higher than those exhibited by fibre-cellophane strip joints. Mohlin [231] later observed higher bond strengths for fibre-fibre bonds as well, but not to the same degree. She postulated that McIntosh and Leopold may have used once dried cellophane with less bonding capability than the never-dried cellophane she had prepared in the laboratory.

An appropriate approach to test the impact of hemicelluloses is to design a model system using hemicellulose and cellulose films. Isolated hemicellulose and cellulose can be dyed using similar methodology to the dyeing of cellulosic fibres and then the contact zone between two films can be probed in a similar manner as before with the fibres.

9.2 Materials and Methods

9.2.1. Materials

Oat spelt xylan, xylitol and Avicel PH-101 microcrystalline cellulose were purchased from Sigma-Aldrich and used without further purification. 7-diethylaminocoumarin-3-carboxylic acid hydrazide (DCCH), and fluorescein-5-thiosemicarbazide (FTSC), were purchased from Invitrogen (Carlsbad, CA, USA) and used as received. Glass slides were cleaned by first rinsing with deionized water followed by immersion in a 7:3 mixture of concentrated sulphuric acid and 50% hydrogen peroxide for 60 minutes and then further rinsing with Barnstead nanopure water. All other chemicals were purchased from Aldrich and used as received.

9.2.2. Preparation of 2,3-Dialdehyde Cellulose

In the event that the films comprised of microcrystalline cellulose did not yield sufficient fluorescent signal, the cellulose was subjected to periodate oxidation using the method of Varma and Kulkarni [171]. Four grams of Avicel PH-101 was suspended in 45- 60 mL deionized water in a round bottom flask with a magnetic stirbar in a water bath at 45°C. Sodium metaperiodate was dissolved in 15-30 mL deionized water and added dropwise to the cellulose suspension with an addition funnel for 60 minutes. After periodate addition had finished, the reaction mixture was further stirred at 45°C for an additional 2-10 hours. Reaction times, volumes and periodate charges are summarized in Table 25. Upon completion, the mixtures were filtered and then thoroughly washed with

approximately one litre of deionized water. The samples were then frozen and lyophilized for 48hrs to remove water.

Table 25. Reaction conditions for periodate oxidation of cellulose

Sample	Total Reaction Time (min)	$NaIO_4$ Added (g)	Starting Volume (mL)	Added Volume (mL)	Total Volume (mL)
1	180	0.86	60	15	75
2	660	1.24	55	20	75
3	660	2.65	45	30	75

9.2.3. Dyeing Polysaccharides

FTSC-xylan was prepared by adding 38 mg of FTSC and 100 µL 1 N aqueous HCl to 1.00 g of oat spelt xylan suspended in 15 mL N,N-dimethylformamide in a 25 mL glass vial. DCCH-xylan was prepared in a similar fashion by the addition of 25 mg DCCH and 120 µL 1 N aqueous HCl to 1.00 g of oat spelt xylan suspended in 15 mL methanol. The dye loading is 90 µmol/g xylan, which is considerably higher than that used for fibres because the number of available reducing ends is assumed to be considerably higher than in the fibres. Dialdehyde cellulose was dyed by adding 65 µL of 1N HCl and 25 mg FTSC or 15 mg DCCH to 0.55 g dialdehyde cellulose in 15 mL of DMF or methanol respectively.

The reaction mixtures were stirred magnetically in the dark overnight at room temperature in vials wrapped in foil. After the reaction time had commenced, the dyed samples were filtered in a Buchner funnel, briefly washed with their respective solvents and then subjected to a mild sodium borohydride reduction (1.3 mmol/L $NaBH_4$ in DMF) for 60 min at room temperature. The dyed samples

were again filtered, rinsed with DMF, and then soxhlet extracted with acetonitrile overnight to remove any non-specifically bound dye.

9.2.4. Synthesis of Trimethylsilyl Cellulose

Trimethylsilyl cellulose (TMSC) and trimethylsilyl dialdehyde cellulose (TMS-DAC) were prepared using a modified procedure from Kontturi *et al* [172-175]. 0.5 grams of cellulose or dialdehyde cellulose was dissolved in 50 mL of 9% (w/w) lithium chloride (LiCl) in N,N-dimethylacetamide (DMAc) by stirring in a 100 mL three-neck round bottom flask in a water bath at 60°C for 3 hours. This method is modified slightly from McCormick *et al* dissolution of cellulose in LiCl/DMAc [176]. After the dissolution was complete and the solution was totally clear, the water bath was heated up to 80°C and 20mL of hexamethyldisilazane was added dropwise for 1 hour while flushing with nitrogen gas. The mixture was then allowed to cool for 1 hour and then 10 mL methanol was added to induce precipitation of TMS-DAC which was left overnight. The precipitate was collected by filtration and then purified by dissolving in 20 mL tetrahydrofuran and then filtering that solution into 500 mL of methanol. The re-precipitated dyed TMS-DAC was then collected by filtration and allowed to air dry. The product was fully soluble in toluene at concentrations up to 80 g/L.

9.2.5. Solid State CP/MAS ^{13}C NMR Characterization

Solid state CP/MAS ^{13}C NMR spectra of carbohydrate samples were recorded by Dr. Yunqiao Pu at room temperature on a Bruker Advance/DMX-400 instrument

operating at 100.06 MHz using a MAS WB CP BB VTN-BL 4 mm probe and ZrO_2 rotors. The MAS spin rate was 5 kHz. Acquisition was performed with a CP pulse sequence using 4.5 μs pulse, 2.0 ms contact pulse and 5.0 s delay between repetitions. 8000 scans were accumulated for each sample.

9.2.6. Fourier Transform Infrared (FTIR) Spectroscopy

Fourier Transform Infrared (FTIR) transmission spectra were collected for each of the carbohydrate samples in the solid state using a Magna-IR System 550 (Nicolet Instrument Corporation). Pellets were formed by pressing mixtures of 3 mg of dry sample and 500 mg of dry spectroscopy grade potassium bromide (KBr) at 15000 psi for 3 min. under vacuum.

9.2.7. Molecular Weight Distribution Analysis

Molecular weight distributions of cellulose and xylan starting materials were determined by Dr. Yunqiao Pu as follows:

9.2.7.1. Molecular weight of cellulose samples

Avicel PH-101 microcrystalline cellulose samples were thoroughly dried over P_2O_5 under vacuum. The dried samples were derivatized with phenyl isocyanate. About 15 mg of dry cellulose sample was soaked in 4 ml anhydrous pyridine in a 25 ml flask, and 0.5 ml phenyl isocyanate was added. The flask was sealed with Teflon-lined cap. The reaction mixture was stirred magnetically in an oil bath at 65 C for 2 ~ 3 days until the cellulose was completely dissolved. After the

reaction completed, the solution was cooled and 1 ml methanol was added to consume unreacted phenyl isocyanate. The mixture was then poured into 100 ml water-methanol (3:7). The precipitated cellulose tricarbanilates were purified through centrifuging at 8000 rpm by repeated washing with water-methanol 3 times, and water 2 times. The cellulose tricarbanilates were then freeze-dried and vacuum dried for analysis.

The molecular weight (MW) and molecular weight distribution analysis of the cellulose tricarbanilates was determined using a Hewlett Packard 1090 series HPLC system consisting of in-line filter and an auto-sampler, a UV detector, and three columns of Styragel HR1, HR3 and HR4 (Waters Inc., USA) linked in series. Tetrahydrofuran (THF) was used as the eluent with a flow rate of 0.8 ml/min at room temperature. The system was calibrated with standard narrow polystyrene samples. The cellulose tricarbanilate samples were dissolved in THF (1 mg/ml) and then filtered with a 0.2 μm filter. The filtered sample (10 μl) was injected into the column system with UV detection at 236 nm. Data were collected with Agilent ChemStation Rev. A.10.01 and analyzed with Agilent GPC Add-on Rev. A.02.02 software. The number-average molecular weight (M_n), weight-average molecular weight (M_w) and polydispersity index were calculated by using the same software.

9.2.7.2. Molecular weight of xylan samples

Xylan samples were collected and dried over P_2O_5 under vacuum before size exclusion chromatography (SEC) analysis. The SEC analyses were carried out using a Hewlett Packard 1090 series HPLC system consisting of in-line filter and an auto-sampler, a 1047A Hewlett Packard refractive index (RI) detector, and three columns of Ultrahydrogel 120, 250 and 500 (Waters Inc., USA) linked in series. The RI detector was set at 35° C. The eluent was 0.1 M sodium nitrate containing 0.02% sodium azide and the flow rate was 0.5 ml/min. The xylan samples were dissolved in mobile phase (1 mg/ml) and then filtered with a 0.2 µm filter. The filtered sample (10 µl) was injected into the SEC column system for analysis. Pullulan standard samples were used as narrow calibration standards. The RI detector was connected to a Hewlett Packard 35900C Multichannel Interface and the signal was processed utilizing the Agilent ChemStation Rev. A.10.01 and GPC Addon Rev. A.02.02 software.

9.2.8. Casting Xylan and Trimethylsilyl Cellulose Films

Xylan films were prepared using a modified method from Grondahl *et al.* and Gabrielli *et al.* [177, 178]. Mixtures of 0.23 g dyed xylan, 0.14g undyed xylan and 0.09 g were dissolved in 12 mL of deionized water and 4 mL of pH 11 buffer (prepared from a 1:1 mixture of 0.05 N NaOH and 0.025 M sodium tetraborate decahydrate) by stirring at 95°C for 15 minutes. After cooling to room temperature, the solution was poured into 86 mm diameter polystyrene Petri dishes. The films were allowed to dry at 50% relative humidity and 22°C for 24

hours. This gave 75 g/m^2 xylan films containing 20% xylitol as a plasticizer. The films are easily peeled from the polystyrene dishes and handled.

Cellulose films were prepared by dissolving 25 mg of dyed TMS-DAC and 225 mg blank TMSC in 8.0 mL of toluene. This required vigorous shaking and some heating. The solution was then filtered through some cotton wool to remove any dust particles and poured into a 78 mm polytetrafluoroethylene (PTFE) dish. The toluene evaporated in approximately 30 minutes and then the film was peeled from the dish. The films were desilylated by briefly soaking them in 2 N aqueous HCl for 60 seconds followed by repeated rinsing with deionized water and then soaking in 0.025M sodium tetraborate buffer for 5 minutes followed by air drying at 50% relative humidity and 22°C for 24 hours.

9.2.9. Preparation of Film Samples for Microscopy

Strips of DCCH or FTSC dyed cellulose and xylan were cut manually with a razor blade and then arranged into 12 crossings on a clean 25 X 75 mm glass slide. The strips were approximately 10 mm long and 0.25 mm in width. Cellulose crossings were then pressed by placing a PTFE screen down on the crossings along with two wet blotters followed by pressing either with a 7 kg weight (35 kPa) or in the automated press with 900 lb load for 5 minutes or 20 minutes. Xylan crossings were pressed under a glass coverslip using the same conditions without any added water. Unfortunately, it was not possible to wet press the

xylan crossings because they are nearly water soluble and deform too easily to be handled when wet.

9.2.10. Fluorescence Microscopy

Fluorescence micrographs of film crossings were collected using an inverted reflected light microscope system. The microscope was equipped with a fluorescence disc that allows quick changing of three different filter sets without disturbing the sample, a 50 watt metal halide light source, and a Hamamatsu ORCA-ER digital camera. Exposure time was held constant between filter set changes and the film crossings were minimally exposed to excitation light to prevent photobleaching. Each film intersection was analyzed by collecting three fluorescence micrographs using three different custom filter sets manufactured by Chroma Technology Corp. (Brattleboro, VT). The custom filter sets are designed to capture three separate signals from each fibre crossing: the donor emission (D), the directly excited acceptor emission (A), and the acceptor emission due to FRET (F). Images of the films were collected using 100X magnification.

9.2.11. Image Analysis

The three fluorescent micrographs of the film intersection are analyzed using Gordon's 1997 FRETN algorithm [157]. The FRETN correction method requires values for samples containing exclusively donor or acceptor dye. These values are obtained using average gray scale intensities from adjacent non-crossing

regions on each of the fibres using three filter sets as shown in Figure 2. Donor only, acceptor only, and both donor and acceptor conditions are measured with each of the three filter sets giving a total of nine values for the analysis. These nine values are then used to calculate the corrected FRETN value at each pixel in the crossing using MATLAB and the MATLAB Image Analysis Toolpak. This procedure is described in detail in Chapter 4.11.

9.3 Results and Discussion

The films prepared in this experiment are intended to mimic the contributions of hemicellulose and cellulose to the cellulosic fibre bond. Although this model has some inherent flaws that will be discussed later, this approach should provide some insight into the structure and behaviour of the fibre bond. The cellulose films prepared in this study were comprised of cellulose regenerated from its trimethylsilyl (TMS) derivative which formed nice smooth films by solvent casting from toluene. The TMS derivatives were identified by their characteristic IR and NMR spectra. The IR spectra for microcrystalline cellulose and TMSC are shown in Figure 71. The silylation of cellulose is apparent by the decrease in the OH stretch at 3600-3000 cm^{-1} and the appearance of absorption peaks due to C-Si at 1250 and 850 cm^{-1}. There is also a noticeable change at 2960 cm^{-1}, where the asymmetric stretches of CH_3 groups from TMSC are apparent.

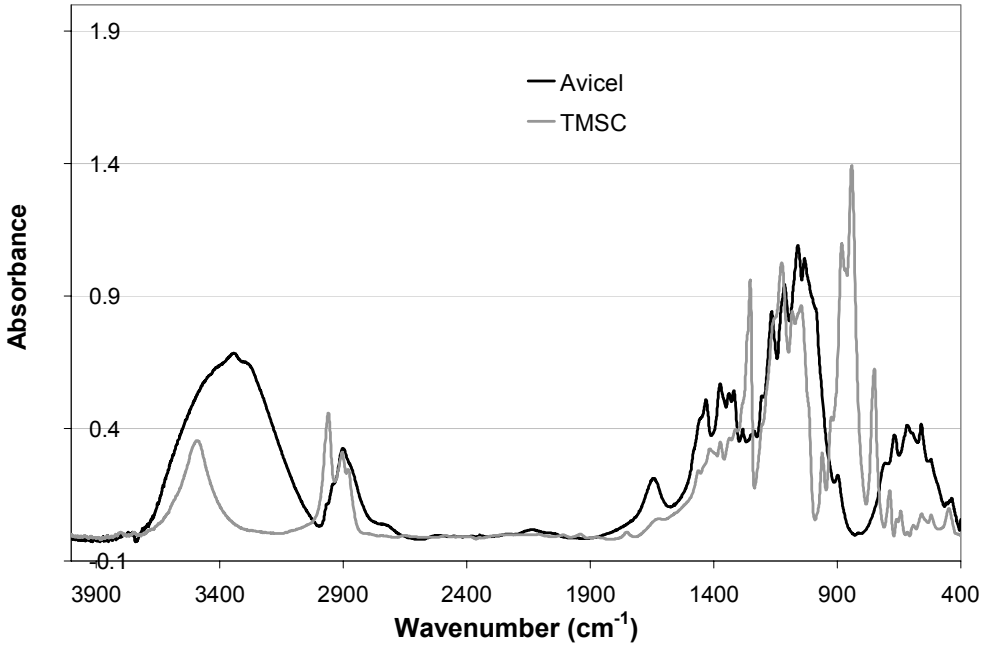

Figure 71. FTIR spectra of cellulose and TMSC

Solid state CPMAS ^{13}C NMR provides further information about the cellulose materials used in this work. Figure 72 and Figure 73 show the NMR spectra of untreated and periodate oxidized cellulose respectively. The chemical shifts are in good agreement with prior work by Varma *et al.* for CPMAS ^{13}C NMR of cellulose and dialdehydecellulose [244]. Figure 74 shows the NMR spectra for TMSC. The most noticeable difference is the appearance of the large peak at zero ppm chemical shift due to the TMS methyl groups. The spectra of TMSC also lose much of the finer structure in the 75-90 ppm range for the C2-5 carbons. The chemical shifts of the C1 and C6 carbons are much less altered compared to the untreated cellulose. In fact, it appears as though those carbons are all contained

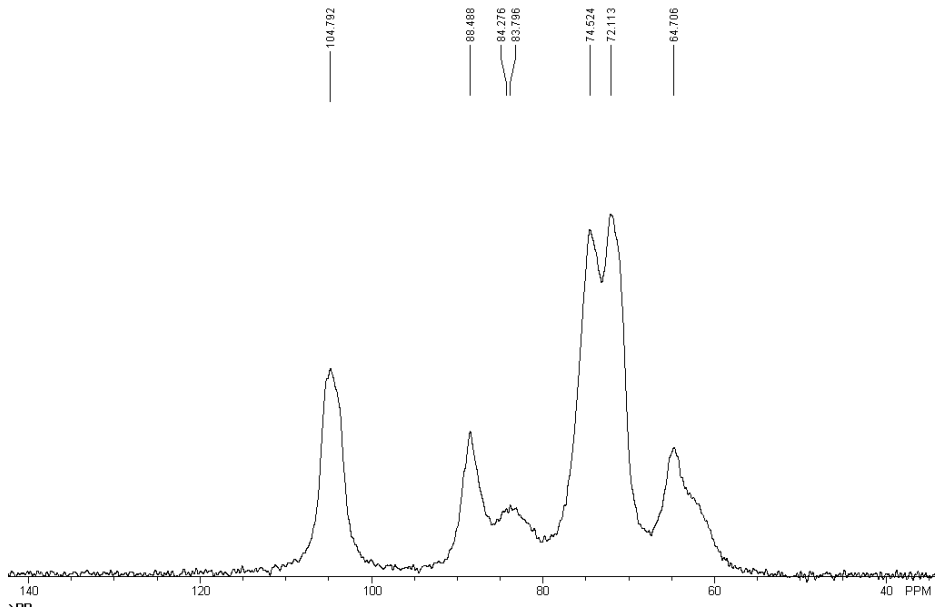

Figure 72. Solid state CPMAS ^{13}C NMR spectra of untreated Avicel PH-101 microcrystalline cellulose

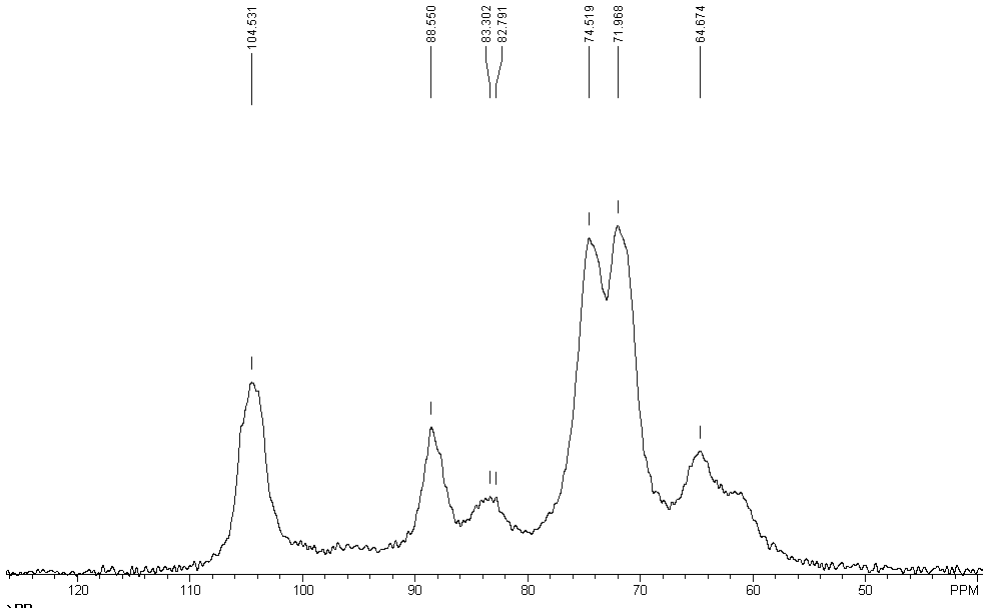

Figure 73. Solid state CPMAS ^{13}C NMR spectra of periodate oxidized cellulose

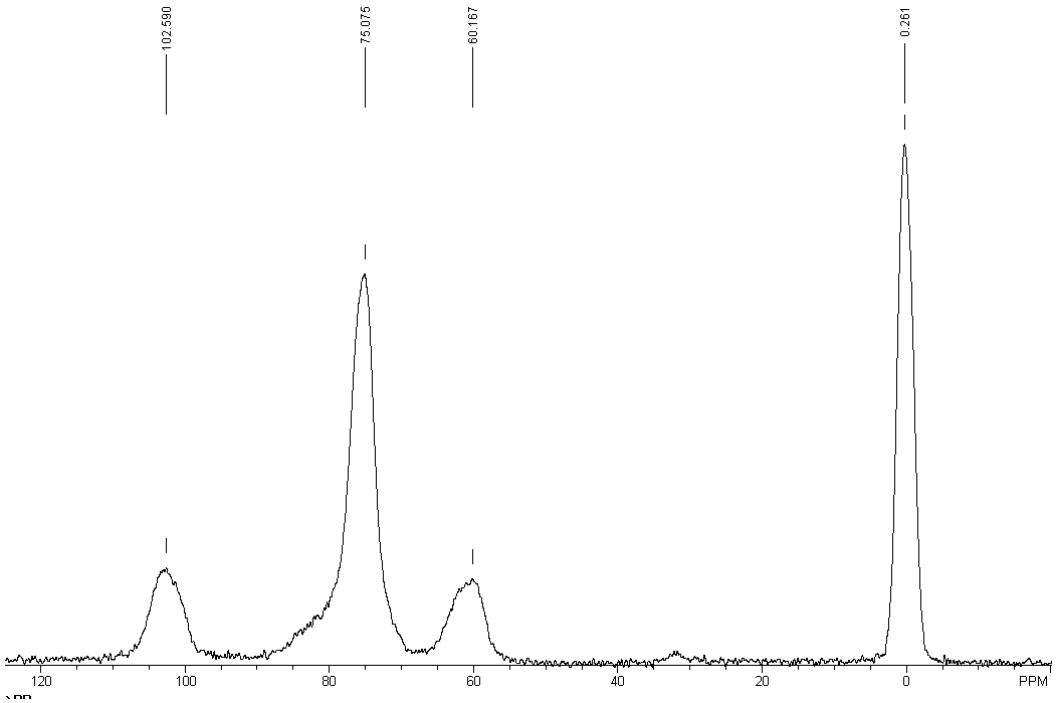

Figure 74. Solid state CPMAS ^{13}C NMR spectra of trimethylsilyl cellulose

It was also observed that the water droplet contact angle was much smaller on the treated films and they have little or no solubility in toluene which indicated that the acid hydrolysis treatment successfully deprotected the cellulose. The xylan films were considerably rougher and less robust than the cellulose films. However, the inclusion of 20% xylitol by mass allowed for films that could be easily handled.

Table 26. Molecular weights of cellulose and xylan as determined by GPC

	M_n	M_w	D
Cellulose	228000	1510000	6.6
Xylan	118000	1870000	15.8

The cellulose and xylan starting materials were also characterized by GPC size exclusion chromatography. The results are summarized in Table 26. The

difference between the molecular weights of cellulose and xylan are much different than expected. One reason for this is that the cellulose used here is microcrystalline cellulose which is typically prepared by steeping cellulose in strong acid to consume amorphous cellulose. This typically reduces the molecular weight considerably. Furthermore, it is likely that pullulan is not a good molecular weight standard for oat spelt xylan. Oat spelt xylan has some branching which may result in an apparent size that is not reflective of the molecule's actual weight when compared to linear macromolecule standards such as pullulan.

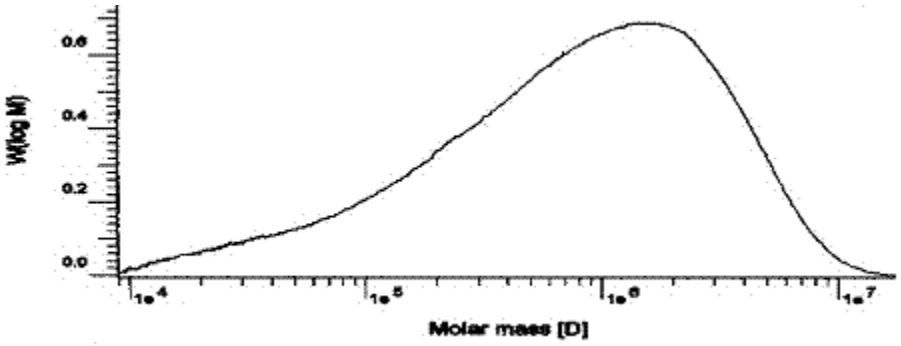

Figure 75. GPC molar mass distributions for cellulose starting material

A comparison of the chromatograms of cellulose and xylan in Figures 75 and 76 respectively, do show considerable differences in the distributions. The cellulose distribution in Figure 75 is quite broad, but the main peak is greater than one million molar mass. The xylan distribution in Figure 76 is clearly bimodal with a significant fraction of the molecules having average molecular weights below 100,000.

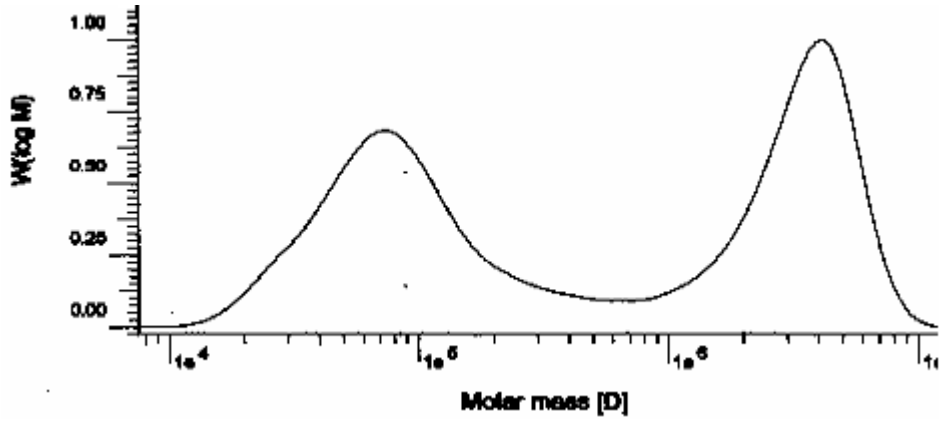

Figure 76. GPC molar mass distributions for oat spelt xylan starting material

Table 27. Conditions used for cellulose films

Cellulose Condition	Pressing Load (kPa)	Pressing Time (min)
1	2070	20
2	35	5
3	35	20
4	2070	5

The key variables of interest in this experiment are of course the type of polysaccharide, pressing load and pressing time. The importance of pressing load has been observed on several occasions in the previous chapters and should have an impact on the model system as well. Although pressing time has not been specifically addressed as an important variable in the work with fibres, it should be important to an interface development mechanism dependent on diffusion as suggested by Voyutskii [113]. Time has proven important for the drying of single fibre crossings as observed in Chapter 8; however that may or may not be a manifestation of diffusion as water removal is surely the predominant factor. Tables 27 and 28 show the conditions used for cellulose and xylan films respectively.

Table 28. Conditions used for xylan films

Xylan Condition	Pressing Load (kPa)	Pressing Time (min)
1	35	5
2	2070	20
3	35	20
4	2070	5

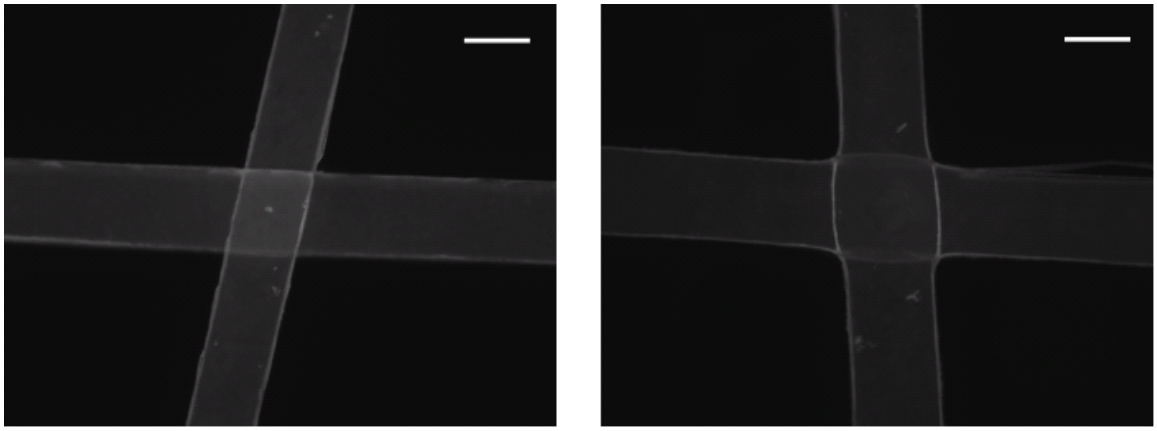

Figure 77. Micrographs of pressed xylan strips at 100X magnification

35 kPa (left) and 2070 kPa (right), bar is 175μm

Figure 77 shows the fluorescent micrographs of a pair of typical xylan strip intersections. The deformation at the crossing in the highly pressed sample is clearly evident and was commonly observed for the highly pressed xylan samples regardless of pressing time. The cellulose intersections did not demonstrate this degree of deformation. Figure 78 shows the familiar FRETN pixel histograms for all four conditions for the xylan samples. Conditions 1 and 3 were the low pressing levels and conditions 2 and 4 were subjected to high pressing loads. It should be clear from the histograms that the pressing load appears to be the most significant variable for FRETN at the xylan interface. This is a very interesting result when put in the context of the observations for the natural wood fibres, where pressing load was also a significant variable.

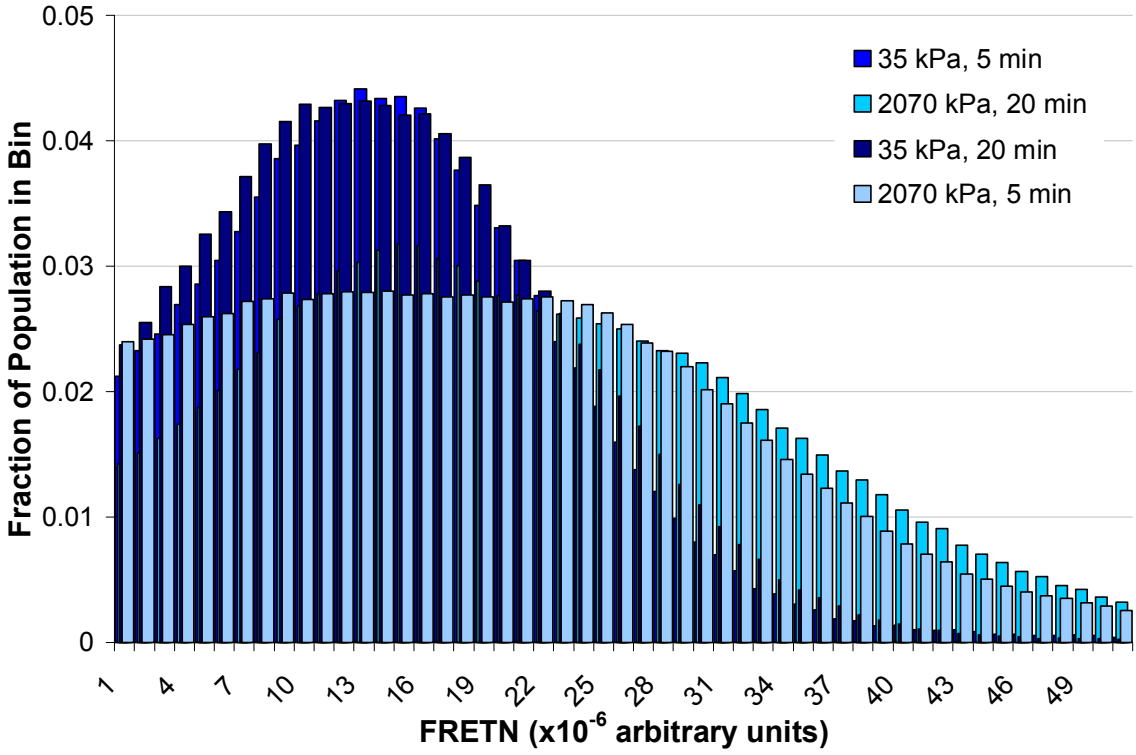

Figure 78. Histograms of xylan strip intersections pressed under different conditions

The histograms for the cellulose conditions are shown in Figure 79. The FRETN pixel distributions appear to change relatively little with different pressing loads or increased pressing time. This result is very similar to the observed wet pressing response for viscose fibres. It appears that the surfaces of these regenerated cellulose films are not capable of undergoing significant interdiffusion at these conditions. The cellulose films appear to have higher value FRETN pixels and a more broad distribution as compared to the results observed for the pressing of viscose fibres in Figure 64 in Chapter 7.

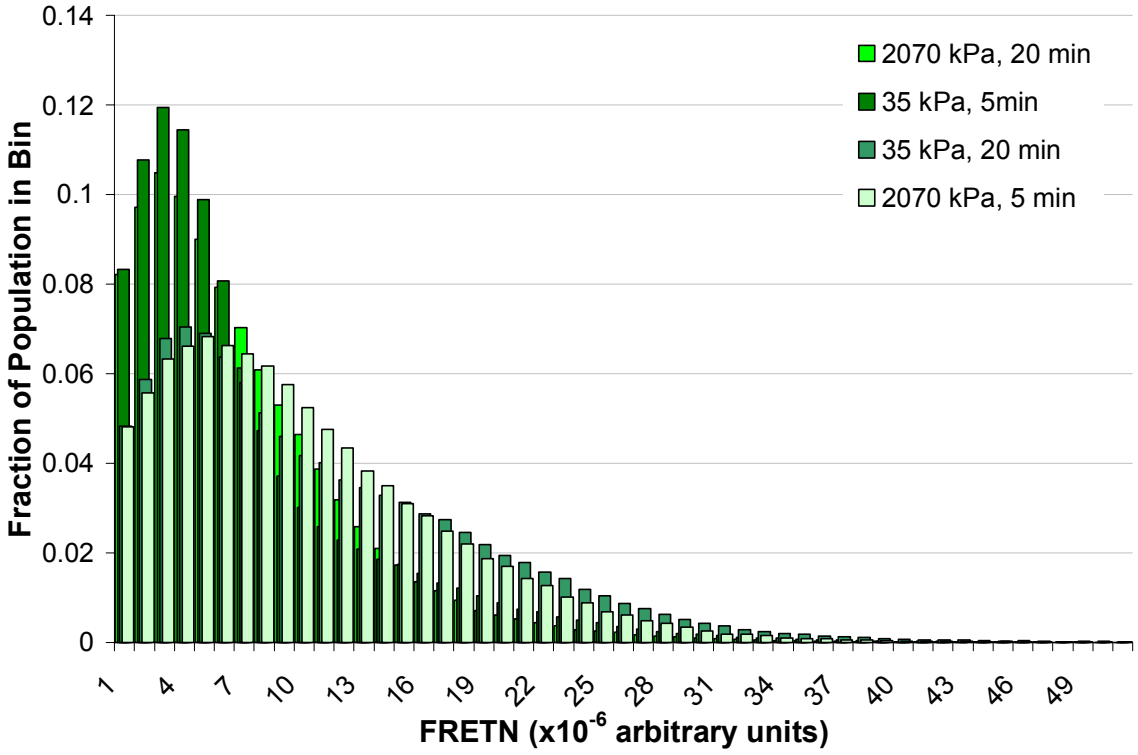

Figure 79. Histograms of cellulose strip intersections pressed under different conditions

It is unclear why this is the case, but it is likely related to the difference in morphology of the two systems. The viscose fibre intersections were dominated by the ridges on the surfaces of those fibres. It is unwise to make more specific comparisons between the fibres and films beyond a comparison of the general trends. The main reason for this is that the fibres are much smaller (25 – 75 μm wide) than the strips of film (200 – 250 μm). This created a problem with the image analysis because Excel can only handle 65536 rows of data in one column. At the 600X magnification level used for the fibres, the much larger film crossings had far too many FRETN pixels to be transferred into Excel. As a result, the film strips had to be cut as thin as possible and the magnification had

to be reduced to 100X to ensure that the number of FRETN pixels for a given crossing could be accommodated by Excel. This is a drastic decrease in resolution and likely prevents any fine grained analysis of the fibre/film comparison. It is likely that the MATLAB program could be re-written such that multiple columns of data could be exported to Excel to fix this problem while retaining resolution.

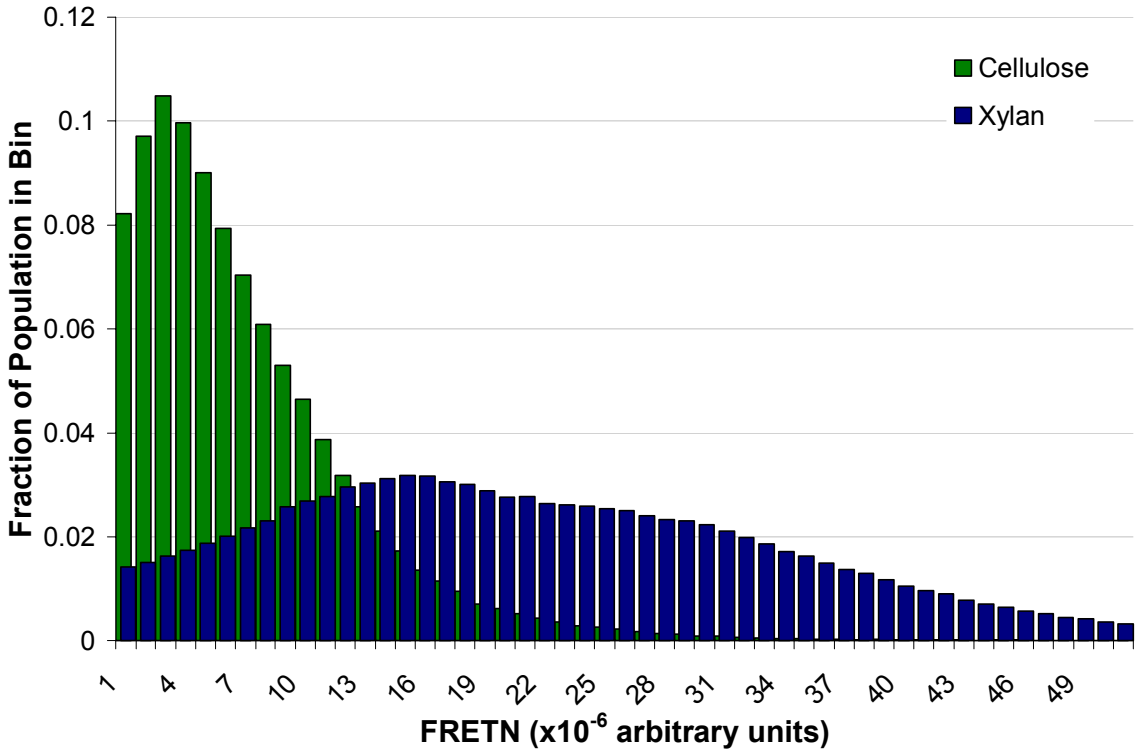

Figure 80. Comparison of FRETN pixel histograms of xylan and cellulose film intersections

Both samples were pressed at 2070 kPa for 20 min

Figure 80 compares the FRETN pixel distributions for xylan and cellulose films pressed at 2070 kPa for 20 minutes. This is yet another familiar histogram and is very reminiscent of the initial comparison of pulp and viscose fibres in Figure 55 from Chapter 6. There is a pronounced difference in the two distributions. The

FRETN distribution for xylan does have a higher mean value than for cellulose but is also characterized by considerably more variance and consequently a larger number of pixels with higher FRETN values. The mean values for total FRETN/bond area are shown in Table 29. This data is less informative than the histograms and although it reflects the similarity of the cellulose responses it does not adequately reflect the pressing response for the xylan samples.

Table 29. Total FRETN/bond area values for xylan and cellulose films

Pressing Load (kPa)	Pressing Time (min)	Total FRETN/Bond area	
		Xylan	Cellulose
35	5	12.1 (1.7)	5.9 (3.0)
35	20	11.3 (1.0)	9.9 (3.6)
2070	5	12.5 (2.0)	7.3 (1.2)
2070	20	17.0 (3.1)	5.9 (2.2)

9.4 Conclusions

Although the model systems employed in this study have some key differences from the fibre systems previously studied, the results are in agreement with the earlier conclusions. Cellulose is less capable of reducing the average interfibre distance either through resistance to deformation, the inability to interdiffuse or some combination of the two factors. As a result, cellulose film interfaces did not show a significant change in the FRETN pixel distribution in response to pressing. On the other hand, the xylan films had broad distributions of FRETN pixels and demonstrated a wet pressing response that was similar to that observed for natural wood fibres. The results of the FRETN analysis of the

polysaccharide film model systems indicate that lower molecular weight carbohydrates are likely to be significant contributors to fibre interface development.

Chapter 10: Overall Conclusions

The original ideas about the fibre bond that inspired this work are quite different from the concepts that have developed throughout this research program. The first chapter of this thesis provided a review of previous ideas and theories about the fibre bond as well a description of some of the methods and experiments that have been used to provide evidence for those theories. Both the classical works in the field as well as the current state of the art has been carefully considered as context for the results obtained in this study.

Although it was not possible to develop a trustworthy method for measuring FRET at fibre-fibre interfaces in a paper sheet, the other main objectives outlined in Chapter 3 were reasonably successful. Natural and regenerated cellulosic fibres were successfully labelled with a known FRET dye pair. This achievement made it possible to proceed with the main objective of the project which was to image fibre-fibre interface topography with nanometre resolution. It would not be possible to select proper filters for the fluorescence microscope without determining the absorptive and emissive properties of these dyes tethered to fibres.

Steady-state epi-fluorescence micrographs of fibre crossings were analyzed using the FRETN correction algorithm. The results suggested that energy transfer from coumarin dyed fibers to fluorescein dyed fibres was occurring. The FRETN surface for spruce fibre interfaces was distinctly different from that

observed in viscose fibre. The fibrillar structure of spruce fibre surfaces and the presence of low molecular weight hemicelluloses is likely responsible for this difference.

Further verification of the FRET microscopy technique was achieved in this work via the application to wet pressing. Image analysis of fluorescence micrographs of both natural and regenerated cellulose indicates a FRET signal is being produced at fibre crossings and that it can be manipulated with wet pressing load. The distribution of FRETN pixels shifts towards larger FRETN values with increased wet pressing for bleached white spruce fibres but did not do so for viscose fibres. A screening experiment further indicated that the effects of wet pressing and fibre fraction on FRETN signal are statistically significant, but that the effect of refining is not significant.

FRET microscopy provided evidence that there is considerable fibre bond development after wet pressing and that FRET is capable of observing coalescence of the fibre-fibre interface during drying. These results were both interesting on their own while simultaneously providing further verification that FRET is occurring in this system. It was possible to image the coalescence of the interface and observe a logarithmic relationship between increasing average FRETN values and drying time. The FRET signal from once-dried fibre crossings increases dramatically after rewetting and wet pressing for a second time. This

indicates that the material within the fibre bonds is still compliant after a single drying cycle.

Lastly, a model system of polysaccharides films was employed to investigate the root cause of the dichotomy between natural and regenerated cellulose fibre interfaces. It was found that cellulose is less capable of reducing the average interfibre distance either through resistance to deformation or the inability to participate in interdiffusion. On the other hand, the xylan films demonstrated a wet pressing response that was similar to that observed for natural wood fibres. The results of the FRETN analysis of the polysaccharide film model systems indicate that lower molecular weight carbohydrates are likely to be significant contributors to fibre interface development.

Chapter 11: Recommendations for Future Work

There are several avenues available for further work in this field. Some particularly attractive options are as follows:

- It would be useful to develop an approach to relate optical contact area with the FRET results. This is a technical issue regarding insufficient contrast at the fibre crossing that could be resolved with different optics or an alternative approach.
- It would be very useful to investigate the contribution and mechanism of common dry strength aids. The surface grafting of carboxymethylcellulose (CMC) appears to be well suited to this particular technique, since the additive could be tagged using similar chemistry and then fixed to fibres which are easily manipulated.
- Switching the technique to confocal laser scanning microscopy could allow the relative measurement of interfacial distances in fibre bonds within sheets.
- Further refinement using an empirical treatment to calibrate the results would be a valuable contribution as it would allow a more quantitative analysis. Possible approaches could include coupling FRET microscopy with AFM or examining the coalescence of well defined films containing the dye pair used in this work in a similar approach to that used by Winnik's group over the past few decades.

Appendix: Copyright Permission

Dear Mr Thomson

We hereby grant you permission to reprint the material detailed below at no charge **in your thesis** subject to the following conditions:

1. If any part of the material to be used (for example, figures) has appeared in our publication with credit or acknowledgement to another source, permission must also be sought from that source. If such permission is not obtained then that material may not be included in your publication/copies.

2. Suitable acknowledgment to the source must be made, either as a footnote or in a reference list at the end of your publication, as follows:

> "This article was published in Publication title, Vol number, Author(s), Title of article, Page Nos, Copyright Elsevier (or appropriate Society name) (Year)."

3. Your thesis may be submitted to your institution in either print or electronic form.

4. Reproduction of this material is confined to the purpose for which permission is hereby given.

5. This permission is granted for non-exclusive world **English** rights only. For other languages please reapply separately for each one required. Permission excludes use in an electronic form. Should you have a specific electronic project in mind please reapply for permission.

6. This includes permission for UMI to supply single copies, on demand, of the complete thesis. Should your thesis be published commercially, please reapply for permission.

Yours sincerely

Steph Smith

Rights Assistant
Elsevier Ltd
The Boulevard
Langford Lane
Kidlington
Oxford OX5 1GB

_____

From: Cameron Thomson [mailto:Cameron.Thomson@ipst.gatech.edu]
Sent: 27 June 2007 19:39
To: Rights and Permissions (ELS)
Subject: Re: Permission

Ms. Truter,

I would like to request permission to reproduce the text, tables and figures from the manuscript entitled "Imaging cellulose fibre interfaces with fluorescence microscopy and resonance energy transfer" by Cameron Thomson, Robert Lowe, and Arthur Ragauskas. It appeared in Carbohydrate Polymers, Vol 69, No. 4, p. 799-804. As first author, I would like to include this paper as part of my PhD dissertation which will be published by the Georgia Institute of Technology in Atlanta, Georgia, USA.

Thank you for your time,

Cameron

Cameron Thomson
Ph.D. Candidate
School of Chemistry and Biochemistry
Institute of Paper Science and Technology
Georgia Institute of Technology
500 10th Street, NW
Atlanta, GA 30332-0620
404-894-7862 (Office)
404-894-4778 (Fax)

References

1. Saka, S., *Chemical Composition and Distribution*, in *Wood and Cellulosic Chemistry*, D.S. Hon and N. Shirashi, Editors. 1991, Marcel Dekker: New York. p. 59-88.

2. Okamura, K., *Structure of Cellulose*, in *Wood and Cellulosic Chemistry*, D.S. Hon and N. Shirashi, Editors. 1991, Marcel Dekker: New York. p. 89-112.

3. Heiningen, A.v., et al., *Relationship between Alkaline Pulp Yield and the Mass Fraction and Degree of Polymerization of Cellulose in the Pulp.* Journal of Pulp and Paper Science, 2004. **30**(8): p. 211-217.

4. Suckling, I.D., et al., *Monitoring Cellulose Degradation During Conventional and Modified Kraft Pulping.* Journal of Pulp and Paper Science, 2001. **27**(10): p. 336-341.

5. Saxena, I.M. and R.M. Brown, Jr., *Cellulose biosynthesis: Current views and evolving concepts.* Annals of Botany (Oxford, United Kingdom), 2005. **96**(1): p. 9-21.

6. Hult, E.-L., P.T. Larsson, and T. Iversen, *A comparative CP/MAS ^{13}C-NMR study of cellulose structure in spruce wood and kraft pulp.* Cellulose, 2000. **7**(1): p. 35-55.

7. Hult, E.-L., P.T. Larsson, and T. Iversen, *Cellulose fibril aggregation - an inherent property of kraft pulps.* Polymer, 2001. **42**(8): p. 3309-3314.

8. Bouchard, J., et al., *Combined Effects of Polysulphide Pulping and ECF Bleaching on Softwood Polysaccharides.* Journal of Pulp and Paper Science, 2004. **30**(6): p. 172-176.

9. Atalla, R.H. and D.L. VanderHart, *Native cellulose: a composite of two distinct crystalline forms.* Science, 1984. **223**(4633): p. 283-5.

10. Langan, P., et al., *Synchrotron X-ray structures of cellulose Ib and regenerated cellulose II at ambient temperature and 100 K.* Cellulose, 2005. **12**(6): p. 551-562.

11. Maunu, S., et al., *Carbon-13 CP/MAS NMR investigations of cellulose polymorphs in different pulps.* Cellulose, 2000. **7**(2): p. 147-159.

12. Thygesen, A., et al., *On the determination of crystallinity and cellulose content in plant fibres.* Cellulose, 2005. **12**(6): p. 563-576.

13. Liitia, T., et al., *Cellulose crystallinity and ordering of hemicelluloses in pine and birch pulps as revealed by solid-state NMR spectroscopic methods.* Cellulose, 2003. **10**(4): p. 307-316.

14. Sun, R., X.F. Sun, and J. Tomkinson, *Hemicelluloses and their derivatives*, in *Hemicelluloses: Science and Technology*, P. Gatenholm and M. Tenkanen, Editors. 2004, ACS: Washington, D.C.

15. Stenius, P., ed. *Forest Products Chemistry*. Papermaking Science and Technology, ed. J. Gullichsen and H. Paulapuro. Vol. 3. 2000, Fapet Oy: Helsinki. 350.

16. Ragauskas, A.J., et al., *From wood to fuels: Integrating biofuels and pulp production.* Industrial Biotechnology, 2006. **2**(1): p. 55-65.

17. Timell, T.E., *Recent Progress in the Chemistry of Wood Hemicelluloses.* Wood Science and Technology, 1967. **1**(1): p. 45-70.

18. Ebringerova, A. and T. Heinze, *Xylan and xylan derivatives - biopolymers with valuable properties, 1. Naturally occurring xylans structures, isolation procedures and properties.* Macromolecular Rapid Communications, 2000. **21**(9): p. 542-556.

19. Dahlman, O., A. Jacobs, and J. Sjoeberg, *Molecular properties of hemicelluloses located in the surface and inner layers of hardwood and softwood pulps.* Cellulose (Dordrecht, Netherlands), 2003. **10**(4): p. 325-334.

20. Isenberg, I.H., *Pulpwood of the United States and Canada, Vol I - Conifers*. 3rd ed. Vol. 1. 1981, Appleton: Institute of Paper Chemistry. 219.

21. Stalbrand, H., et al., *Isolation, Characterization, and Enzymatic Hydrolysis of Acetyl-Galactoglucomannan from Spruce (Picea abies)*, in *Hemicelluloses: Science and Technology*, P. Gatenholm and M. Tenkanen, Editors. 2004, ACS: Washington, D.C. p. 66-78.

22. Isenberg, I.H., *Pulpwood of the United States and Canada, Vol II - Hardwoods*. 3rd ed. Vol. 2. 1981, Appleton: Institute of Paper Chemistry. 168.

23. Grace, T.M. and E.W. Malcolm, eds. *Pulp and Paper Manufacture Vol 5. Alkaline Pulping*. Pulp and Paper Manufacture, ed. M.J. Kocurek. Vol. 5. 1989, Technical Section Canadian Pulp and Paper Association: Montreal.

24. Jacobs, A. and O. Dahlman, *Characterization of the molar masses of hemicelluloses from wood and pulps employing size exclusion chromatography and matrix-assisted laser desorption ionization time-of-flight mass spectrometry.* Biomacromolecules, 2001. **2**(3): p. 894-905.

25. Ralph, J., et al., *Lignins: Natural polymers from oxidative coupling of 4-hydroxyphenylpropanoids.* Phytochemistry Reviews, 2004. **3**(1-2): p. 29-60.

26. Sjostrom, E., *Wood Chemistry: Fundamentals and Application*. 1993, Orlando: Academic Press. 293.

27. Sarkanen, K.V. and C.H. Ludwig, eds. *Lignin:Occurrence, Formation, Structure and Reactions*. 1971, Wiley Interscience: New York. 916.

28. Boerjan, W., J. Ralph, and M. Baucher, *Lignin biosynthesis.* Annu Rev Plant Biol FIELD Full Journal Title:Annual review of plant biology, 2003. **54**: p. 519-46.

29. Chakar, F.S. and A.J. Ragauskas, *Review of current and future softwood kraft lignin process chemistry.* Industrial Crops and Products, 2004. **20**(2): p. 131-141.

30. Karhunen, P., et al., *The formation of dibenzodioxocin structures by oxidative coupling. A model reaction for lignin biosynthesis.* Tetrahedron Letters, 1995. **36**(25): p. 4501-4.

31. Karhunen, P., et al., *Dibenzodioxocins; a novel type of linkage in softwood lignins.* Tetrahedron Letters, 1995. **36**(1): p. 169-70.

32. Panshin, A.J. and C.d. Zeeuw, *Textbook of Wood Technology*. 4th ed. 1980, New York: McGraw-Hill.

33. Côté, W.A., *Wood ultrastructure. An atlas of electron micrographs*. 1967, Seattle: University of Washington Press.

34. Lehtonen, L.K., J.H. Lehto, and A.W. Rudie, *Development of unbonded and bonded areas in relation to populus species wood characteristics in grinding.* Journal of Pulp and Paper Science, 2004. **30**(10): p. 275-278.

35. Laine, J., R. Hynynen, and P. Stenius, *The effect of surface chemical composition and charge on the fiber and paper properties of unbleached and bleached kraft pulps.* Fundamentals of Papermaking Materials, Transactions of the Fundamental Research Symposium, 11th, Cambridge, UK, Sept. 1997, 1997. **2**: p. 859-892.

36. Li, K. and D.W. Reeve, *The origins of kraft pulp fibre surface lignin.* Journal of Pulp and Paper Science, 2002. **28**(11): p. 369-373.

37. Duchesne, I., et al., *Surface Chemical Composition and Morphology of ITC Kraft Fibres as Determined by XPS and FE-SEM.* Journal of Pulp and Paper Science, 2003. **29**(3): p. 71-76.

38. Risen, J., A.H. Hulten, and M. Paulsson, *Surface Characterization of Softwood and Hardwood Kraft Pulp Fibers from Different Stages in a Bleaching Sequence.* Journal of Wood Chemistry and Technology, 2004. **24**(4): p. 307-321.

39. Risen, J., A.H. Hulten, and M. Paulsson, *Influence of Fiber Properties on the Network Strength of Softwood and Hardwood Kraft Pulp Fibers from Different Stages of a Bleaching Sequence.* Journal of Wood Chemistry and Technology, 2004. **24**(4): p. 289-306.

40. Freese, M., I. Schmidt, and K. Fischer, *Hemicellulose composition in the outer cell wall layers of paper grade and dissolving pulp.* Macromolecular Symposia, 2006. **232**(Hemicelluloses): p. 13-18.

41. Sjoeberg, J., et al., *Cross-Sectional Analysis of the Polysaccharide Composition in Cellulosic Fiber Materials by Enzymatic Peeling/High-Performance Capillary Zone Electrophoresis.* Biomacromolecules, 2005. **6**(6): p. 3146-3151.

42. Dence, C.W. and D.W. Reeve, eds. *Pulp Bleaching: principles and practice*. 1996, TAPPI Press: Atlanta. 868.

43. Laine, J., et al., *The effect of elemental chlorine-free (ECF) and totally chlorine-free (TCF) bleaching on the surface chemical composition of kraft pulp as determined by ESCA.* Nordic Pulp & Paper Research Journal, 1996. **11**(3): p. 201-210.

44. Retulainen, E., K.J. Niskanen, and N. Nilsen, *Fibres and Bonds*, in *Paper Physics*, K.J. Niskanen, Editor. 1998, Fapet Oy: Helsinki. p. 54-87.

45. Lindstrom, T., L. Wagberg, and T. Larsson. *On the Nature of Joint Strength in Paper - A Review of Dry and Wet Strength Resins Used in Paper Manufacturing*. in *13th Fundamental Research Symposium*. 2005. Cambridge, United Kingdom: The Pulp and Paper Fundamental Research Society.

46. Nissan, A.H. *General Principles of Adhesion: With Particular Reference to the Hydrogen Bond*. in *Transactions of the IInd Fundamental Research Symposium*. 1961. Oxford: FRC.

47. Notley, S., B. Petterson, and L. Wagberg, *Direct Measurement of Attractive van der Waals' Forces between Regenerated Cellulose Surfaces in an Aqueous Environment.* Journal of the American Chemical Society, 2004. **126**: p. 13930-13931.

48. Notley, S.M. and L. Wagberg, *Morphology of Modified Regenerated Model Cellulose II Surfaces Studied by Atomic Force Microscopy: Effect of*

Carboxymethylation and Heat Treatment. Biomacromolecules, 2005. **6**(3): p. 1586-1591.

49. Wagberg, L. and G. Annergren. *Physicochemical Characterization of Papermaking Fibres*. in *The Fundamental of Papermaking Materials, Transactionsof the XIth Fundamental Research Symposium*. 1997. Cambridge: FRC.

50. Page, D.H., *A Theory for the Tensile Strength of Paper.* TAPPI, 1969. **52**(4): p. 674-681.

51. Page, D.H., *Fibre-to-fibre bonds; Part 1-A method for their direct observation.* Paper Technology, 1960. **1**(4): p. 407-411.

52. Page, D.H. and J.W. Sargent. *The fine structure of fibre bonding*. in *The Formation and Structure of Paper, Transactions of the IInd Fundamental Research Symposium*. 1961. Oxford: FRC.

53. Page, D.H. and P.A. Tydeman, *Fibre-to-fibre bonds; Part 2-A preliminary study of their properties in paper sheets.* Paper Technology, 1960. **1**(5): p. 519-530.

54. Page, D.H., P.A. Tydeman, and M. Hunt. *A study of fibre-to-fibre bonding by direct observation*. in *The formation and structure of paper*. 1962. Oxford: Technical Section of the British Paper and Board Makers' Assoc.

55. Ratliff, F.T., *The possible correlation between hemicelluloses and the physical properties of bleached kraft pulps.* TAPPI, 1949. **32**(8): p. 357-367.

56. Ingmanson, W.L. and E.F. Thode, *Factors contributing to the strength of a sheet of paper; II. Relative bonded area.* TAPPI, 1959. **42**(1): p. 83-93.

57. Emerton, H.W., *Fundamentals of the Beating Process; The theory of the development in pulps of papermaking characteristics by mechanical treatment*. 1957, Kenley: The British Paper and Board Industry Research Assoc. 198.

58. Barkas, W.W., Proc. Tech. Sect. Brit. Paper and Board Makers' Assoc., 1950. **31**(3): p. 463.

59. Asunmaa, S. and B. Steenberg, *Beaten pulps and the fibre-to-fibre bond in paper.* Svensk Papperstidning, 1958. **61**(18b): p. 686-695.

60. Asunmaa, S.K. and D.W. Schwab, *Aspen holocellulose and morphology of interfibre bonding - an electron microscope study.*, in *Cellular Ultrastructure of Woody Plants*, W.A. Cote, Editor. 1965, Syracuse University Press: Syracuse, NY. p. 573-593.

61. Jayme, G. and G. Hunger, *Electron microscope 2- and 3-dimensional classification of fibre bonding*, in *Formation and Structure of Paper, Transactions of the IInd Fundamental Research Symposium*, F. Bolam, Editor. 1961, FRC: Oxford. p. 135-170.

62. Haselton, W.R., *An Investigation of the Adsorption of Gases by Wood and its Components and of Gas Adsorption Techniques as a Means of Studying the Area and Structure of Pulp and Paper*, in *Physics Department*. 1953, The Institute of Paper Chemistry: Appleton, WI. p. 172.

63. Borch, J., *Optical and Appearance Properties*, in *Handbook of Physical Testing of Paper*, J. Borch, et al., Editors. 2001, Marcel Dekker, Inc.: New York. p. 127-138.

64. Kortum, G., *Reflectance Spectroscopy*. 1969, New York: Springer-Verlag. 366.

65. Scallan, A.M. and J. Borch, *An interpretation of paper reflectance based upon morphology; I. Initial considerations.* TAPPI, 1972. **55**(4): p. 583-588.

66. Scallan, A.M. and J. Borch, *An interpretation of paper reflectance based upon morphology: general applicability.* TAPPI, 1974. **57**(5): p. 143-147.

67. Scallan, A.M. and J. Borch, *An interpretation of paper reflectance based upon morphology - The effect of mass distribution.* TAPPI, 1976. **59**(10): p. 102-105.

68. Uesaka, T., et al., *Determination of Fiber-Fiber Bond Properties*, in *Handbook of Physical Testing of Paper*, R. Mark, et al., Editors. 2002, Marcel Dekker, Inc: New York. p. 873-900.

69. Nordman, L.S. *Bonding in paper sheets*. in *Fundamentals of Papermaking Fibres, Trans. Ist Fund. Res. Symp.* 1957. Cambridge: FRC.

70. Haselton, W.R., *An Investigation of the Adsorption of Gases by Wood and its Components and of Gas Adsorption Techniques as a Means of Studying the Area and Structure of Pulp and Paper*. 1953, The Institute of Paper Chemistry: Appleton, WI. p. 172.

71. Ebeling, K.I., *Distribution of energy consumption during straining of paper*. 1970, The Institute of Paper Chemistry: Appleton, WI. p. 680.

72. Alince, B., J. Porubska, and T.G.M. Van De Ven, *Light scattering and microporosity in paper.* Journal of Pulp and Paper Science, 2002. **28**(3): p. 93-98.

73. Lehtonen, L.K. and T.J. Dyer, *Light-scattering coefficient as a measure of specific surface area in mechanical pulp laboratory sheets.* Paperi ja Puu, 2005. **87**(8): p. 517-524.

74. Haselton, W., *Gas Adsorption by Wood, Pulp, and Paper.* Tappi Journal, 1955. **38**(12): p. 716-723.

75. McKenzie, A., *The Structure and Properties of Paper Part XXI: The Diffusion Theory of Adhesion Applied to Interfibre Bonding.* APPITA, 1984. **37**(7): p. 580-583.

76. Haselton, W.R., *Gas Adsorption by Wood, Pulp and Paper; II. the application of gas adsorption techniques to the study of the area and structure of pulps and the unbonded and bonded area of paper.* TAPPI, 1955. **38**(12): p. 716-723.

77. Swanson, J.W. and A.J. Steber, *Fiber surface area and bonded area.* TAPPI, 1959. **42**(12): p. 986-994.

78. Barber, H.A., *Determination of the energy site distribution of the surface of cellulose fibers by gas adsorption methods*. 1969. p. 110 pp.

79. Dietrich, W.H., *A comparison of adsorptive potential energies for argon and nitrogen adsorption on the surface of cellulose fibers*. 1970, Institute of Paper Chemistry: Appleton, WI. p. 184.

80. Davies, G.W., *A Microscopic Study of Paper Made from Pinus radiata.* TAPPI, 1968. **51**(10): p. 454-461.

81. Bates, N.A., *Polyamide-Epichlorohydrin Wet-Strength Resin; I. Retention by Pulp.* TAPPI, 1969. **52**(6): p. 1157-1161.

82. Allen, K.W., *Theories of Adhesion*, in *Handbook of Adhesion*, D.E. Packham, Editor. 2005, John Wiley and Sons: Chichester. p. 533-538.

83. Steiner, T., *Reviews: The hydrogen bond in the solid state.* Angewandte Chemie, International Edition, 2002. **41**(1): p. 48-76.

84. Parthasarathi, R., V. Subramanian, and N. Sathyamurthy, *Hydrogen bonding without borders: an atoms-in-molecules perspective.* Journal of Physical Chemistry A, 2006. **110**(2): p. 3349-3351.

85. Umeyama, H. and K. Morokuma, *The origin of hydrogen bonding. An energy decomposition study.* Journal of the American Chemical Society, 1977. **99**(5): p. 1316-32.

86. Desiraju, G.R., *Hydrogen Bridges in Crystal Engineering: Interactions without Borders.* Accounts of Chemical Research, 2002. **35**(7): p. 565-573.

87. Bletzinger, J.C., *Effect of acetylation on water binding properties of cellulose.* Industrial and Engineering Chemistry, 1943. **35**(4): p. 474-480.

88. Higgins, H.G., A.W. McKenzie, and K.J. Harrington, *The structure and properties of paper. VII. Study of the mechanisms of beating and interfiber bonding by means of esterification.* Tappi, 1958. **41**: p. 193-204.

89. McKenzie, A.W. and H.G. Higgins, *Reactivity of cellulose. I. The effect of beating and other physical treatments on rate of acetylation.* Holzforschung, 1956. **10**: p. 150-3.

90. Nissan, A.H. and S.S. Sternstein, *Cellulose fiber bonding.* Tappi Journal, 1964. **47**(1): p. 1-6.

91. Page, D.H., *The rheology of paper in terms of its molecular structure.* Tappi, 1963. **46**(12): p. 750-756.

92. Broughton, G. and J.P. Wang, *The Mechanical Properties of Paper - Part III.* TAPPI, 1955. **38**(7): p. 412-415.

93. Corte, H., H. Schaschek, and O. Broens, *The rupture energy of paper and its dependence on the stress-time characteristics during drying.* Tappi, 1957. **40**(6): p. 441-447.

94. Tabor, D., *Recent studies of short range forces.* Journal of Colloid and Interface Science, 1969. **31**(3): p. 364-371.

95. Bergstrom, L., *Hamaker constants of inorganic materials.* Advances in Colloid and Interface Science, 1997. **70**(1): p. 125-169.

96. Bergstrom, L., et al., *Spectroscopic ellipsometry characterization and estimation of the Hamaker constant of cellulose.* Cellulose, 1999. **6**(1): p. 1-13.

97. Notley, S.M., B. Pettersson, and L. Wagberg, *Direct Measurement of Attractive van der Waals' Forces between Regenerated Cellulose Surfaces in an Aqueous Environment.* Journal of the American Chemical Society, 2004. **126**(43): p. 13930-13931.

98. Barzyk, D., D.H. Page, and A.J. Ragauskas, *Acidic group topochemistry and fibre-to-fibre specific bond strength.* Journal of Pulp and Paper Science, 1997. **23**(2): p. J59-J61.

99. Scallan, A.M., *The effect of acidic groups on the swelling of pulps: a review.* Tappi Journal, 1983. **66**(11): p. 73-5.

100. Scallan, A.M. and J. Grignon, *The effect of cations on pulp and paper properties.* Svensk Papperstidning, 1979. **82**(2): p. 40-7.

101. Scallan, A.M. and A.C. Tigerstroem, *Swelling and elasticity of the cell walls of pulp fibers.* Journal of Pulp and Paper Science, 1992. **18**(5): p. 188-93.

102. Laine, J., et al., *Studies on topochemical modification of cellulosic fibers. Part 1. Chemical conditions for the attachment of carboxymethyl cellulose onto fibers.* Nordic Pulp & Paper Research Journal, 2000. **15**(5): p. 520-526.

103. Laine, J., et al., *Studies on topochemical modification of cellulosic fibres Part 5: Comparison of the effects of surface and bulk chemical modification and beating of pulp on paper properties.* Nordic Pulp & Paper Research Journal, 2003. **18**(3): p. 325-332.

104. Laine, J., et al., *Studies on topochemical modification of cellulosic fibres. Part 2. The effect of carboxymethyl cellulose attachment on fibre swelling and paper strength.* Nordic Pulp & Paper Research Journal, 2002. **17**(1): p. 50-56.

105. Furuta, T. and D.G. Gray, *Direct force-distance measurements on wood-pulp fibers in aqueous media.* Journal of Pulp and Paper Science, 1998. **24**(10): p. 320-324.

106. Hanley, S.J. and D.G. Gray, *Atomic force microscopy (AFM) images in air and water of kraft pulp fibers.* Journal of Pulp and Paper Science, 1999. **25**(6): p. 196-200.

107. Pang, L. and D.G. Gray, *Heterogeneous fibrillation of kraft pulp fiber surfaces observed by atomic force microscopy.* Journal of Pulp and Paper Science, 1998. **24**(11): p. 369-372.

108. Chhabra, N., et al., *An investigation of pulp fiber surfaces by atomic force microscopy.* Journal of Pulp and Paper Science, 2005. **31**(1): p. 52-56.

109. Persson, B.N.J. and E. Tosatti, *The effect of surface roughness on the adhesion of elastic solids.* Journal of Chemical Physics, 2001. **115**(12): p. 5597-5610.

110. Israelachvili, J., et al., *Effects of sub-angstrom (pico-scale) structure of surfaces on adhesion, friction, and bulk mechanical properties.* Journal of Materials Research, 2005. **20**(8): p. 1952-1972.

111. Maeda, N., et al., *Adhesion and friction mechanisms of polymer-on-polymer surfaces.* Science, 2002. **297**(5580): p. 379-382.

112. Chen, N., et al., *Adhesion and friction of polymer surfaces: the effect of chain ends.* Macromolecules, 2005. **38**(8): p. 3491-3503.

113. Voyutskii, S.S., *Autohesion and Adhesion of High Polymers*. Polymer Reviews, ed. H.F. Mark and E.H. Immergut. Vol. 4. 1963, New York: Interscience. 272.

114. Turro, N.J., *Modern Molecular Photochemistry*. 1 ed. 1978, Menlo Park, CA: Benjamin/Cummings Publ. Co. 628.

115. Harris, D.C. and M.D. Bertolucci, *Symmetry and Spectroscopy: an introduction to vibrational and electronic spectroscopy*. 1989, Mineola, NY: Dover Publications.

116. Lakowicz, J.R., *Principles of Fluorescence Spectroscopy*. 1983, New York: Plenum Press. 496.

117. McQuarrie, D.A. and J.D. Simon, *Physical Chemistry: a molecular approach*. 1 ed. 1997, Sausalito, CA: University Science Books. 1270.

118. Guilbault, G.G., *Practical Fluorescence*. 2 ed. 1990, New York: Marcel Dekker. 812.

119. Pekcan, O., et al., *Energy transfer in restricted dimensions: a new approach to latex morphology.* Macromolecules, 1990. **23**(8): p. 2210-16.

120. Pekcan, O. and M.A. Winnik, *Energy transfer studies on polymer membrane films. Materials with variable apparent dimensionality.* Chemical Physics, 1990. **146**(3): p. 283-9.

121. Pekcan, O., M.A. Winnik, and M.D. Croucher, *Direct energy-transfer studies on doped and labeled polymer latex particles.* Physical Review Letters, 1988. **61**(5): p. 641-4.

122. Pekcan, O., M.A. Winnik, and M.D. Croucher, *Fluorescence studies of coalescence and film formation in poly(methyl methacrylate) nonaqueous dispersion particles.* Macromolecules, 1990. **23**(10): p. 2673-8.

123. Stryer, L., *Fluorescence energy transfer as a spectroscopic ruler.* Annual Review of Biochemistry, 1978. **47**: p. 819-46.

124. Hoffmann, C., et al., *A FlAsH-based FRET approach to determine G protein-coupled receptor activation in living cells.* Nature Methods, 2005. **2**(3): p. 171-176.

125. Somogyi, B., et al., *Foerster-type energy transfer as a probe for changes in local fluctuations of the protein matrix.* Biochemistry, 1984. **23**(15): p. 3403-11.

126. Mitsui, T., H. Nakano, and K. Yamana, *Coumarin-fluorescein pair as a new donor-acceptor set for fluorescence energy transfer study of DNA.* Tetrahedron Letters, 2000. **41**(15): p. 2605-2608.

127. Forster, T., *Mechanism of energy transfer*, in *Comprehensive Biochemistry*, M. Florkin and E.H. Statz, Editors. 1967, Elsevier: New York. p. 61-77.

128. Haugland, R.P., J. Yguerabide, and L. Stryer, *Dependence of the kinetics of singlet-singlet energy transfer on spectral overlap.* Proceedings of the National Academy of Sciences, 1969. **63**(1): p. 23-30.

129. Herman, B., *Fluorescence Microscopy*. 2nd ed. 1998. 170 pp.

130. Guillet, J., *Polymer photophysics and photochemistry*. 1985, New York: Cambridge University Press. 391.

131. Cheung, H.C., *Chapter 3: Resonance Energy Transfer*, in *Principles of fluorescence spectroscopy*, J.R. Lakowicz, Editor. 2002, Plenum Press: New York. p. 127-176.

132. Grunwell, J.R., et al., *Monitoring the Conformational Fluctuations of DNA Hairpins Using Single-Pair Fluorescence Resonance Energy Transfer.* Journal of the American Chemical Society, 2001. **123**(18): p. 4295-4303.

133. Somogyi, B., et al., *Forster-Type Energy Transfer as a Probe for Changes in Local Fluctuations of the Protein Matrix.* Biochemistry, 1984. **23**: p. 3403-3411.

134. Lakowicz, J.R., *Principles of Fluorescence Spectroscopy*. Third ed. 2006, New York: Springer. 954.

135. Shiah, T.Y.-J. and H. Morawetz, *New fluorescence technique for characterizing polymer self diffusion.* Macromolecules, 1984. **17**: p. 792-794.

136. vanDrooge, D.J., et al., *Characterization of the mode of incorporation of lipophilic compounds in solid dispersions at the nanoscale using fluorescence resonance energy transfer.* Macromolecular Rapid Communications, 2006. **27**: p. 1149-1155.

137. Winnik, M.A., O. Pekcan, and M.D. Croucher, *Fluorescence Techniques in the Study of Polymer Colloids*, in *Scientific Methods for the Study of*

Polymer Colloids and Their Applications, F. Candau and R.H. Ottewill, Editors. 1990, Kluwer. p. 225-245.

138. Winnik, M.A., et al., *Fluorescence quenching studies of core and stabilizer-labeled non-aqueous dispersions: the nature of the core-stabilizer interface.* Journal of Colloid and Interface Science, 1990. **139**(1): p. 251-9.

139. Ye, X., et al., *Polymer Diffusion in PBMA Latex Films Using a Polymerizable Benzophenone Derivative as an Energy Transfer Acceptor.* Macromolecules, 2003. **36**(23): p. 8749-8760.

140. Oh, J.K., et al., *Film Formation and Polymer Diffusion in Poly(vinyl acetate-co-butyl acrylate) Latex Films. Temperature Dependence.* Macromolecules, 2003. **36**(15): p. 5804-5814.

141. Mazuel, F., et al., *Interdiffusion and Self-Cross-Linking in Acetal-Functionalized Latex Films.* Macromolecules, 2004. **37**(16): p. 6141-6152.

142. Wu, J., et al., *Temperature Dependence of Polymer Diffusion in Poly(vinyl acetate-co-dibutyl maleate) Latex Films.* Macromolecules, 2004. **37**(6): p. 2299-2306.

143. Wang, Y. and M.A. Winnik, *Polymer diffusion across interfaces in latex films.* Journal of Physical Chemistry, 1993. **97**(11): p. 2507-15.

144. Feng, J. and M.A. Winnik, *Effect of water on polymer diffusion in latex films.* Macromolecules, 1997. **30**(15): p. 4324-4331.

145. Jones, C.D., J.G. McGrath, and L.A. Lyon, *Characterization of Cyanine Dye-Labeled Poly(N-isopropylacrylamide) Core/Shell Microgels Using Fluorescence Resonance Energy Transfer.* Journal of Physical Chemistry B, 2004. **108**(34): p. 12652-12657.

146. Gan, D. and L.A. Lyon, *Fluorescence nonradiative energy transfer analysis of crosslinker heterogeneity in core-shell hydrogel nanoparticles.* Analytica Chimica Acta, 2003. **496**(1-2): p. 53-63.

147. Gan, D. and L.A. Lyon, *Interfacial Nonradiative Energy Transfer in Responsive Core-Shell Hydrogel Nanoparticles.* Journal of the American Chemical Society, 2001. **123**(34): p. 8203-8209.

148. Merzlyakov, M., et al., *Spectral Forster resonance energy transfer detection of protein interactions in surface supported bilayers.* Langmuir, 2006. **22**: p. 6986-6992.

149. Parthasarathy, R., et al., *Nonequilibrium Adhesion Patterns at Lipid Bilayer Junctions.* Journal of Physical Chemistry B, 2004. **108**(2): p. 649-657.

150. Wong, A.P. and J.T. Groves, *Topographical Imaging of an Intermembrane Junction by Combined Fluorescence Interference and Energy Transfer Microscopies.* Journal of the American Chemical Society, 2001. **123**(49): p. 12414-12415.

151. Wong, A.P. and J.T. Groves, *Molecular topography imaging by intermembrane fluorescence resonance energy transfer.* Proceedings of the National Academy of Sciences of the United States of America, 2002. **99**(22): p. 14147-14152.

152. Niles, W.D., J.R. Silvius, and F.S. Cohen, *Resonance Energy Transfer Imaging of Phospholipid Vesicle Interaction with a Planar Phospholipid Membrane.* Journal of General Physiology, 1996. **107**: p. 329-351.

153. Kuhn, H., *Classical aspects of energy transfer in molecular systems.* Journal of Chemical Physics, 1970. **53**(1): p. 101-108.

154. Jares-Erijman, E.A. and T.M. Jovin, *FRET imaging.* Nature Biotechnology, 2003. **21**(11): p. 1387-1395.

155. Stanley, M., *An introduction to FRET with an emphasis on the optics involved*, in *Application Notes*. 2003, Chroma Technology Corp.: Burlington, VT. p. 14.

156. Stanley, M., *Image registered, sub-pixel resolution filter sets*, in *Application Notes*. 2005, Chroma Technology Corp.: Burlington, VT. p. 5.

157. Gordon, G.W., et al., *Quantitative Fluorescence Resonance Energy Transfer Measurements Using Fluorescence Microscopy.* Biophysical Journal, 1998. **74**: p. 2702-2713.

158. Youvan, D.C., et al., *Calibration of Fluorescence Resonance Energy Transfer in Microscopy Using Genetically Engineered GFP Derivatives on Nickel Chelating Beads.* Biotechnology et alia, 1997. **3**: p. 1-18.

159. Xia, Z. and Y. Liu, *Reliable and Global Measurement of Fluorescence Resonance Energy Transfer Using Fluorescence Microscopes.* Biophysical Journal, 2001. **81**: p. 2395-2402.

160. Gu, Y., et al., *Quantitative fluorescence resonance energy transfer measurement with acceptor photobleaching and spectral unmixing.* Journal of Microscopy, 2004. **215**(2): p. 162-173.

161. Hoppe, A., K. Christensen, and J. Swanson, *Fluorescence resonance energy transfer-based stoichiometry in living cells.* Biophysical Journal, 2002. **83**(6): p. 3652-3664.

162. Nanko, H., O. J., and A. Okagawa, *How to see interfibre bonding in paper sheets.* Journal of Pulp and Paper Science, 1989. **15**(1): p. J17-J23.

163. Nanko, H. and J. Ohsawa, *Mechanisms of fibre bond formation*, in *Fundamentals of Papermaking, Trans. IXth Fund. Res. Symp.*, C.F. Baker and V.W. Punton, Editors. 1989, FRC: Cambridge. p. 783-830.

164. Haselton, W.R., TAPPI, 1954. **37**(9): p. 404-412.

165. Page, D.H., P.A. Tydeman, and M. Hunt. *A study of fibre-to-fibre bonding by direct observation*. in *The Formation and Structure of Paper, Transactions of the IInd Fundamental Research Symposium*. 1961. Oxford: FRC.

166. Van Den Akker, J.A., *Structural Aspects of Bonding.* TAPPI, 1959. **42**(12): p. 940-947.

167. Anderson, J.M., *Fluorescent hydrazides for the high-performance liquid chromatographic determination of biological carbonyls.* Analytical Biochemistry, 1986. **152**(1): p. 146-53.

168. Martin, M.M. and L. Lindqvist, *The pH dependence of fluorescein fluorescence.* Journal of Luminescence, 1975. **10**: p. 381-390.

169. Mirenda, M., M.G. Lagorio, and E.S. Roman, *Photophysics on surfaces: determination of absolute fluorescence quantum yields from reflectance spectra.* Langmuir, 2004. **20**: p. 3690-3697.

170. Lowe, R.M., D.H. Page, and A.J. Ragauskas. *Imaging Fiber Deformations*. in *13th Fundamental Research Symposium*. 2005. Cambridge: Pulp and Paper Fundamental Research Society.

171. Varma, A.J. and M.P. Kulkarni, *Oxidation of cellulose under controlled conditions.* Polymer Degradation and Stability, 2002. **77**(1): p. 25-27.

172. Kontturi, E., P.C. Thuene, and J.W. Niemantsverdriet, *Trimethylsilylcellulose/Polystyrene Blends as a Means To Construct Cellulose Domains on Cellulose.* Macromolecules, 2005. **38**(26): p. 10712-10720.

173. Kontturi, E., et al., *Introducing open films of nanosized cellulose-atomic force microscopy and quantification of morphology.* Polymer, 2005. **46**(10): p. 3307-3317.

174. Kontturi, E., P.C. Thuene, and J.W. Niemantsverdriet, *Cellulose model surfaces -- simplified preparation by spin coating and characterization by X-ray photoelectron spectroscopy, infrared spectroscopy, and atomic force microscopy.* Langmuir, 2003. **19**(14): p. 5735-5741.

175. Kontturi, E., P.C. Thune, and J.W. Niemantsverdriet, *Novel method for preparing cellulose model surfaces by spin coating.* Polymer, 2003. **44**(13): p. 3621-3625.

176. McCormick, C.L., P.A. Callais, and B.H. Hutchinson, *Solution studies of cellulose in lithium chloride and N,N-dimethylacetamide.* Macromolecules, 1985. **18**: p. 2394-2401.

177. Grondahl, M., L. Eriksson, and P. Gatenholm, *Material properties of plasticized hardwood xylans for potential application as oxygen barrier films.* Biomacromolecules, 2004. **5**: p. 1528-1535.

178. Gabrielii, I., et al., *Separation, characterization and hydrogel-formation of hemicellulose from aspen wood.* Carbohydrate Polymers, 2000. **43**(4): p. 367-374.

179. Liu, Y., et al., *Microspectroscopic analysis and kappa determination of single pulp fibres stained with acridine orange.* Journal of Pulp and Paper Science, 1999. **25**(10): p. 351-355.

180. Li, K. and D.W. Reeve, *Fluorescent labeling of lignin in the wood pulp fibre wall.* Journal of Wood Chemistry and Technology, 2004. **24**(2): p. 169-181.

181. Mathews, J., R. Gustafson, and K. Hodgson, *A method to determine the charge demand of single pulp fibers.* Nordic Pulp & Paper Research Journal, 2004. **19**(4): p. 453-459.

182. Potthast, A., et al., *A novel method for the determination of carbonyl groups in cellulosics by fluorescence labeling. 3. Monitoring oxidative processes.* Biomacromolecules, 2003. **4**(3): p. 743-9.

183. Rohrling, J., et al., *Synthesis and testing of a novel fluorescence label for carbonyls in carbohydrates and cellulosics.* Synlett, 2001(5): p. 682-684.

184. Rohrling, J., et al., *A novel method for the determination of carbonyl groups in cellulosics by fluorescence labeling. 2. Validation and applications.* Biomacromolecules, 2002. **3**(5): p. 969-75.

185. Rohrling, J., et al., *A novel method for the determination of carbonyl groups in cellulosics by fluorescence labeling. 1. Method development.* Biomacromolecules, 2002. **3**(5): p. 959-68.

186. Alpenfels, W.F., *A rapid and senstive method for the determination of monosaccharides as their dansyl hydrazones by high performance liquid chromatography.* Analytical Biochemistry, 1981. **114**(1): p. 153-157.

187. Houdier, S., et al., *A new fluorescent probe for sensitive detection of carbonyl compounds.* Analytica Chimica Acta, 1999. **382**(1): p. 253-263.

188. Boturyn, D., et al., *Synthesis of fluorescent probes for the detection of abasic sites in DNA.* Tetrahedron, 1997. **53**(15): p. 5485-5492.

189. Czworkowski, J., O.W. Odom, and B. Hardesty, *Fluorescence study of the topology of messenger RNA bound to the 30S ribosomal subunit of Escherichia coli.* Biochemistry, 1991. **30**(19): p. 4821-30.

190. Takakusa, H., et al., *A novel design method of ratiometric fluorescent probes based on fluorescence resonance energy transfer switching by spectral overlap integral.* Chemistry--A European Journal, 2003. **9**(7): p. 1479-1485.

191. Takakusa, H., et al., *Design and Synthesis of an Enzyme-Cleavable Sensor Molecule for Phosphodiesterase Activity Based on Fluorescence Resonance Energy Transfer.* Journal of the American Chemical Society, 2002. **124**(8): p. 1653-1657.

192. Jacquemin, D., et al., *The geometries, absorption and fluorescence wavelengths of solvated fluorescent coumarins: A CIS and TD-DFT comparative study.* Chemical Physics Letters, 2007. **438**(4-6): p. 208-212.

193. Nguyen, K.A., P.N. Day, and R. Pachter, *Effects of solvation on one- and two-photon spectra of coumarin derivatives: a time-dependent density functional theory study.* Journal of Chemical Physics, 2007. **126**(9): p. 094303/1-094303/10.

194. Raikar, U.S., et al., *Rotational Diffusion and Solvatochromic Correlation of Coumarin 6 Laser Dye.* Journal of Fluorescence, 2006. **16**(6): p. 847-854.

195. Raikar, U.S., et al., *Solvent effects on the absorption and fluorescence spectra of coumarins 6 and 7 molecules: Determination of ground and excited state dipole moment.* Spectrochimica Acta, Part A: Molecular and Biomolecular Spectroscopy, 2006. **65A**(3-4): p. 673-677.

196. Das, K., B. Jain, and P.K. Gupta, *Photophysics of Coumarin 500 and Coumarin 151 in AOT reverse micelles.* Chemical Physics Letters, 2005. **410**(1-3): p. 160-164.

197. Vishwanath, K., et al., *Fluorescence quenching by polystyrene microspheres in UV-visible and NIR tissue-simulating phantoms.* Optics Express, 2006. **14**(17): p. 7776-7788.

198. Brooke, F., J.C. Andre, and G. Mathis, *Kinetics of partly diffusion controlled reactions XXII: Competition between long-distance energy transfer and collision quenching-first results.* Journal of Photochemistry and Photobiology, A: Chemistry, 1989. **46**(2): p. 181-91.

199. Lopez Arbeloa, I., *Fluorescence self-quenching of halofluorescein dyes.* Journal of Photochemistry, 1982. **18**(2): p. 161-8.

200. Bridgwater, A.V., *Renewable fuels and chemicals by thermal processing of biomass.* Chemical Engineering Journal (Amsterdam, Netherlands), 2003. **91**(2-3): p. 87-102.

201. Council, N.R., *Biobased industrial products: priorities for research and commercialization*, N.A.o. Sciences, Editor. 2000, National Academy Press. p. 147.

202. Ragauskas, A.J., et al., *The Path Forward for Biofuels and Biomaterials.* Science (Washington, DC, United States), 2006. **311**(5760): p. 484-489.

203. Gindl, W., T. Schoeberl, and J. Keckes, *Structure and properties of a pulp fibre-reinforced composite with regenerated cellulose matrix.* Applied Physics A: Materials Science & Processing, 2006. **83**(1): p. 19-22.

204. Zadorecki, P., H. Karnerfors, and S. Lindenfors, *Cellulose fibers as reinforcement in composites: determination of the stiffness of cellulose fibers.* Composites Science and Technology, 1986. **27**(4): p. 291-303.

205. Berglund, L., *Cellulose-based nanocomposites.* Natural Fibers, Biopolymers, and Biocomposites, 2005: p. 807-832.

206. Choi, Y. and J. Simonsen, *Cellulose nanocrystal-filled carboxymethyl cellulose nanocomposites.* Journal of Nanoscience and Nanotechnology, 2006. **6**(3): p. 633-639.

207. Eichhorn, S.J., et al., *Chemical functionalisation and geometrical modification of cellulose fibrous networks for tissue engineering.* Abstracts of Papers, 231st ACS National Meeting, Atlanta, GA, United States, March 26-30, 2006, 2006: p. CELL-122.

208. Dufresne, A., *Interfacial phenomena in nanocomposites based on polysaccharide nanocrystals.* Composite Interfaces, 2003. **10**(4-5): p. 369-387.

209. Favier, V., et al., *Mechanical percolation in cellulose whisker nanocomposites.* Polymer Engineering and Science, 1997. **37**(10): p. 1732-1739.

210. Forster, T., *Intermolecular energy transference and fluorescence.* Ann. Physik [6 Folge], 1948. **2**: p. 55-75.

211. Van Der Meer, B.W., G. Coker, III, and S.S.Y. Chen, *Resonance Energy Transfer: Theory and Data*. 1994. 184 pp.

212. McIntosh, D.C. and B. Leopold. *Bonding strength of fibres*. in *Formation and Structure of Paper; Trans. IInd Fund. Res. Symp.* 1961. Oxford: FRC.

213. Mohlin, U.-B., *Cellulose Fibre Bonding Part 4. Effect of chemical modification on rayon fibre bonding ability.* Svensk Papperstidning, 1975. **10**: p. 373-375.

214. Torgnysdotter, A. and L. Wagberg, *Study of the joint strength between regenerated cellulose fibres and its influence on the sheet strength.* Nordic Pulp and Paper Research Journal, 2003. **18**(4): p. 455-459.

215. Eichhorn, S.J., et al., *Current international research into cellulosic fibers and composites.* Journal of Materials Science, 2001. **36**(9): p. 2107-2131.

216. Borja, Y., G. Riess, and K. Lederer, *Synthesis and characterization of polypropylene reinforced with cellulose I and II fibers.* Journal of Applied Polymer Science, 2006. **101**(1): p. 364-369.

217. Hartler, N. and U.-B. Mohlin, *Cellulose fibre bonding Part 2. Influence of pulping on interfibre bond strength.* Svensk Papperstidning, 1975. **78**(8): p. 295-299.

218. Goring, D.I. *Thermal softening, adhesive properties and glass transitions in lignin, hemicellulose and cellulose*. in *Consolidation of the Paper Web, Trans. IIIrd Fund. Res. Symp.* 1965. Cambridge: FRC.

219. Retulainen, E. and K. Ebeling, *Fiber-Fiber Bonding and Ways of Characterizing Bond Strength.* APPITA Journal, 1993. **46**(4): p. 282-288.

220. Nordman, L., *Bonding in Paper Sheets*, in *Transactions of the Ist Fundamental Research Symposium*, F. Bolam, Editor. 1957, FRC: Cambridge. p. 333-347.

221. Alexander, S. and R. Marton, TAPPI, 1968. **51**(6): p. 283-288.

222. Nordman, L., P. Aaltonen, and T. Makkonen. *Relationships Between Mechanical and Optical Properties of Paper Affected by Web Consolidation*. in *Transactions of the IIIrd Fundamental Research Symposium*. 1965. Cambridge: FRC.

223. Yapoudjian, S., et al., *Surface fluorescence resonance energy transfer studies on interfacial adsorption of Thermomyces (Humicola) lanuginosa*

lipase, using monomolecular films of cis-parinaric acid. Biopolymers, 2002. **65**(2): p. 121-128.

224. Lindstrom, T., *Chemical Factors affecting the behaviour of fibres during papermaking.* Nordic Pulp and Paper Research Journal, 1992(4): p. 181-192.

225. McKenzie, A., *The Structure and Properties of Paper Part XXI: The Diffusion Theory of Adhesion Applied to Interfibre Bonding.* APPITA Journal, 1984. **37**(7): p. 580-583.

226. Pelton, R., *A model of the external surface of wood pulp fibers.* Nordic Pulp and Paper Research Journal, 1993(1): p. 113-119.

227. Pelton, R., et al., *The role of surface polymer compatibility in the formation of fiber/fiber bonds in paper.* Nordic Pulp and Paper Research Journal, 2000. **15**(5): p. 400-406.

228. Chhabra, N., et al., *An Investigation of Pulp Fibre Surfaces by Atomic Force Microscopy.* Journal of Pulp and Paper Science, 2005. **31**(1): p. 52-56.

229. Furuta, T. and D.G. Gray, *Direct Force-Distance Measurements on Wood-Pulp Fibres in Aqueous Media.* Journal of Pulp and Paper Science, 1998. **24**(10): p. 320-324.

230. Mohlin, U.-B., *Cellulose fibre bonding; Part 4: Effect of chemical modification on rayon fibre bonding ability.* Svensk Papperstidning, 1975. **78**(10): p. 373-375.

231. Mohlin, U.-B., *Cellulose fibre bonding; Determination of interfibre bond strength.* Svensk Papperstidning, 1974. **77**(4): p. 131-137.

232. Clark, J., *Pulp Technology and Treatment for Paper*. 1985, San Francisco: Miller Freeman.

233. Paavilainen, L., *Conformability - flexibility and collapsibility - of sulphate pulp fibres.* Paperi ja Puu, 1993. **75**(9): p. 689-702.

234. Page, D.H., *The meaning of Nordman bond strength.* Nordic Pulp & Paper Research Journal, 2002. **17**(1): p. 39-44.

235. Page, D.H., *Fibre-to-fibre bonds: Part 1 - A method for their direct observation.* Paper Technology, 1960. **1**(4): p. 407-411.

236. Campbell, W.B., in *Forest Service Bulletin No. 84*. 1933, Canada Dept. Interior.

237. Thomson, C.I., R.M. Lowe, and A.J. Ragauskas, *Imaging cellulose fibre interfaces with fluorescence microscopy and resonance energy transfer.* Carbohydrate Polymers, 2007. **69**(4): p. 799-804.

238. Mohlin, U.-B., *Cellulose fibre bonding; Part 3. The effect of beating and drying on interfibre bonding.* Svensk Papperstidning, 1975. **78**(9): p. 338-341.

239. Gurnagul, N., S. Ju, and D.H. Page, *Fibre-fibre bond strength of once-dried pulps.* Journal of Pulp and Paper Science, 2001. **27**(3): p. 88-91.

240. Torgnysdotter, A. and L. Wagberg, *Tailoring of fibre/fibre joints in order to avoid the negative impacts of drying on paper properties.* Nordic Pulp and Paper Research Journal, 2006. **21**(3): p. 411-418.

241. Notley, S., M. Eriksson, and L. Wagberg, *Visco-elastic and adhesive properties of adsorbed polyelectrolyte multilayers determined in situ with QCM-D and AFM measurements.* Journal of Colloid and Interface Science, 2005. **292**: p. 29-37.

242. McIntosh, D.C., *Tensile and bonding strengths of Loblolly Pine kraft fibers cooked to different yields.* Tappi, 1963. **46**(5): p. 273-277.

243. Touchette, R.V. and L.C. Jenness, *Effect of surface-active agents on drainage and physical strength of sulfite pulp.* Tappi, 1960. **43**: p. 484-9.

244. Varma, A.J., V.B. Chavan, and P.R. Rajmohanan, *Some observations of the high-resolution solid-sate CP-MAS ^{13}C-NMR spectra of periodate oxidised cellulose.* Polymer Degradation and Stability, 1997. **58**: p. 257-260.